NTNU
Norwegian University of
Science and Technology

# The effects of press cooling and artificial aging on fatigue and ductility of an aluminium alloy

**Musaad Nidal Najeeb**

Materials Science and Engineering, MIMT
Submission date: July 2020
Supervisor: Professor Ola Jensrud, IMA

Norwegian University of Science and Technology
Department of Materials Science and Engineering

# Preface

This report is submitted as the product of ¨ TMT4920 Materials Technology, Master's thesis ¨ in fulfilment of the degree of Master of Science in Materials science and engineering at the Norwegian University of Science and Technology. This Master's thesis is conducted in collaboration with SINTEF Manufacturing AS. The research has been conducted at the Department of Materials Science and Engineering under supervision of Professor Ola Jensrud.

Trondheim, July 2020
Musaad Najeeb

# Acknowledgement

I would like to express my gratitude to my supervisor Ola Jensrud for valuable guidance, advice, help and encouraging during the semester.

I would like to thank my contact person from SINTEF AS, Senior Adviser Tanja Pettersen for her guidance, discussions, and help.

I would like to thank the Research Scientist Kai Zhang for valuable advice and feedbacks about my results.

I would like to thank M.Sc. Metallurg Benedikte Myrold for guidance, help, discussions and feedbacks about my results.

I would like to thank chief engineer Pål Christian Skaret for the cooperation during the conduction of the experimental work.

Thanks to the mechanical engineering workshop and staff engineer Øystin Gjervan Hagemo for the machining samples.

Finally, I would like to thank Staff Engineer Berit Vinje Kramer for helping me during my work in metallography laboratory during preparing my samples.

# Abstract

The modern automotive industry demands new lightweight solutions regarding producing light vehicles to reduce gas emissions and increase the fuel-efficiency.
Age hardenable aluminium alloys are attractive choices to replace the steel to reduce the weight of vehicles. Age hardenable aluminium alloys combine high strength and good ductility. In this study, two age hardenable aluminium alloys AA6082 and AA6010 that belong to AA-6xxx series have been used. During the heat treatment, an integrated in-die quenching, and hot forming method was used. This method is more suitable for high volume production than the conventional production process. An improved flat pressing tool was used to deform and quench the samples after solution heat treatment.
The last step of the heat treatment procedures was the artificial aging. Three different states of the artificial aging have been tested: under-aged condition, peak-aged condition, and over-aged conditions.
During the mechanical tests, low cycle fatigue behavior was the main focus. After artificial aging, age hardenable aluminium alloys get better strength and lower ductility. Therefore, low cycle fatigue tests were done to distinguish the relation between the strength and ductility, and to compare between the under-aged, peak-aged, and over-aged condition results. Effect of the artificial aging on the low fatigue properties was studied by aging the samples to three different periods. For AA6082, samples were divided in three groups. The first group of samples was artificially aged for 40 minutes to the under-aged state, the second group of samples was artificially aged for 3 hours to the peak-aged for state, and the last group of samples was artificially aged for 8 hours to the over-aged state. For AA6010, the same process was done. The periods of the artificial aging were 2 hours for the peak-aged state, 5 hours for the peak-aged state and 20 hours for the over-aged state. Results exhibit that samples that have the higher tensile strength have the lower fatigue life. The over-aged condition gives the higher number of cycles to failure.

# Sammendrag

Den moderne bilindustrien krever nye løsninger når det gjelder å produsere lette kjøretøyer for å redusere utslipp og øke drivstoffeffektiviteten. Utherdbare aluminiumslegeringer er attraktive erstatninger for stål for å redusere vekten på kjøretøyer.

Utherdbare aluminiumslegeringer kombinerer høy styrke og god duktilitet. I denne studien ble det brukt to utherdbare aluminiumslegeringer, AA6082og AA6010, som tilhører AA6-xxxx-serien. Under varmebehandlingen ble det brukt en integrert in-die quenching og varmeformingsmetode. Denne metoden er mer egnet for høyvolumproduksjon enn den konvensjonelle produksjonsprosessen. Et forbedret flatpresse-verktøy ble brukt til å deformere og slukke prøvene etter oppløsningsvarmebehandling.

Det siste trinnet i varmebehandlingsprosedyrene var kunstig aldring. Legeringer ble testet til tre tilstander med den kunstige aldringen; under-aldret, topp-aldret og over-aldret tilstander. Under de mekaniske testene var utmattelsesatferd med lav syklus hovedfokus. Etter kunstig aldring får utherdbare aluminiumslegeringer bedre styrke og lavere duktilitet. Derfor ble det utført utmattelsestester med lav syklus for å skille sammenhengen mellom styrke og duktilitet, og for å sammenligne mellom under-aldrede, topp-aldrede og over-aldrede tilstandsresultater. Effekten av den kunstige aldringen på egenskapene med lav utmattelse ble studert ved å utherde prøvene til tre forskjellige perioder. For AA6082 ble prøvene delt inn i tre grupper. Den første gruppen av prøver ble kunstig aldret i 40 minutter til under-aldret tilstand, den andre gruppen av prøver ble kunstig aldret i 3 timer til topp-aldret tilstand, og den siste gruppen av prøver ble kunstig aldret i 8 timer til overaldret tilstand. For AA6010 er den samme prosessen blitt utført. Men periodene med den kunstige aldringen var 2 timer for under-aldret tilstand, 5 timer for topp-aldret tilstand og 20 timer for over-aldret tilstand. Resultatene viser at prøver med høyere strekkfasthet har lavere utmattelses-levetid. Over-aldret tilstand tåler høyest antall sykluser før at det skjer brudd i prøven.

# Table of contents

# 1 Introduction

Nowadays automotive industry has new environmental, economic, and technological challenges. Improving efficient manufacturing processes is an important issue to achieve more success in the environmental field [2].

Serious attention has been focused to reduce the weight of vehicles by replacing cast iron and steel by aluminium and its alloys [21]. Steel has been the dominant material utilized in the automotive industry since 1920s. In 1947 was the average of aluminium content in motor vehicles around 3 Kg and this amount of aluminium been increased up to 156 kg in 2009 [21].

Properties of aluminium alloys, high strength stiffness to weight ratio, good corrosion resistance and good form ability make aluminium the desired metal to replace conventional materials (steel, wood) to assure lighter weight and more fuel-efficient vehicles [14]. Aluminium alloys are the most used non-ferrous alloys in the engineering application in the automotive, aerospace, and structural industries [2]. Extrusion of aluminium alloys has relatively very low cost compared to the steel and that make aluminim alloys suitable for a lot of application regarding to the economy [2].

Interest of using aluminium alloys in automotive industry have been increased very widely due to the desired properties of aluminium which led to reduction in the weight of the vehicle, and that might rise the fuel efficiency and reduce gas emissions of the vehicle (Co2) [4].

## 1.1 The aim of project

The main purpose of this study is to determine the low cycle fatigue properties of two aluminium alloys (AA6082-AA6010) under three different artificial aging conditions. The three types of artificial aging treatments are: Under-aged condition (U.A), Peak-aged condition (P.A) and Over-aged condition (O.A).

Samples have been tempered to the T6 temper by using a new method which is known as integrated hot forming and in-die quenching. This study also includes the hardening curves of AA6082 and AA6010, and the grain structure of AA6082 and AA6010 alloys.

The mechanical properties of AA6082 and AA6010 have been determined by hardness measurements, tensile tests, low cycle fatigue tests and fractography study.

# 2 Theory

## 2.1 Aluminium and its alloys

Aluminium is the most used non-ferrous metal in the world [11]. Aluminium alloys are second only to steels in the use in structural applications [24].

The color of aluminium is silver-white. The atomic number of aluminium is 13 [11]. Density of aluminium is relatively low (2,7 g/cm$^3$) approximately half the density of steel 7.83 g/cm$^3$ [24]. Thermal and electrical conductivity of aluminium are very high. The crystal structure of aluminium is face-centered cubic (FCC) and the crystal structure is closely packed. Pure aluminium is a soft metal and has a low strength, like all pure metals. Therefore, alloying elements should be added to improve the mechanical properties, like strength. The properties of aluminium alloys depend on the developing of the chemical composition and microstructure features of the alloys during the solidification, deformation process, and heat treatment.

Aluminium and its alloys are increasingly utilized in automotive industry, building constructions and aerospace equipment due to its light weight, high strength, good corrosion resistance, and the good formability [11].

### 2.1.1 Designation of aluminium alloys

Several alloying elements are essentially used in order to strengthen the aluminium. Aluminium alloys can be formed by using alloys elements like: Mg, Si, Cu, Li, Zn and Mn. The following table, table 2.1, presents the series of wrought aluminium alloys according to which alloying elements is presented in each series [16].

| Alloying elements | Series designation |
|---|---|
| Pure aluminium | AA1XXX |
| Copper | AA2XXX |
| Manganese | AA3XXX |
| Silicon | AA4XXX |
| Magnesium | AA5XXX |
| Magnesium and silicon | AA6XXX |
| Zinc | AA7XXX |
| Lithium | AA8XXX |

Table 2.1: Four-digit numeric designation of aluminium alloys.

### 2.1.2 Heat-treatable aluminium alloys

Aluminium alloys which are able to respond to the strengthening after heat treatment procedures are called heat treatable alloys, and the heat treatable alloys are covered by three series: 2xxx (Al-Cu, Al-Cu-Mg), 6xxx (Al-Mg-Si) and 7xxx (Al-Zn-Mg, Al-Zn-Mg-Cu). These series depend on the aging to achieve better strength properties. These alloys can be categorized into two groups: alloys that have medium strength (like Al-Mg-Si and Al-Zn-Mg), and alloys that have high strength which are used for aircraft construction (like Al-Cu, Al-Cu-Mg, and Al-Zn-Mg-Cu). Figure 2.1 shows representation of both age hardening alloys (heat treatable alloys) and non-age hardening alloys [21].

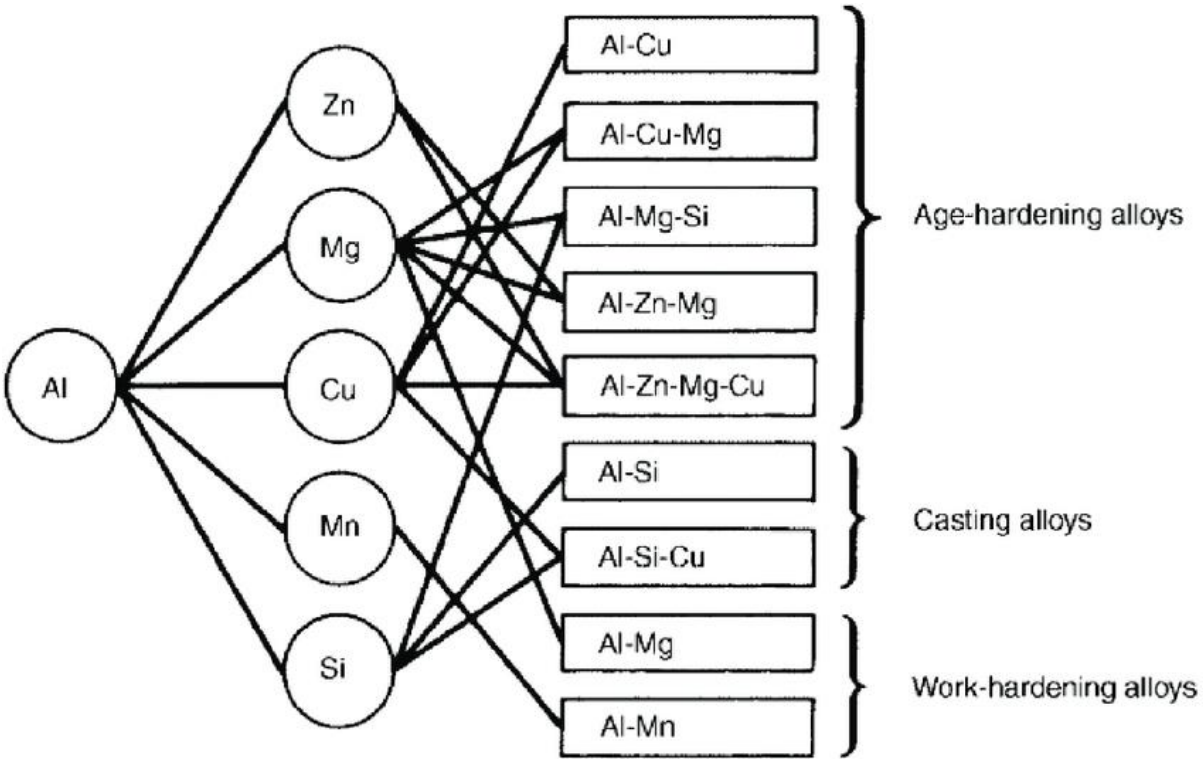


Figure 2.1: Representation of alloying elements in relation to aluminium alloys.

### 2.1.3 Temper states of aluminium alloys

The most important effects on the properties of the wrought aluminium alloys can be achieved by the final heat treatments. The tempers designation system is used to designate the heat treatment performed on the aluminium. This designation is used for all cast and wroght aluminium alloys, expect ingot.

The basic temper designations are: F as fabricated, O annealed (only for wrought products), W solution heat treated, and T heat treated to produce more stable tempers than F and O. The following table indicates some of the specific sequences of heat treatments of designation T: [13]

| | |
|---|---|
| T1 | Cooled from elevated temperature shaping process and naturally aged. |
| T2 | Annealed (for cast products only) |
| T3 | Solution heat treated and naturally aged to substantially stable conditions. (Applies to products which are cold worked) |
| T4 | Solution heat treated and naturally aged to substantially stable conditions. (Applies to products which are not cold worked) |
| T5 | Cooled from elevated temperature shaping processes and artificially aged. |
| T6 | Solution heat treated and artificially aged. |

Table 2.2: Some of the most used temper states. [13]

### 2.1.4 AL-Mg-Si alloys (6xxx series)

Al-Mg-Si alloys are mainly used in transportation applications. These alloys have high variation of solute aggregation states. This variety of solute aggregation states rely on the temperature, alloy compositions, and aging time [18].

Commercial Al-Mg-Si alloys are split into three categories. Those categories are illustrated in figure 2.2 according to the chemical composition and strength (at T6).

The first group covers alloys which have balanced amount of magnesium and silicon adding up to between 0.8 wt % and 1.2 wt %. This type of alloys can be easily extruded, and they may be quenched immediately when the alloy emerges hot from the extrusion die. The strength may be developed by age-hardening at 160-190 °C. The most typical used alloy in this group is AA6063, and the typical tensile properties are 215 MPa yield strength and 245 MPa tensile strength. Those alloys are used for architectural and decorative finishes. The other two groups contain more than 1.4% magnesium and silicon. Those two groups offer better strength on aging. The amount of Magnesium and silicon in the commercial alloys should be balanced to form quasi-binary Al-$_{Mg2Si}$ alloys (Mg:Si 1.73:1), or with extra addition of silicon to get $Mg_2Si$. 6061 alloy is one common example of these groups which has a balanced composition that is very common in North America, AA6061 contains balanced compositions (Al-1Mg-0.6Si) with an addition amount 0,25% copper to improve the mechanical properties and with further addition with 0.2% chromium to compensate any adverse influence of copper on corrosion

resistance. This category of alloys is usually used as structural materials [21]. The alloys in the last two groups involve silicon in excess of what is necessary to form $Mg_2Si$, and this excess of silicon improves the effect of age-hardening by refining the size of $Mg_2Si$ particles and the precipitation of silicon. On the other hand, this excess may reduce the ductility and cause intergranular embrittlement. This is because of the ability of silicon to segregate to the grain boundaries. However, chromium (AA6151) and manganese (AA6351) revers this effect by improving the fine grain size and suppressing the crystallization during solution treatment. Those alloys are typically used as extruded or forged [21].

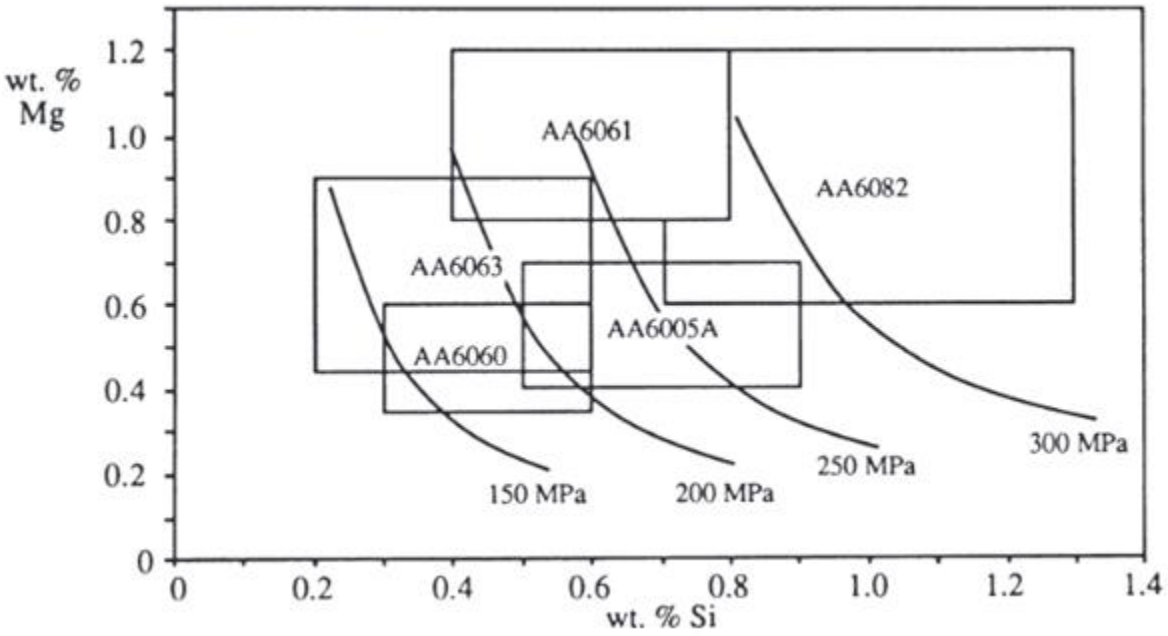


Figure 2.2: Compositions limits of some common AL-6XXX alloys. The additional curves exhibit corresponding peak aged (T6) yield strength. [21]

## 2.1.5 Microalloying effects on AA6xxx

The presence of minor amounts of certain elements may strongly affect the precipitation reactions, especially when the following conditions are present: increasing the GP zones solvus, preferential interactions between vacancies which minimize the rate of nucleation of GP zones, simulating nucleation of an existing precipitate, boost formation of a different precipitate, supplying heterogeneous sites, and rising supersaturation [20].

The presence of copper in AA-6xxx has a ratable influence. Addition of adjustable amount of copper to aluminium alloys leads to substantial solid solution and precipitation strengthening. The presence of Mg and Si in AA6xxx alloys, and the addition of copper lead

to age hardening effects at room temperatures. This effect of copper minimizes the weldability and corrosion resistance [16].

The presence of small amounts of Fe in AA6xxx alloys, has a negative influence on the mechanical properties. This presence of Fe trace forms coarse constituent with Al and the other elements which are involved in AA6xxx alloys. That leads to reduction in ductility and toughness, and also, decreased fatigue resistance [16].

Figure 2.3 and figure 2.4 illustrate alloy selection challenge and how to combine between the desired mechanical properties (strength) and the addition of both Mg and Si. Increasing the Mg and Si content will increase the strength but that occurs on expense of formability and corrosion resistance [8].

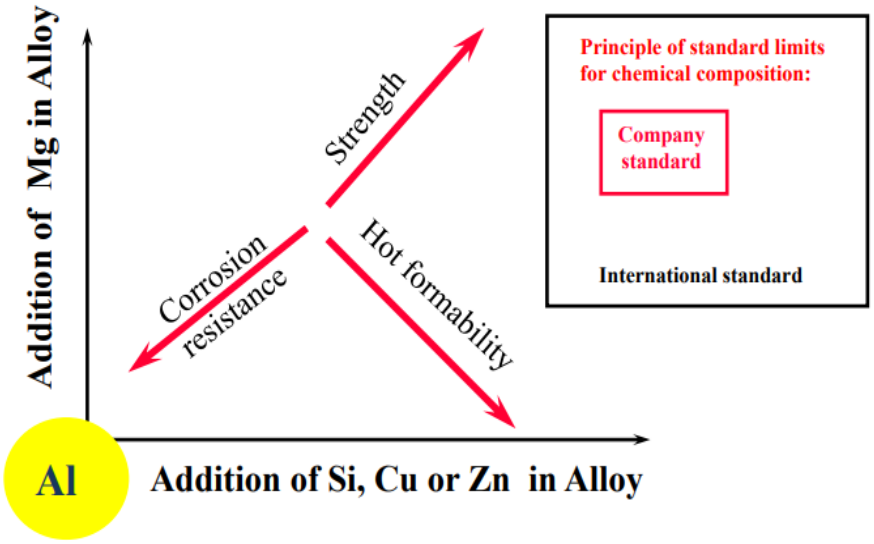


Figure 2.3: Principle of combinations Al+ Mg+ (Si or Cu or Zn). [8]

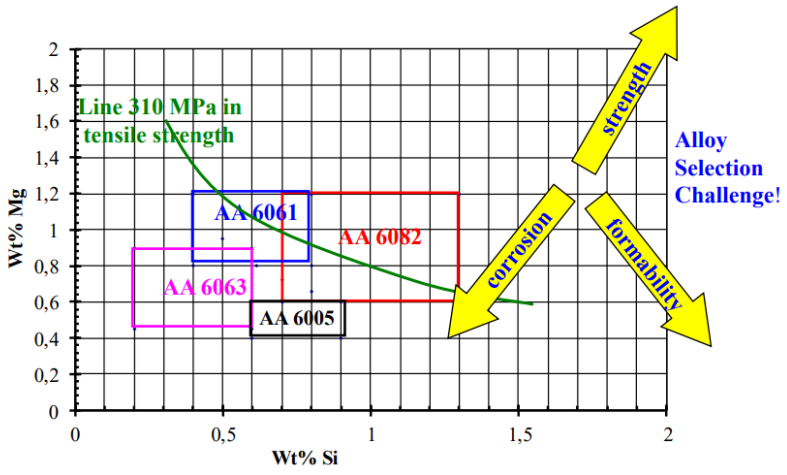


Figure 2.4: Principle of combinations Al+ Mg+ Si. [8]

### 2.1.6 Overview on AA6082 and AA6010

Aluminium alloy 6082 is one of the most popular alloys in 6xxx series. AA6082 is usuallyused as extruded or rolled. The most Typical heat treatment for AA6082 is to be tempered at (T6 orT4) [4]. The chemical composition of AA6082.25 that been used in this study is illustrated in the table 2.3 [12].

| Element | Si | Mg | Cu | Mn | Fe | Zn | Ti | Cr | Al |
|---|---|---|---|---|---|---|---|---|---|
| Wt % | 0.92 | 0.64 | 0.01 | 0.55 | 0.17 | 0.02 | 0-0.1 | 0.15 | Balance |

Table 2.3: Chemical composition of AA6082.25. [12]

AA6082 is very commonly used for machining in the flat shape. It has medium strength and very good corrosion resistance. After tempering, AA6082 gets higher strength but lower ductility. Table 2.4 shows the mechanical properties of AA6082 and T6 conditions [29].

| Tensile strength, $\sigma_{UTS}$ (MPa) | Hardness, $Hv_{0.2}$ | Elongation, $\varepsilon_r$ (%) | Yield strength, $\sigma_{YS}$ (MPa) |
|---|---|---|---|
| 330 | 115 | 10 | 307 |

Table 2.4: Mechanical properties of AA6082 at T6.

AA6010 is another type of alloy in 6xxx series. The chemical composition of AA6010 that been used in this study is given in table 2.5 [4], and the mechanical properties for AA6010 at T4 tempering condition is illustrated in table 2.6.[12]

| Element | Mg | Si | Cu | Fe | Mn | Zn | Cr | Zr | Ti | Al |
|---|---|---|---|---|---|---|---|---|---|---|
| Wt % | 0.73 | 1 | 0.24 | 0.29 | 0.51 | 0.2 | 0.005 | 0.0001 | 0.023 | Balance |

Table 2.5: Chemical composition for AA6010. [12]

| Tensile strength, $\sigma_{UTS}$ (MPa) | Elongation at break (%) | Yield strength, $\sigma_{YS}$ (MPa) |
|---|---|---|
| 349 | 4 | 318 |

Table 2.6: Mechanical properties of AA6010 at T6 conditions. [12]

## 2.2 Hot forming and in-die quenching

¨ Hot forming and in-die quenching ¨ is a novel method to improve the low form ability at room temperatures. The hot forming and in-die quenching technique for an aluminium alloy include

the solution heat treatment and deforming in cold dies. Deforming aluminium alloys which are heated to elevated temperature gives better formability and ease forming to complex shapes. Hot forming and in-die quenching step is followed by artificial aging to improve the strength. The following figure 2.5 illustrates an example for the steps of heat treatments of an aluminium alloy AA6082, the workpiece heated to 500 C ° at a rate 10 C °/s and after that heated to 525 C ° at a rate 5 c °/sec to avoid overheating. The workpiece is kept at 525 C° for 300 sec. The deformation started at 500 C ° and the workpiece quenched to room temperature [28].

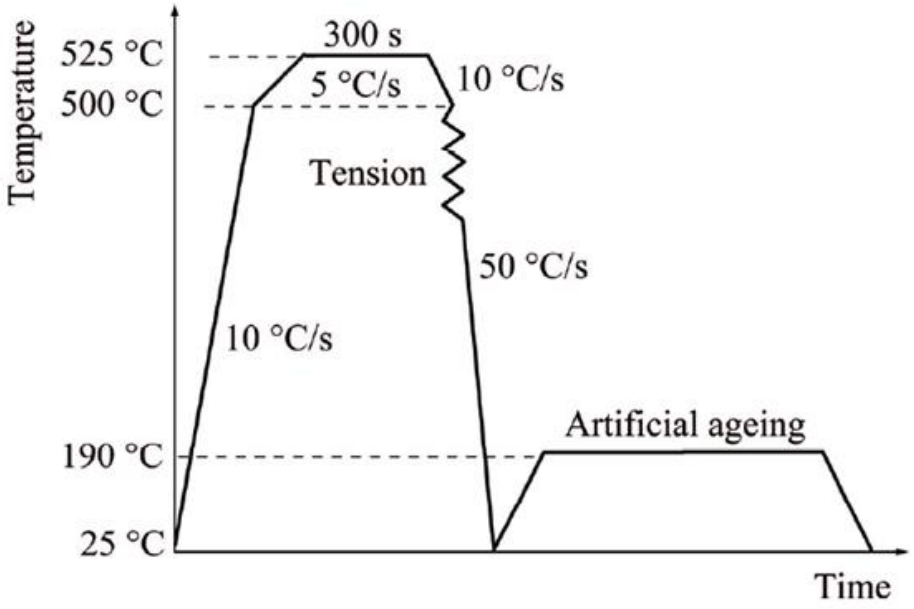


**Figure 2.5:** Temperature profile of simulated thermal experiments.

## 2.4 Work hardening and annealing

Work hardening, known as strain hardening, is an essential method to strength the metal by plastic deformation. The strengthening happens due to the movement of dislocations and the generation of dislocations into the crystal structure of the metal. [3]

### 2.4.1 Influence of deformation on aluminium alloys

Deformation of alloys or metals cause rising in the extent of dislocation as dislocation happens faster than annihilation, which can happen by dynamic recovery. The strength increases during deformation because of several influencing factors: Dislocations tangles, cells and sub grains are formed, grain shapes and internal structure changes. These factors reduce the mean free path and thus increase the strength [19]. Figure 2.6 shows the microstructure of a

rolled aluminium alloy and explains how the features was developed during the deformation. Slips has occurred in the individual grains and the grains have become elongated which gives increased grain boundary area. Figure 2.6 illustrates how the deformation band (a) into one grain separates two internal areas that have improved two distinguished orientations during the deformation process. And that appears in the figure 2.6 where there is a big cutout (d) which is called a shear band. These bands tend to appear in areas of high strain (true strain> 1) [20].

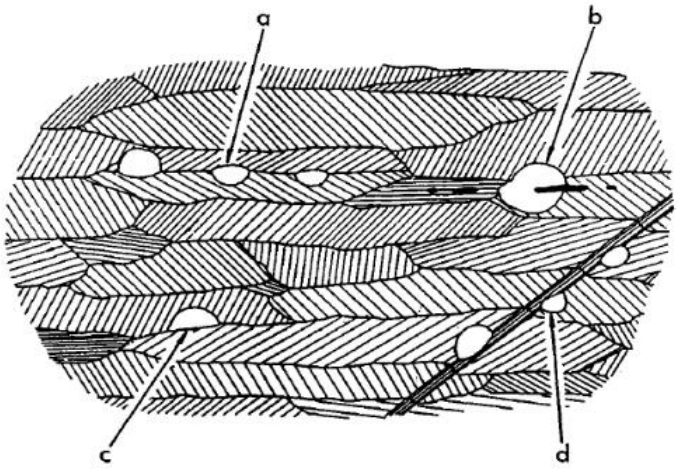


Figure 2.6: shows the possible nucleation sites for recrystallized grains in a rolled alloy.

However, deformation might be more inhomogeneous in alloys which have several phases, like multi-phase aluminium alloys that contain coarse and fine intermetallic particles. Figure 2.7 shows how substructures develop severely around the coarse particles in the deformed zones [20].

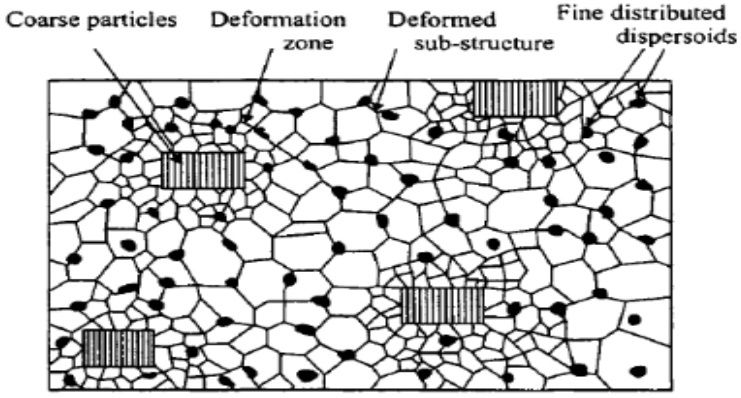


Figure 2.7: Schematic drawing of the substructure of cold worked alloy that contains fine and coarse intermetallic particles.

It is important to notice that chemical elements in solid solution state may affect deformation behavior by enhancing rates at which dislocation can multiply, reducing the mobility of

dislocations and thus gives more influential barriers to metal flow, and decreasing rates of recovery during thermal mechanical procedures. Copper is the most influential element which can affect deformation process, magnesium has lesser efficiency on an equi-atomic basis. However, magnesium has higher value than the other element because of its great solubility [20].

### 2.4.2 Annealing after hot deformation

Annealing is the process of altering the microstructure of a metal or an alloy by heat treatment to get better mechanical properties like strength, ductility and hardness. The process of annealing can be divided into three main steps: recovery, recrystallization and grain growth [3]. Recrystallization and recovery have an essential technological rule after conducting hot deformation procedures. Because the cooling rate of the material which has been conducted to hot deformation is very low. Therefore, recovery, recrystallization and grain growth happen directly after hot deformation. Dynamic recovery happens during hot deformation. However, after deformation, further recovery takes place which is called static recovery. This recovery is generally small and involves sub grain growth, dislocation rearrangement (Ouchi and Okita,1983) and consequent softening (Sellars et al., 1986) [7].

### 2.4.3 Dynamic recovery and dynamic recrystallization

During deformation at high temperatures. Metals or alloys experience the restoration procedures of recovery and recrystallization. These restoration processes which occur during deformation are called dynamic recovery and dynamic recrystallization. Dynamic recovery and dynamic recrystallization have an essential role during metal forming processes like hot rolling and extrusion. This is of importance because they decrease the flow stress in the material, and consequently make the material more able to be deformed [7]. Dynamic recovery occurs very fast at elevated temperatures for metals which have high stacking fault energy, like aluminum alloys. Because in this case cross-slip and dislocation climb happen very easily. The stress-strain curve for this situation is illustrated in figure 2.8. During the initial stages of deformation, the flow stress raises highly because of the interaction between dislocations. Therefore, dislocation increase the density. The driving force and the rate of recovery will raise too. At this stage, the microstructure of low-angle boundaries and sub grains grow. After this stage, the rates of work hardening and recovery amount to equilibrium recovery at determined strain. And a steady-state flow stress might be achieved, and the dislocation density will be

steady [7].

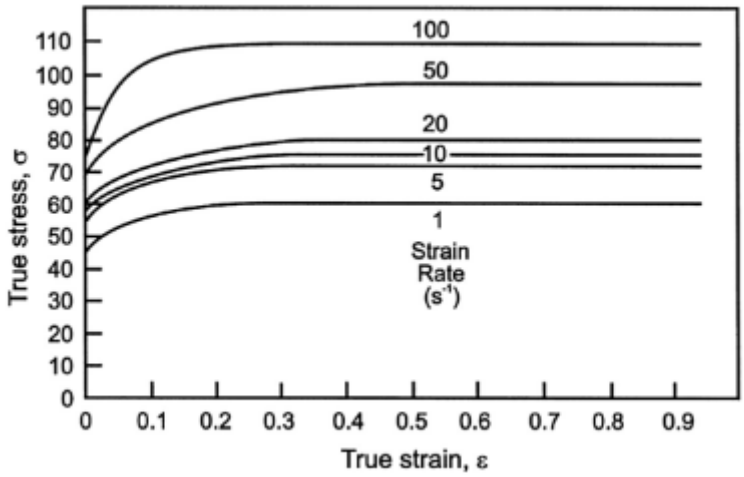


Figure 2.8: Stress-strain curves for Al alloy contains (1%Mg) at 400 °C.

## 2.4.4 Decomposition of supersaturated solid solutions

Decreasing the solid solubility of the alloying elements with decreasing temperature is the main term for an alloy to be able to age-hardening. Typical heat treatment for aluminium alloys involves these three steps. step 1: solution heat treatment at elevated temperature to ensure dissolving of the alloying elements. step 2: rapid cooling to room temperature to achieve a supersaturated solid solution of the alloying elements in aluminium. Step 3: Aging to obtain controlled decomposition of the supersaturated solid solution that leads to final dispersed precipitate. All these three steps are illustrated in figure 2.8 [20].

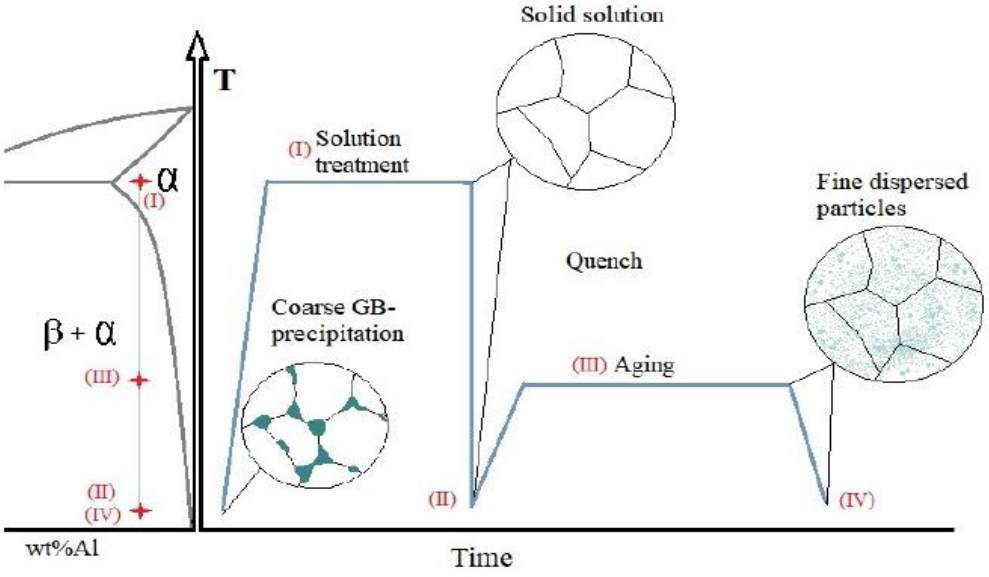


Figure 2.8: General heat treatment for precipitation hardenable alloys.

## 2.5 Fatigue:

It has been noticed that some materials suddenly fail after considerable periods of service. Metals that conducted to a fluctuating or repetitive stress will fail at a stress lower than that required to cause fracture on a single application of load. Fatigue failures are failures that occur under condition of dynamic loading. Fatigue failure is quite dangerous because it occurs without any obvious warning. Today, fatigue failures accounts to more than 90 percent of all metallic component failures, due to mechanical causes [3].

There are three essential factors that are required to cause fatigue failure: sufficiently high value of maximum tensile strength, sufficiently large fluctuation in the applied stress, and high numbers of cycles of the applied stress. Other variables like temperature, corrosion, metallurgical structure and overload may influence the condition for fatigue [3].

### 2.5.1 Relevant definitions and concepts

Fatigue is the failure in response to alternating loads. Typical measuring of fatigue resistance is given according to the numbers of cycles to failure. For a given number of cycles either the strain is specified, or the stress is specified.

Endurance N: The number of applied cycles to failure.

SN curve: A plot of log S (on the Y axis) and log N (on the X axis).

Equations for cyclic stresses:

Stress range: $\Delta\sigma = \sigma_{max} - \sigma_{min}$

Stress amplitude: $\sigma_a = \Delta\sigma/2$

Mean stress: $\sigma_m = (\sigma_{max} + \sigma_{min})/2$

Max stress in a cycle: $\sigma_{max} = \sigma_m + \sigma_a$

Min stress in a cycle: $\sigma_{min} = \sigma_m - \sigma_a$

Stress ratio: $R = \sigma_{min}/\sigma_{max}$

Figure 2.9 illustrates the stress variables and the parameters of a stress cycle at three different stress ratio level [30].

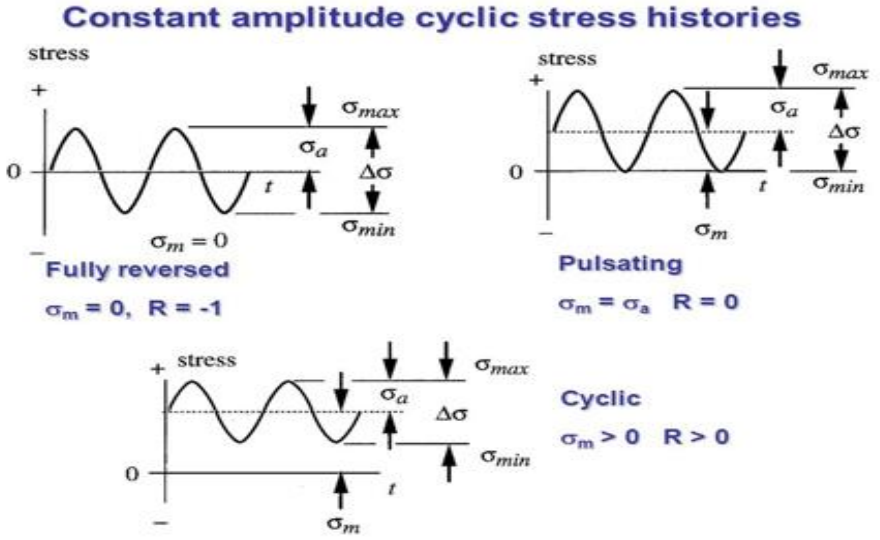


Figure 2. 9: Parameters of a stress cycle and definition of stress variable.

### 2.4.4 The S-N curves

The main way to present fatigue test results is by using S-N curve, by plotting stress S versus number of cycles to failure N. The values of stress which is plotted in the S-N curves can be stress amplitude, maximum stress or minimum stress. The S-N relation is established for a certain value of mean stress $\sigma_m$, stress ratio R, or A. Figure 2.10 shows the typical S-N curves for ferrous, and nonferrous metals [3].

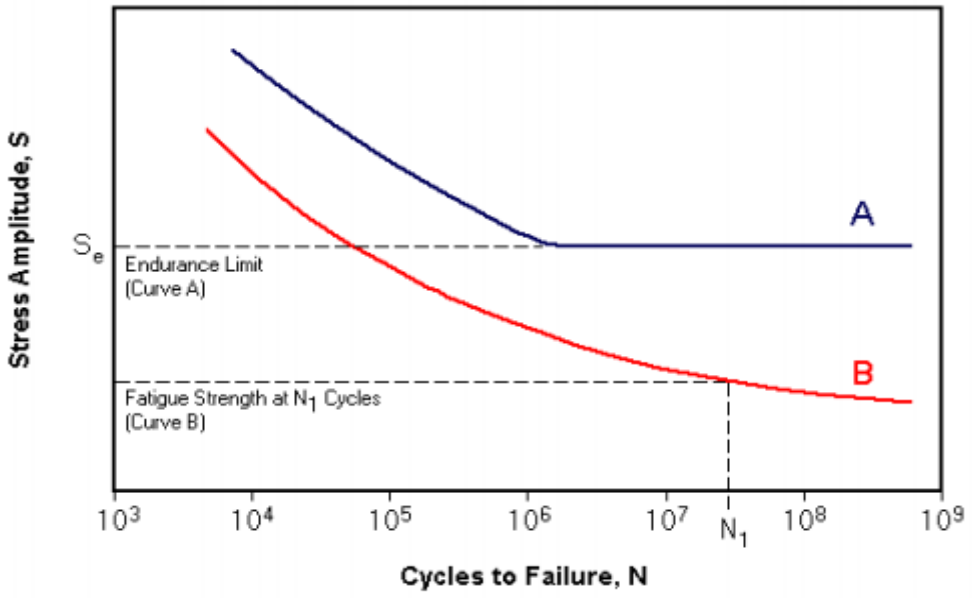


Figure 2. 10: Representation for materials which have a clear endurance limit, like Steel (A) and another material which does not exhibit well-defined endurance limit, like Aluminium (B).

Some materials exhibit certain endurance limit which represents a stress level where the material does not fail below this level and can be cycled infinitely. If the applied stress is much lower than the endurance limit of the metal (like steel), the structure in this case has infinite limit. However, many non-ferrous alloys or metals like aluminium, does not have clear endurance limit. Therefore, attention should be taken in fatigue design because the endurance limit might be altered due to high temperatures, periodic overloads, or corrosive environments [3].

### 2.4.3 Statistical nature of fatigue

The statistical analysis of fatigue data has been an essential study for the researchers because of the variability of fatigue test results. It is important to study the probability of a sample given certain cycles of life at a certain amplitude stress or study the probability of failure at a given stress comparing to the fatigue limit. To determine the statistical parameters to evaluate the probability requires a considerable number of the tested specimens. The main way for representing fatigue data should be a three-dimensional surface illustrating the relationship between stress, number of cycles to failure, and probability of failure. And that is illustrated in two-dimensional plot in figure 2.11 [3].

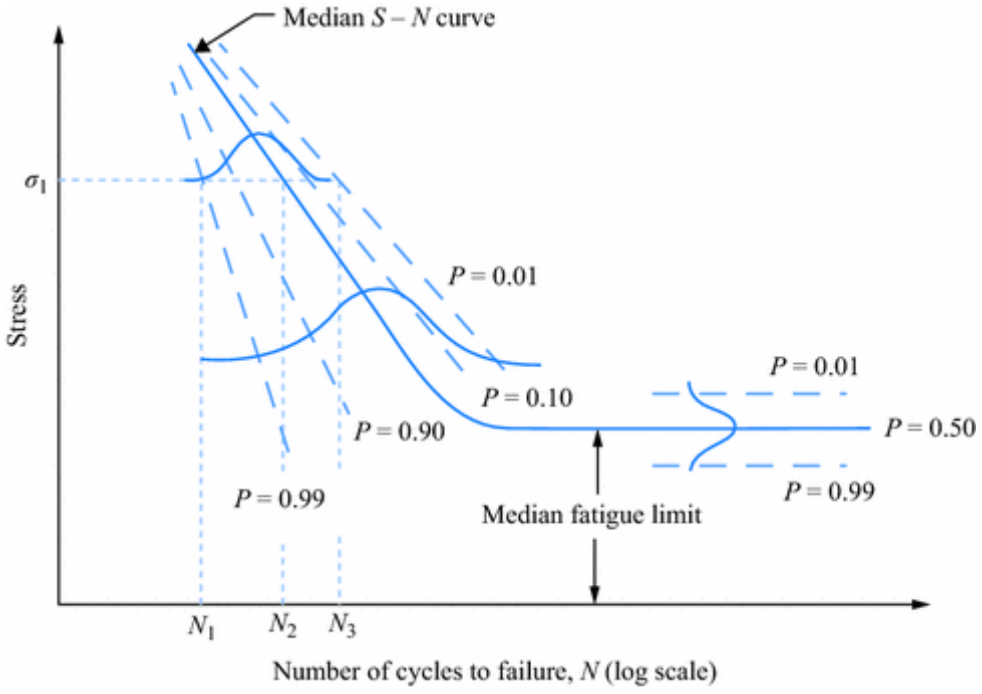


Figure 2.11: Fatigue data on probability basis.

Figure 2.11 shows schematically how the fatigue life can be distributed at a certain constant stress, and how the curves of constant probability of failure are plotted according to the stress

and distribution of fatigue life. Figure 2.11 explains that at $\sigma_1$ the probability of failure is 1 percent at $N_1$ cycles, and 50 percent at $N_2$ cycles, etc. This figure shows also that an increasing stress is usually followed by a decrease in the scatter in fatigue life [3].

### 2.4.4 Fatigue failure of metals

The fracture surface of a metal has almost a characteristic appearance. The fracture surface is typically divided into two different regions. The smooth regions of the surface, which look like beach marks, is weakly deformed and caused by fatigue, and the rough regions which was made by the final fracture. This variation in the fracture surface of metal is due to several stages which happen under cyclic loads. Crack initiation: Fatigue fracture usually starts at the highest loaded position of the structure. Fatigue strength of a component rely on the manufacturing process and the material defect much more than the static strength [23]. Crack propagation: the propagation of fatigue crack in metals occurs by plastic deformation at the tip that outcomes from progressive plastic blunting. The crack grows in the direction normal to ultimate tensile stress [25]. Final fracture: The final fracture occurs when the stress intensity fracture is equal to the fracture toughness $K_{Ic}$ of the metal [23]. Figure 2.12 exhibit schematic representation for the stages of the fatigue failure [15].

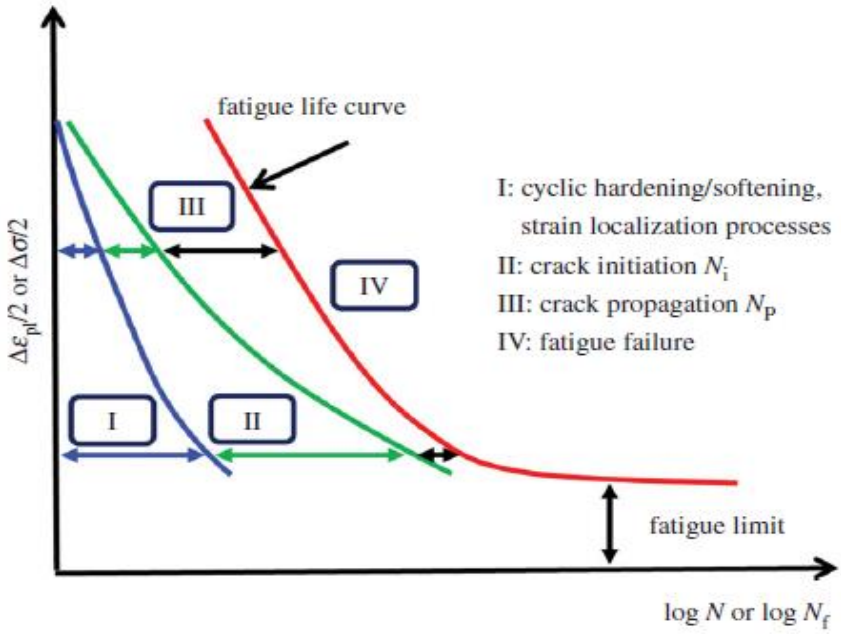


Figure 2.12: Representation of the four stages of fatigue in a ductile metal. [15]

### 2.4.5 Basic concepts on fatigue statics

Fatigue life is governed by loading in three interval ranges. The three categories are: low life region when the fatigue life of a specimen is less than $10^4$ cycles, medium life region when the fatigue life of specimen is between $10^4$ to $10^6$ cycles, and long life region when the fatigue life of a specimen is higher than $10^6$ cycles. [27] Researchers have noticed that many structures have experienced engineering failure at high stress and low number of cycles. This type of failure usually occurs due to repeated stresses from thermal origin Thermal stresses increase from the thermal expansion of the material. Low cycle fatigue should be considered in the design of most types of power machinery. Usually low cycle fatigue tests are strain controlled because it is easier to see the results from cyclic strain rather than from cyclic stresses.

Low cycle fatigue test data is usually plotted by the plastic strain range versus the number of cycles to failure [3].

### 2.4.6 Cyclic hardening and softening

Cyclic hardening and cyclic softening are the hardening or the softening response of a material that has been conducted to repeated loading. Cyclic hardening occurs due to the increasing of the dislocation density, or the interaction between the dislocations and particles during the cyclic straining. Cyclic softening occurs when the precipitated particles present are easily sheared by the dislocation. The presence of the persistent slip bands in the precipitated alloys lead to the cyclic softening [26]. Cyclic hardening leads to increased resistance to the deformation. While cyclic softening leads to reduced resistance to the deformation. Cyclic hardening and softening can be investigated by the variation of the stress amplitude with number of cycles or the variation between the strain amplitude and the fatigue life. Figures 2.13 shows the mutual competition between cyclic hardening and cycle softening [22].

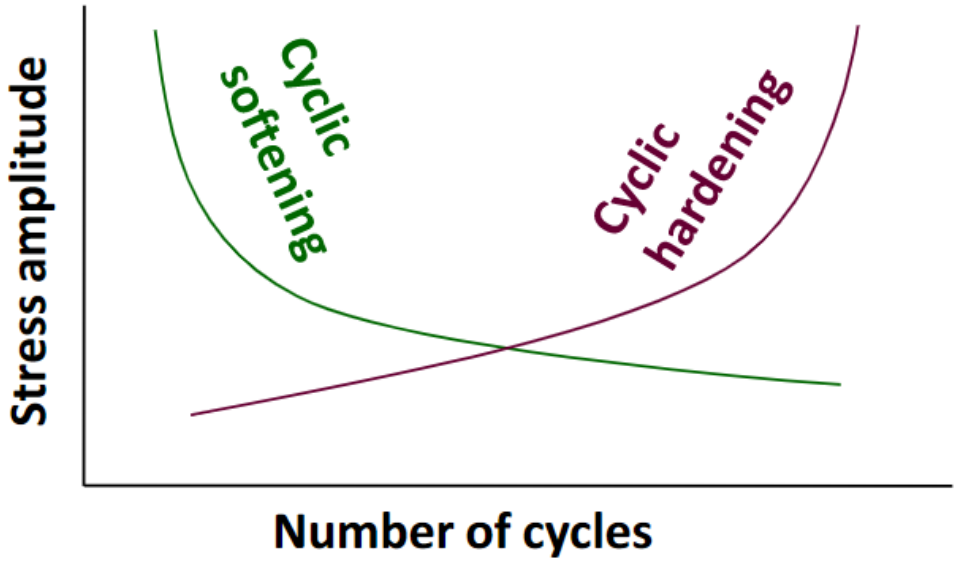


Figure 2.13: Representation of the mutual competition between cyclic hardening and cyclic softening.

## 2.5 Influence of aging on the low fatigue properties of Al-Mg-Si alloys

The structural changes of aged aluminium alloys during fatigue rely on many factors like temperature of cyclic straining, strain rate, plastic strain amplitude and the initial microstructure. Many studies indicate that cyclic response of age hardenable aluminium alloys differs widely with the state of aging (under-aged, peak-aged, or over-aged conditions).Sekhar, Nandy and Das [17] have studied the influence of aging on low cycle fatigue behavior for AA6063 alloys which belongs to the AA-6XXX series. The low cycle fatigue behavior has been studied together with exanimated micro-mechanism during the cyclic deformation of this alloy in the under-aged, peak-aged and over-aged conditions of aging. This research has investigated that the condition of aging has deep effects on the cyclic deformation behavior of Al-Mg-Si alloys.

The cyclic hardening and cyclic softening behaviors are associated with the dislocation-dislocation and dislocation-particle interactions which is determined by the microstructure and the plastic strain amplitude. Analysis of the hysteresis loop reveals that Peak-aged and over-aged alloys exhibit initial hardening followed by progressive softening to failure. While the under-aged alloys show continuous cyclic hardening for strain amplitude higher than 0.4% and cyclic hardening followed by saturation for strain amplitude lesser than 0.4%. Therefore, the hardening rate of the under-aged state is higher than peak-aged and over-

aged states. Regardless of the strain amplitudes, the under-aged state shows Masing behavior due to dislocation-dislocation interactions, the peak-aged state shows non-Masin behavior due to dislocation-precipitate interactions, and the over-aged state shows variation between Masing and non-Masing behavior and this referred to near-Masing behavior. Analysis of the Masing behavior is illustrated in figure 2.14 for under-aged, peak-aged and over-aged conditions [17].

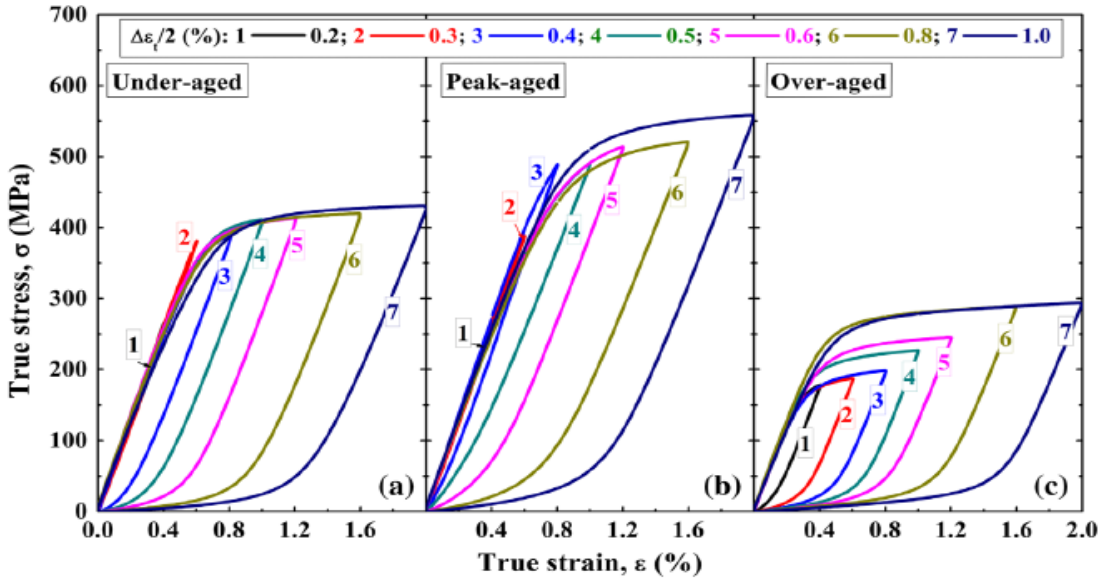


Figure 2.14: Stress-strain curves represent the Masing behavior for alloys under under-aged, peak-aged and over-aged states.

# 3. Experimental work

## 3.1 Delivered materials

The examined materials were Al-Mg-Si alloys which are AA6082 as-extruded and AA6010 as-rolled. The shape of the samples is illustrated in figure 3.1. Both AA6082 and AA6010 have the same dimensions. The samples were made in this form to fit the pressing tool which was used during experimental procedures.

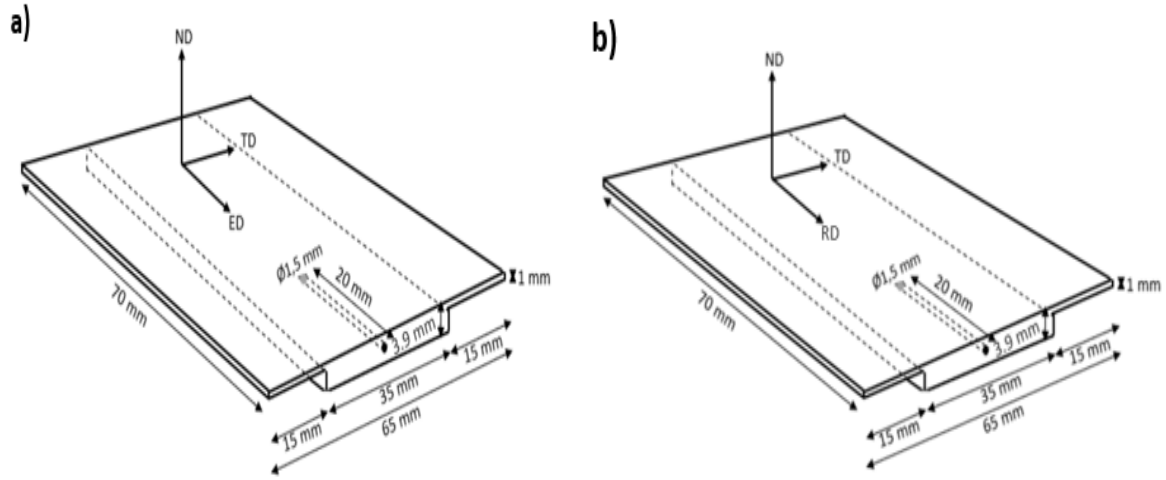


Figures 3.1: Shows the dimensions of the samples as-received: a) extruded samples AA6082, b) rolled samples AA6010. Together with drawing shows the directions of the extrusion for AA6082, and rolling for AA6010.

Figure 3.2 shows the terminology used to address the planes and directions in this study. The extruded profile for AA6082 and the rolled profile for AA6010.

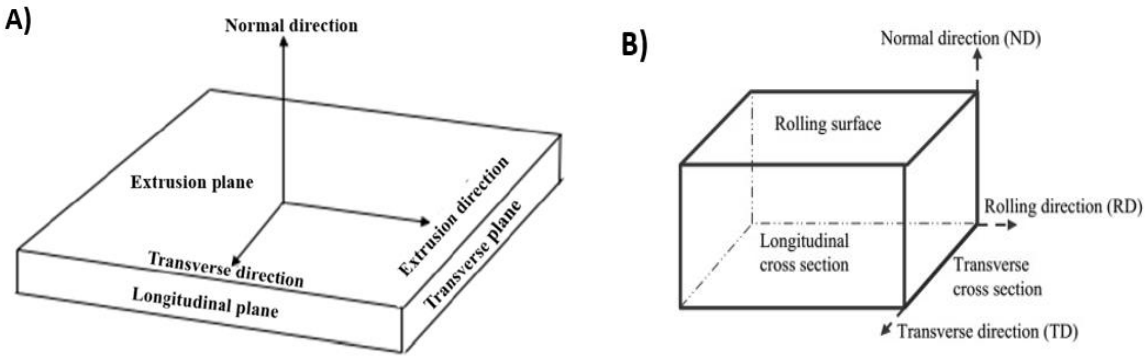


Figure 3.14: Terminology used to address the planes and direction. A) extruded profile AA6082, and B) rolled profile for AA6010.

## 3.2 Hardening curves

Hardening curves have been conducted for both AA6082 and AA6010. The aim of the hardening curves was to examine how the hardness changes with the aging, and to determine under-aged, peak-aged, and over-aged states. Those three different aging states will be used to age the specimens to do the mechanical tests.

For AA6082, one sample was conducted to solution heat treatment for 15 min in a salt bath at 545 °C. This step was followed by quenching in water to room temperature. Then the sample was storage for 30 min after quenching from solution heat treatment. Then, artificial aging was conducted in an oil bath at 185 °C for 24 hours and the hardness measurements were taken many times at different periods. The artificial aging was followed by quenching in water to room temperature. These steps are illustrated in figure 3.3.

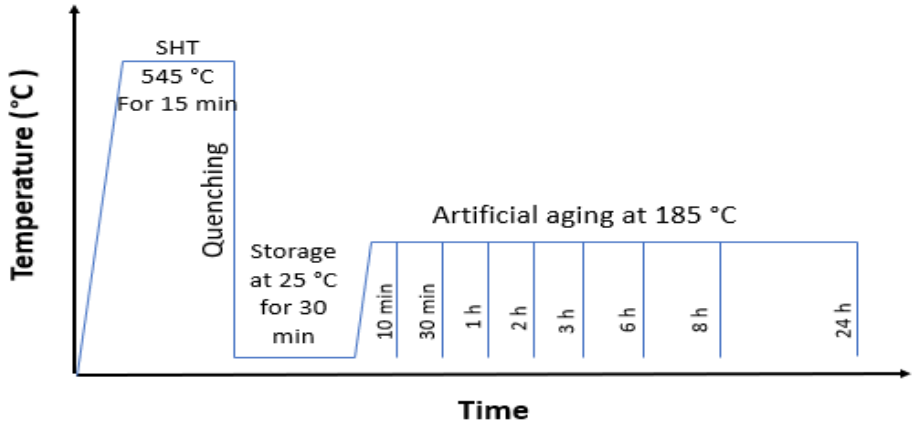


Figure 3.3: Illustration of heat treatment sequence for an AA6082 sample to get the artificial aging curve at 185 °C.

For AA6010, three different specimens were conducted to solution heat treatment for 15 min in a salt bath at 560 °C, followed by quenching in water to room temperature. The specimens were storage for 30 min after quenching from solution heat treatment.

Then, the specimens were conducted to artificial aging up to 48 hours. The first specimen was conducted to artificial aging in the oil bath at 165 °C, the second specimen at 185 °C and the last specimen at 200 °C. The artificially aging was followed by quenching in water after each step of artificial aging. Figure 3.4 illustrates how the artificial aging has been done for AA6010 specimens.

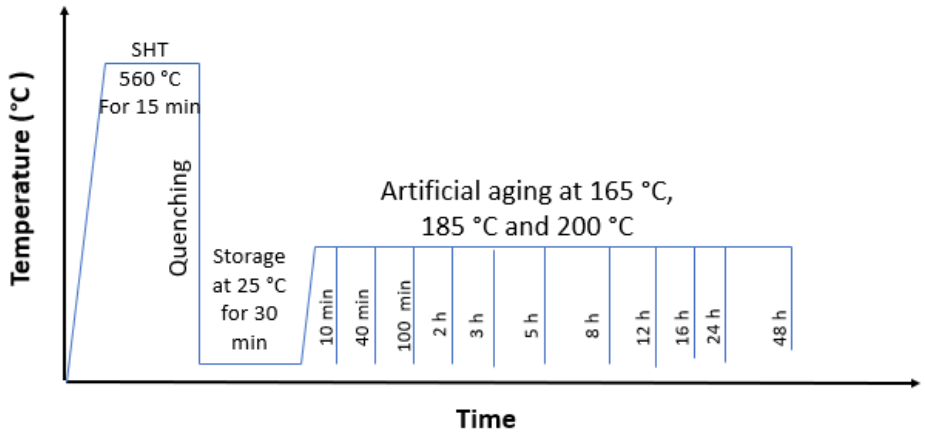


Figure 3.4: Illustration of heat treatment sequence for three different AA6010 samples to get artificial aging curves at 165 °C, 185 °C and 200 °C.

## 3.3 Heat treatment procedure

The heat treatment sequence in this study includes three main stages. Solution heat treatment, integrated hot forming and in-die quenching, and artificial aging.

### 3.3.1 Solution heat treatment

Solution heat treatment was done by a Naberterm N15 air circulation furnace. The samples were heated to elevated temperatures in order to bring the particles into the alloys (Mg-Si particles) to the solid solution, and to make the sample more amenable for deformation process.

The setting of the temperature in the furnace was 545 °C for AA6082 samples and 565 °C for AA6010 samples. Each sample was held in the furnace for 30 minutes.

### 3.3.2 New recipe to multiply the productivity during solution heat treatment

During resolution heat treatment for AA6082 and AA6010 samples, each sample should remain 30 minutes in the furnace. That means using a lot of time for each test. Therefore, a new recipe was investigated to reduce the period for resolution heat treatment. The recipe was putting two samples in the furnace at the same time, thus the first sample should been put in the furnace, and after 15 minutes, the door will be opened and the second sample will be held in the furnace, and after 15 minutes, the door will be opened again, and the first sample will be taken out in order to perform the pressing. During the pressing the door of the furnace was kept

open for around 30 seconds. Then, the next sample (the third one) will be held in the furnace (instead of the first one which is out now), and the door closed again, and so on. That means during doing the resolution heat treatment for each sample, the door will be opened every 15 minutes, and staying open for around 30 seconds (in order to take the sample and do the pressing, and after that putting another sample and closing the door). The influence of interrupting the heating (reducing heating) because of the opening of the door was investigated by measuring the temperature of two samples. Those two samples where conducted to solution heat treatment in the furnace for 30 minutes and this heating was interrupted by opening the door after 15 minutes for 30 seconds. These two samples where compared to another sample which conducted to the heating in the furnace for 30 minutes without opening the door (normal heating without interruption). Solution heat treatment was followed by quenching in water to room temperature. Then, the artificial aging was done in an oil bath at 185 °C. The procedure was done for both AA6082 and AA6010.The hardness measurements were taken for all the samples in order to distinguish the mechanical properties for the samples which had been conducted to interrupted heating by opening the door and the sample which conducted normal heating without interrupting(samples as reference). Hardness measurements are presented in figure3.5 for AA6082 and figure 3.6 for AA6010. The results show that the influence of the interrupted heating on the hardness measurements is very small.

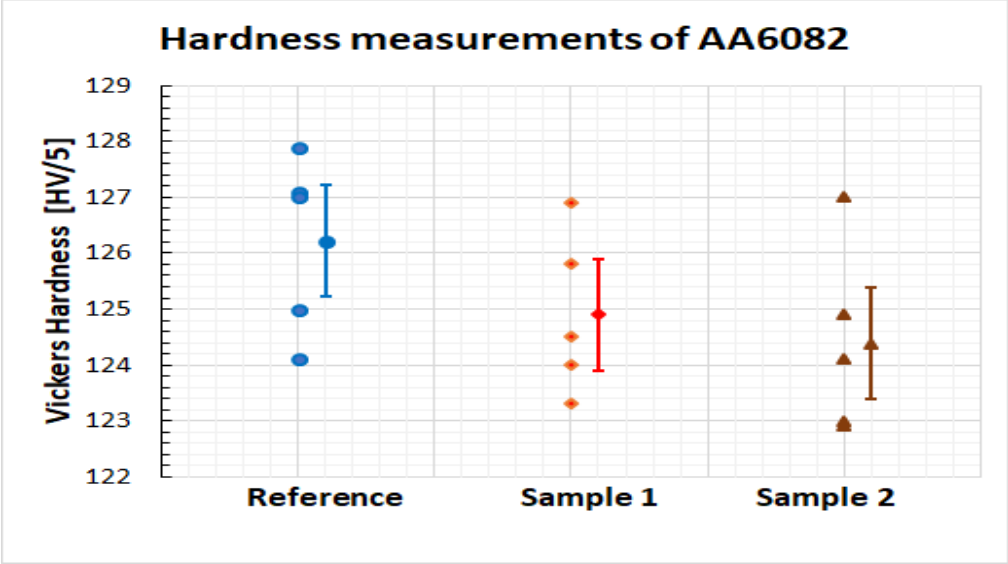


**Figure 3.5:** Hardness measurements for AA6082, for the reference sample which been heat treated normally and the two other samples which were conducted to heat interrupting during solution heat treatment. Together with the average and standard deviation.

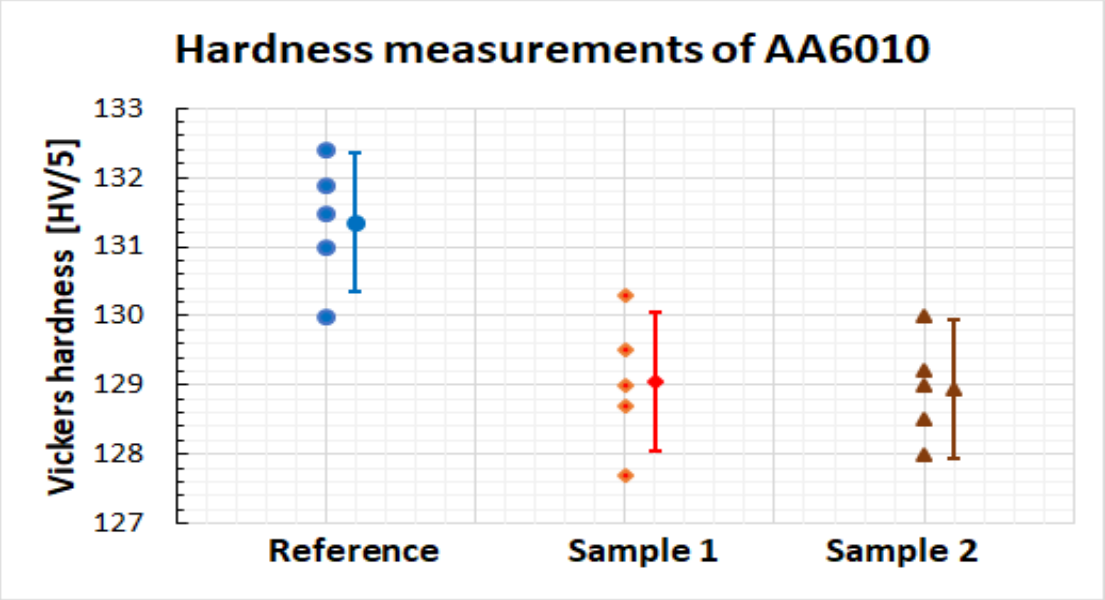


**Figure 3.6:** Hardness measurements for AA6010, for the reference sample which been heat treated normally and the two other samples which were conducted to heat interrupting during solution heat treatment. Together with the average and standard deviation.

For AA6082, the average of hardness measurements for the reference sample is almost 2 units higher (2 HV) than the average for the other two sample that had been subjected to interrupting heating. For AA6010, the average of hardness measurements for the reference sample is almost 1 unit (1 HV) higher than the average for the other two sample that been subjected to interrupting heating.

Furthermore, temperature measurements show that during the 30 seconds with the door opened, the sample lose up to 50 °C, and the spent time to compensate this losing in temperature is almost 2 minutes. Figures 3.7 and figure 3.8 show the temperature curves during these procedures for both AA6082 and AA6010, respectively.

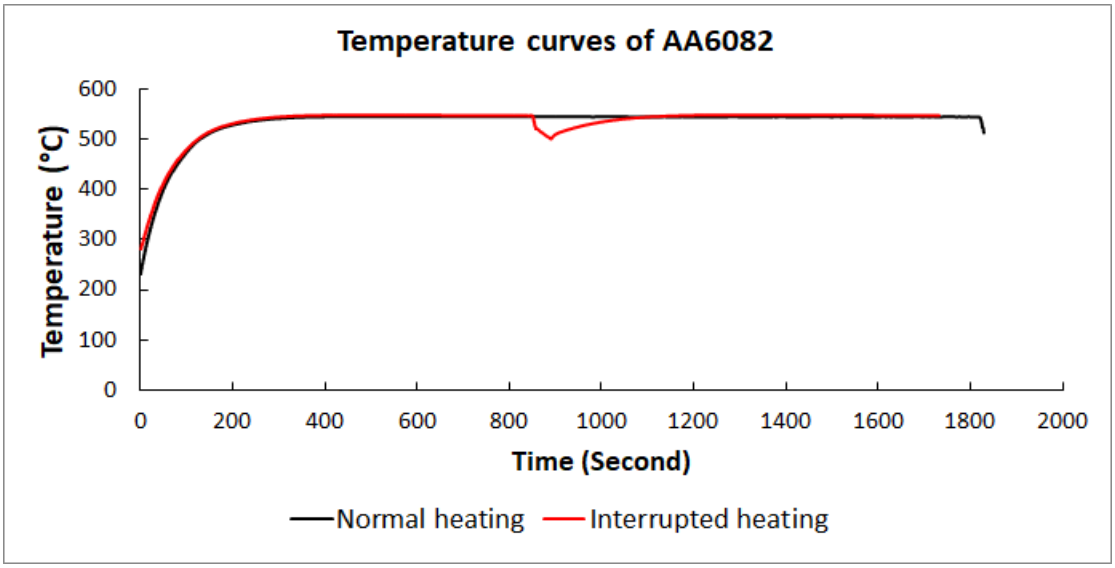


Figure 3.7: Temperature curves for two AA6082 samples, show how the temperature differs between the interrupted and normal heating.

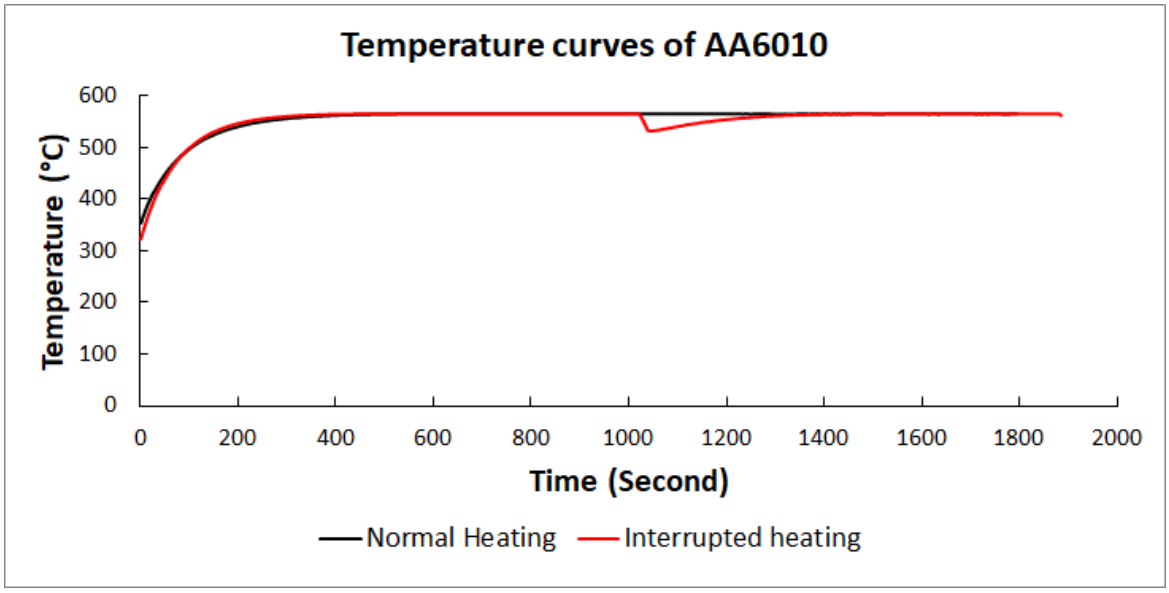


Figure 3.8: Temperature curves for two AA6010 samples, show how the temperature differs between the interrupted and normal heating.

Therefore, the procedures of putting two samples at the same time was very safe and a good way to save half of the time. Hence, this recipe was used in this experiment work.

### 3.3.3 Hot forming and in-die quenching

After solution heat treatment, each sample was carried to integrated hot forming and in-die quenching at the same time by a pressing tool. The used pressing tool was conducted

to a MTS 311-1000 KN hydraulic driven press. The safety limit of the pressing tool is 650 KN. The desired deformation of the samples was 20%. Each sample was moved from the furnace to the pressing tool by a plier. The set of the pressing tool consists of two dies. The lower die is constant while the upper die can move up and down. The dies were built with water channels. Water channels were connected to the upper and lower dies and water goes in from one side and let out from the other side to achieve the quenching to the pressing dies during the pressing process. Cooling process by water channels was done before each pressing test for around three minutes. The lower die was provided by four spikes which stand on springers. Each sample was moved from the furnace to the pressing tool, was put on these four spikes. Then the pressing test starts. The aim of the spikes is to prevent the temperature loos between the sample and the lower die before pressing process. During the process of the pressing, the upper die goes down and press the sample and the spikes go into the lower die. And after pressing the higher die goes up and the spikes go up and held the sample over the low die again, which reduce the temperature missing also when the temperature of the sample is too high. The shape of the pressing tool is presented in figure 3.9.

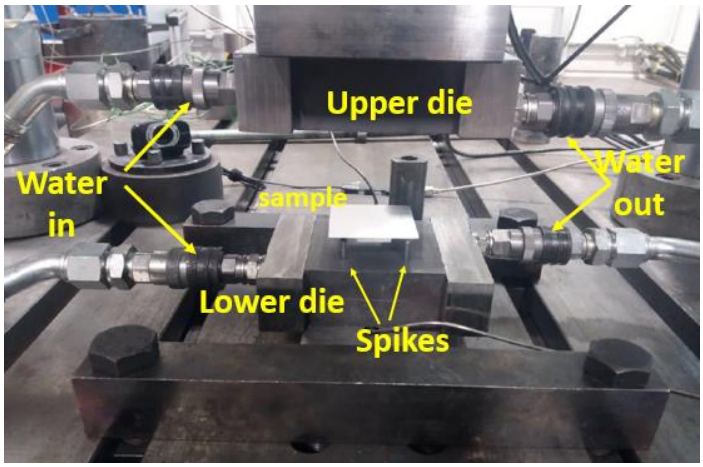


Figure 3.9: The components of the used pressing tool.

To reduce the friction between the sample and the dies, Molykote G-Rapid Plus which is a mineral oil were spread on the dies before the pressing process.

### 3.3.4 Cooling curves for AA6082 and AA6010

The samples were attached to a thermo logger by a thermo element. The thermo element were attached to the datalogger by a thermoelement, the two ends of the thermoelement from the other side had been welded and fixed in the sample by bunching into the hole which has been made already in the samples. The data logger that was used is a Data Taker DT80 and was taken10 measurements per second.

Figures 3.10 and 3.11 show the cooling curves during pressing one sample of AA6082, and one sample of AA6010, respectively.

For AA6082 sample, the furnace setting temperature was 545 °C, the starting temperature for the sample was 540 °C, the used time to move the sample from the furnace to the pressing tool was 6 seconds. In these 6 seconds the temperature dropped from 540 °C to 497 °C. Then, forming/ contact starting at 11,5 second, and at time 12,9 the temperature is dropped below 100 °C. The holding time was 20 seconds. After 15 seconds of the holding time, the temperature was around 30 °C.

Cooling rates from 497 °C to 79,9: (496,7-79,9)/(13,2-11,5) = 245,2 K/s

From 79 to 44 $^{0}$C: (77-44)/(16,3-13,2) = 10,6 K/s

The maximum force is 538 KN.

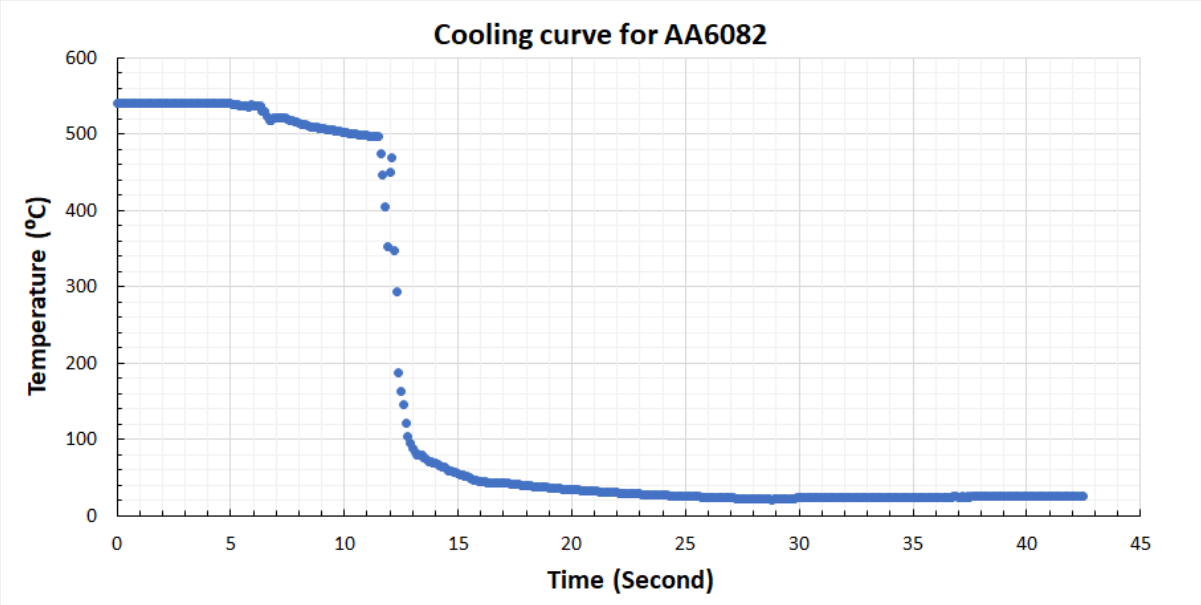


Figure 3.10: Cooling curve for one AA6082 sample during the pressing.

For the AA6010 sample, the furnace setting temperature was 565 °C, the starting temperature of the sample was 563 °C. Moving the sample from the furnace to the pressing tool took around 6 seconds and the loosed temperature in the air was from 563 °C to 539 °C. Then, forming started at time 8,9 second. At time 11,2 second the temperature is dropped below 100 °C. At 20 second, the temperature was 48 °C.

The cooling rate from 516 °C to 79,89 °C: (516-97,89)/(11,2-9) = 190,05 K/s

The cooling rate from 79 °C to 44 °C: (80,8-43,7)/(27,6-12,3) = 2,4 K/s

The maximum force is 548,9 KN.

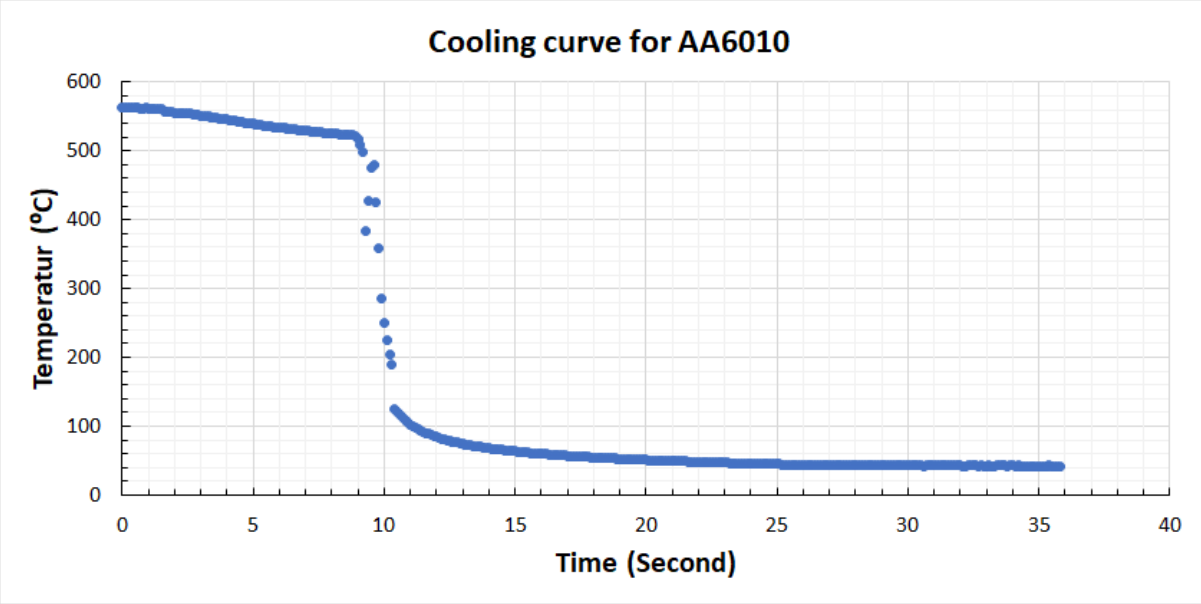


Figure 3.11: Cooling curve for one AA6010 sample during the pressing.

### 3.3.5 Artificial aging

Each sample was conducted to the artificial aging after the integrated hot forming and in-die quenching procedures. During the artificial aging, samples was split to three groups. The first group was aged to the under-aged state, the second group was aged to the peak-aged state, and the last group was aged to the over-aged state. These three different states of aging were determined by the hardening curves for both AA6082 and AA6010.

Table 3.1 shows the values of the required time to obtain the under-aged, peak-aged and over-aged states taken from the previous figures. These values were used for the artificial aging after the quenching and deformation by the pressing tool. These values were taken from the hardening curves which is presented in chapter 4 ¨Results¨

| | Under-aged | Peak-aged | Over-aged |
|---|---|---|---|
| AA6082 | At 40 min | At 3 hours | At 8 hours |
| AA6010 | At 2 hours | At 5 hours | At 20 hours |

Table 3.1: The determined periods to obtain under-aged, peak-aged and over-aged condition for AA6082 and AA6010.

Figure 3.12 shows the equipment which was used during the heat treatment sequence.

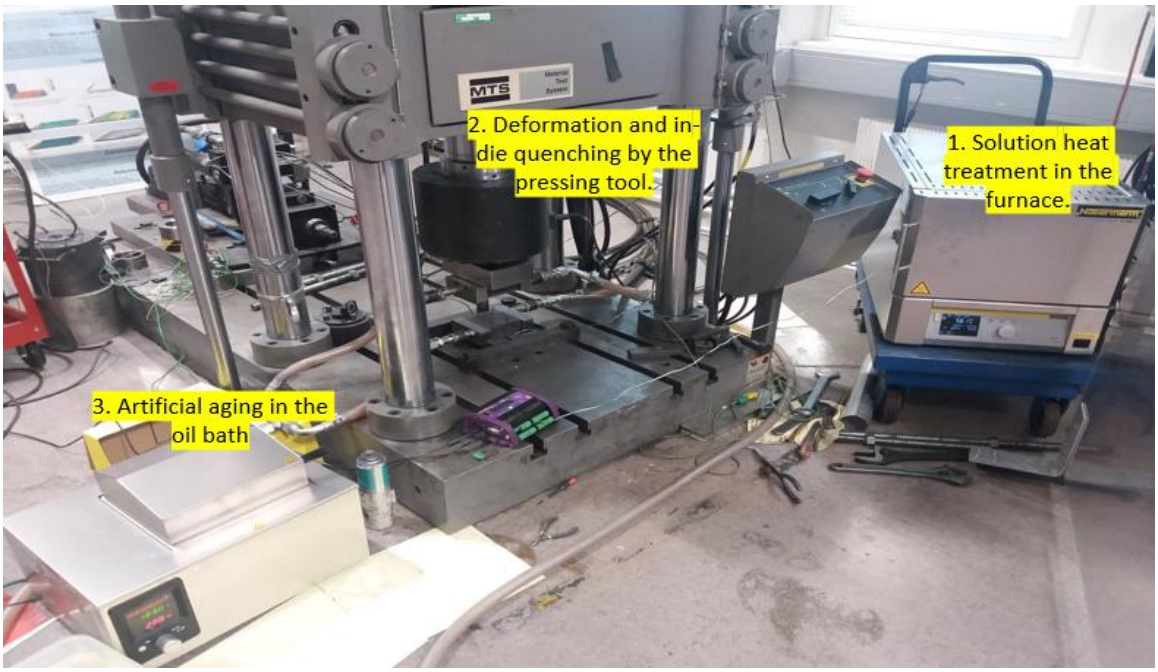


Figure 3.12: The air circulation furnace, the pressing tool, and the oil bath that were used during heat treatment.

## 3.4 Mechanical tests

### 3.4.1 Tensile tests

Tensile tests were performed with (three or four) parallels for each treatment. The geometry of the tensile specimens is illustrated in the figure 3.13. The same geometry was used also for the fatigue test specimens. The thickness of the specimens was obtained during the pressing process. Therefore, there is slight variation in the thickness from specimen to another specimen.

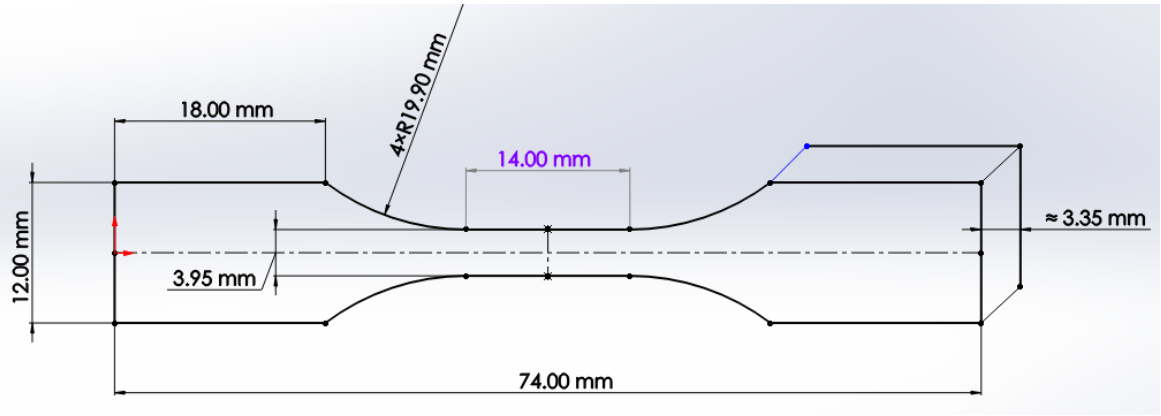


Figure 3.13: Dimension of tensile specimens.

Figure 3.14 shows how tensile and fatigue specimens were obtained from the extruded AA6082 and rolled AA6010 samples as-received.

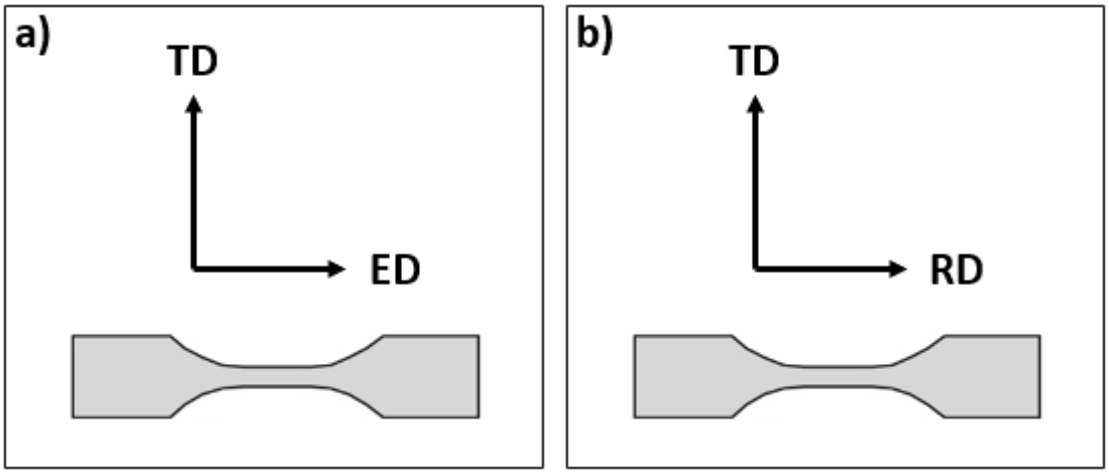


Figure 3.14: How fatigue and tensile specimens where obtained out from the extruded samples AA6082 (a) and the rolled samples AA6010 (b).

### 3.4.2 Hardness measurements on the tensile bars

In order to get better understanding of the previous tensile test results, hardness measurements were taken on the same tensile bars which were tested. An Innovatest Vickers test was used to measure the hardness of the samples. Five measurements were taken per each sample, the red circle in figure 3.15 shows the area where the hardness measurements were taken. The load that was applied during hardness measurements was 10 kg with 10 seconds loading time.

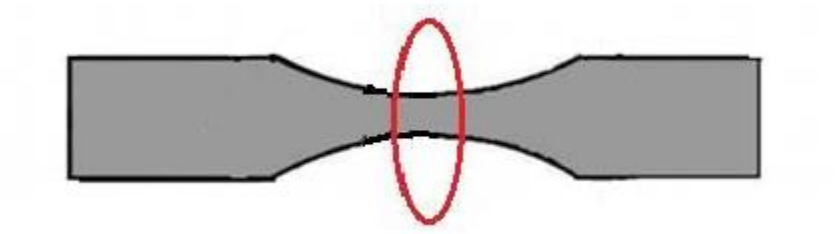

Figure 3.15: Area where the hardness measurements were taken.

### 3.4.3 Percentage reduction of area (Z)

Tensile tests bars were examined again in order to calculate the percentage reduction of area. The percentage reduction of area Z is the maximum change of cross-sectional area, which occurred during the tensile test, expressed as a percentage of the original cross-sectional area.

Z= So-Su/So [%]

So is the original cross-sectional area before testing [$m^2$]

Su is the minimum cross-sectional area after fracture [$m^2$]

The minimum cross-sectional area was measured by using a stereoscope to calculate the percentage reduction of area (Z).

### 3.4.4 Fatigue tests

The low fatigue tests were the main focus in this study. Tensile tests were done prior to the fatigue tests. Fatigue testing was done in a MTS-810 KN servo hydraulic universal testing machine. Eleven tests were done for each treatment. The tests were stress controlled because the samples were very small, and it was very difficult to fix the extensometer on the gauge length.

The tests run at different stress levels. Loading levels were 80% of Rp0.2, 70% of Rp0.2, and 50% of Rp0.2.

During the tests: The strain ratio $R= \sigma_{max}/\sigma_{min}= -1$, $\sigma_a= \sigma_{max}$.

The applied force was in KN, Force= $\sigma_a \times$ Area; Area (thickness × width)

Frequency: $f = 10$ Hz

The geometry of the fatigue specimens is the same of the geometry of the tensile test specimens which was illustrated in figure 3.13. Each sample was grinded by hand with a 1200 SiC papers. This was done to reduce the surface roughness and residual stresses

from machining. The setup of the low cycle fatigue tests is illustrated in figure 3.16.


Figure 3.16: The setup of the fatigue test.

## 3.5 Metallography

### 3.5.1 Microstructure characterization

The grain structure has been characterized for some samples after solution heat treatment, integrated hot forming and in-die quenching, and artificial aging. Transverse plane and longitudinal plane were studied by optical microscopy. Sample preparation included grinding to 2.4 μm with SiC grinding papers and polishing with diamond suspension to 1 μm. Then, anodizing has been done in order to form an oxide layer on the surface to change the reflections of different grains under the polarized light.

To get a better view about how the grains were deformed after integrated hot forming and in-die quenching. The grain structure analysis has been done for some samples after deformation and solution heat treatment, for both AA6082 and AA6010.

The grain structure analysis was done by using electron backscatter analysis EBSD with the LVFESEM Zeiss Ultra 55 VP. For both alloys AA6082 and AA6010, analysis was carried out in the longitudinal and the transverse plans. Samples were prepared to EBSD analysis by

grinding manually up to 2.4 µm by SiC papers. Then, specimens were polished up to 1 µm. Finally, the samples were conducted to the vibration polishing.

### 3.5.2 Fractography

Secondary electron microscopy (SEM) was used to do fractography investigation. The fractography investigation was done for some samples to underline the fatigue properties and to assure that the failure fracture caused due to fatigue and not a random fracture. Fractography analysis was done by LVFESEM Zeiss Supra 55 VP. Before the investigation, samples were held in an ultrasound bath for 3 minutes to clean the specimens and remove any organic material.

# 4. Results

## 4.1 Artificial aging curves

Hardening curves of AA6082 and AA6010 are given in figure 4.1 and figure 4.2, respectively.

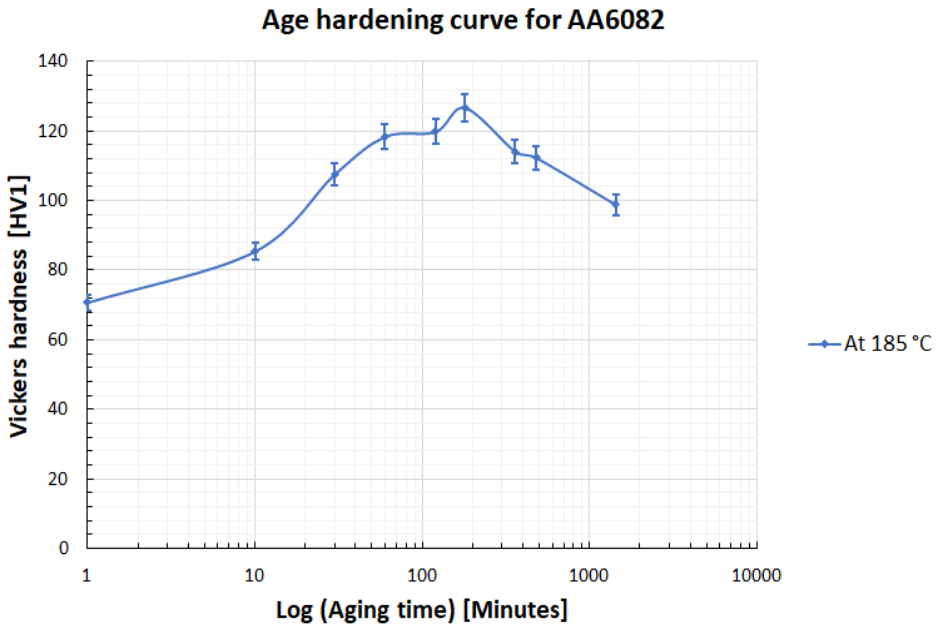


Figure 4.1: Artificial aging response at 185 °C for AA6082.

For AA6010 alloy, three different hardening curves have been done at three different temperatures at 165 °C, 185 °C, and 200 °C. The shortest time to reach the peak-hardness was 5 hours at 185 °C.


Figure 4.2: Artificial aging response for AA6082 samples at 165 °C, 185 °C and 200 °C.

In order to determine the under-aged, peak-aged and over-aged points, a proportional line was made below around 10% from the peak-aged point. Those points are illustrated in figure 4.3 and figure 4.4 for both AA6082 and AA6010, respectively.

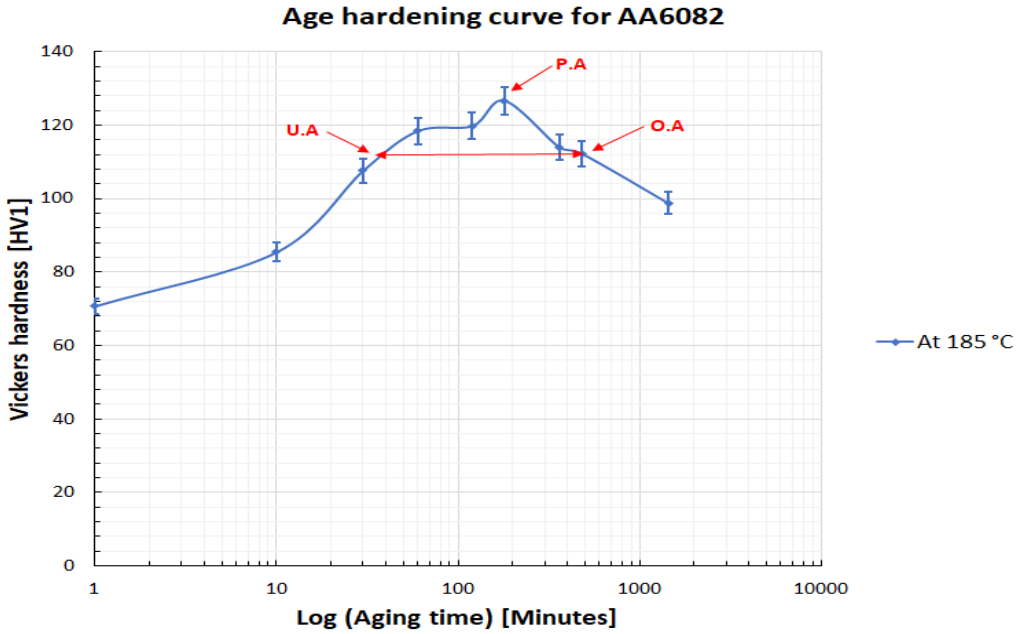


Figure 4.3: Determined points for under-aged, peak-aged and over-aged conditions for AA6082.

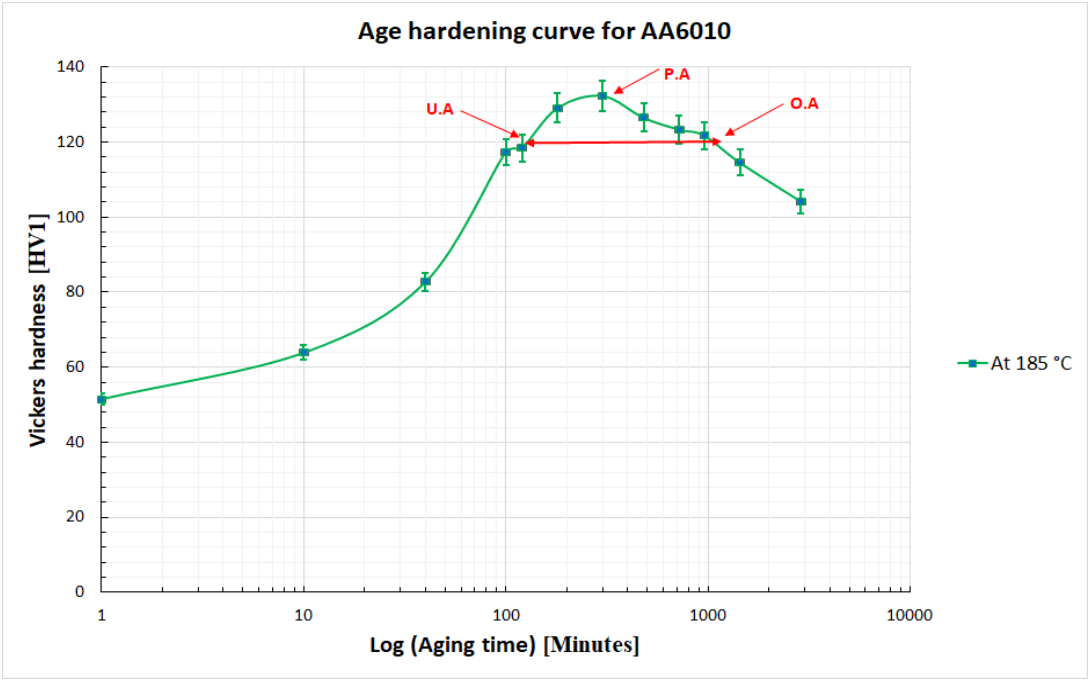


Figure 4.4: The determined points for under-aged, peak-aged and over-aged conditions for AA6010.

## 4.2 Tensile behavior

Results from tensile tests for AA6082 specimens are presented in figure 4.5 for under-aged condition, peak-aged condition and over-aged condition.

Note: The extensometer that was used during the tensile tests couldn't cover all the gage length of the specimens. Thus, in some specimens the fracture occuered in the area that hasnot been covered by the extensometer.

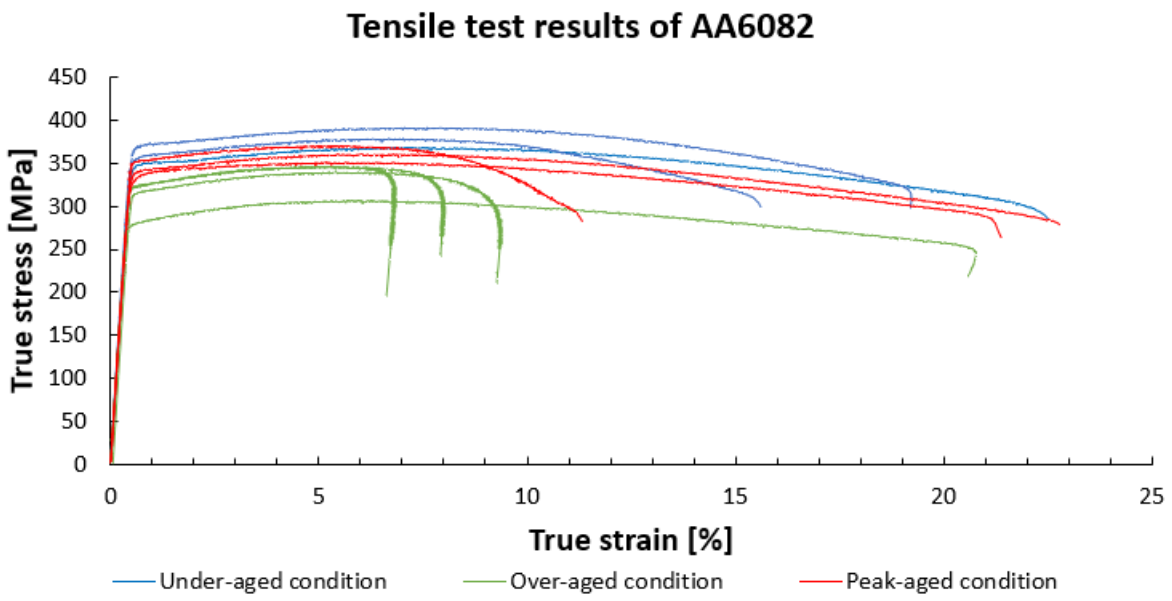


Figure 4.5: Stress-strain curves for AA6082 specimens at under-aged, peak-aged, and over-aged states.

The lowest yield strength and tensile strength values of AA6082 were at over-aged condition. While the average tensile strength and yield strength at the under-aged condition are slightly higher than the average tensile strength and yield strength at the peak-aged condition. That means that the peak-aged value of the hardness which was obtained from the hardening curve for AA6082 (peak hardness at 3 hours) has been changed during in the practice for the other samples.

Results from tensile tests for AA6010 samples are presented in figure 4.6 for under-aged condition, peak-aged condition and over-aged condition.

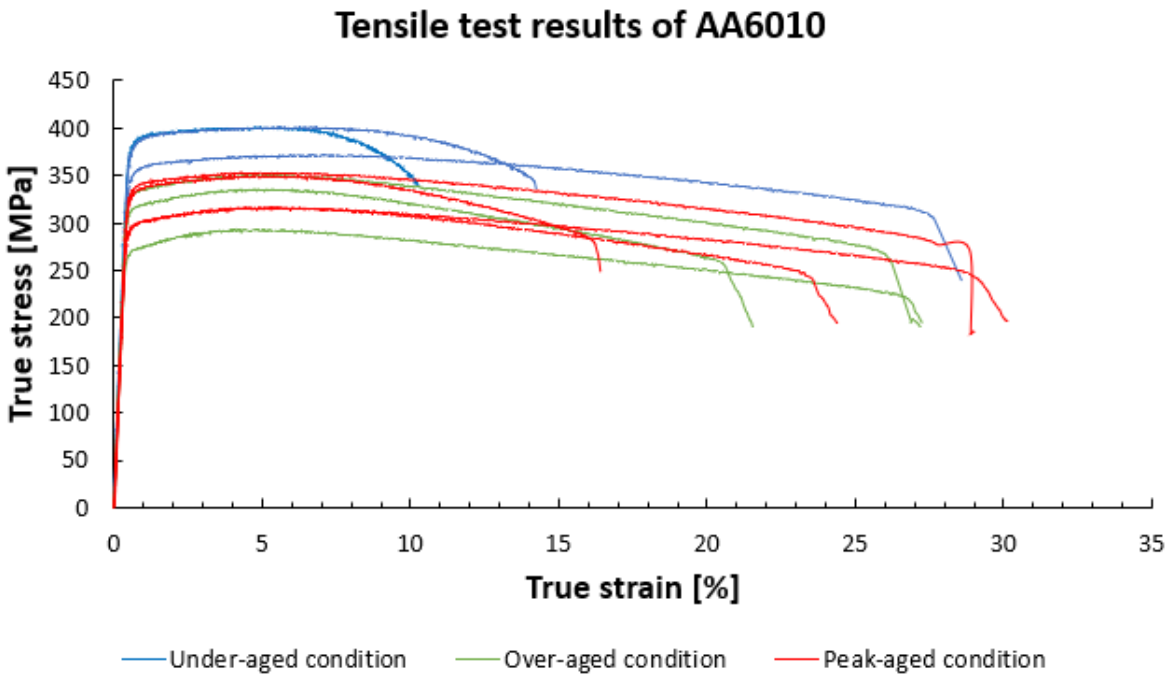


Figure 4.6: Stress-strain curves for AA6010 specimens at under-aged, peak-aged, and over-aged states.

For AA6010, the highest tensile strength and yield strength were obtained at the under-aged condition. While the lowest tensile strength and yield strength values were at the over-aged condition.

Tensile results show that the yield strength of the samples that have been aged to the peak hardness is lower than the yield strength for the samples that have been aged to the under-aged state. Samples that have been aged to the over-aged state have the lowest yield strength. These results do not match with the hardening curves for AA6082 and AA6010 for the samples which have been aged to the peak-aged and under-aged conditions. However, the yield strength for AA6082 and AA6010 samples match better with the aging curves for the over-aged conditions.

## 4.3 Hardness measurements

Hardness measurements had been taken on the same tensile bars that have been conducted to the tensile tests. The results are illustrated in figure 4.7 and figure 4.8 for both AA6082 and AA6010, respectively.

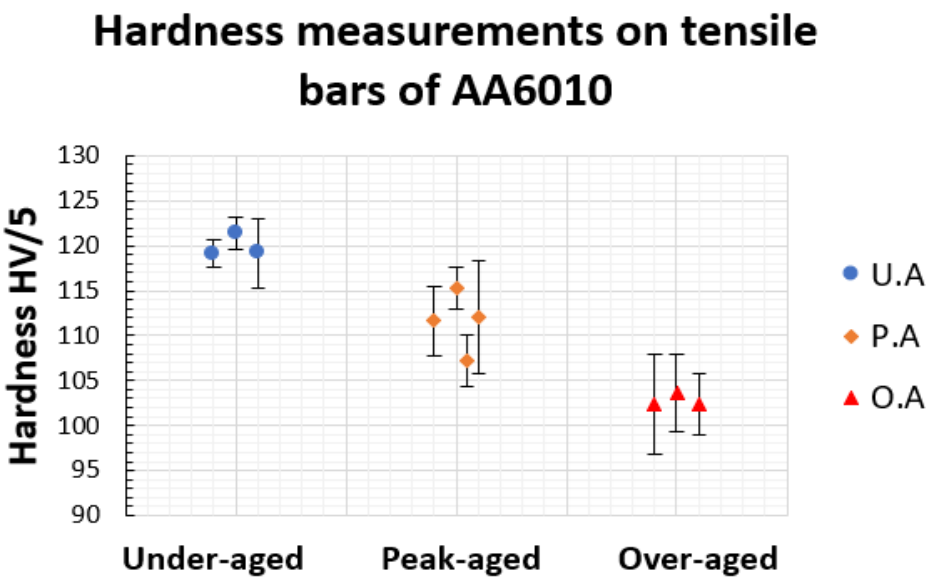


Figure 4.7: Hardness measurements on AA6082 tensile test bars that have been artificial aged to under-aged conditions (40 min), peak-aged condition (3 hours) and over aged condition (8hours).

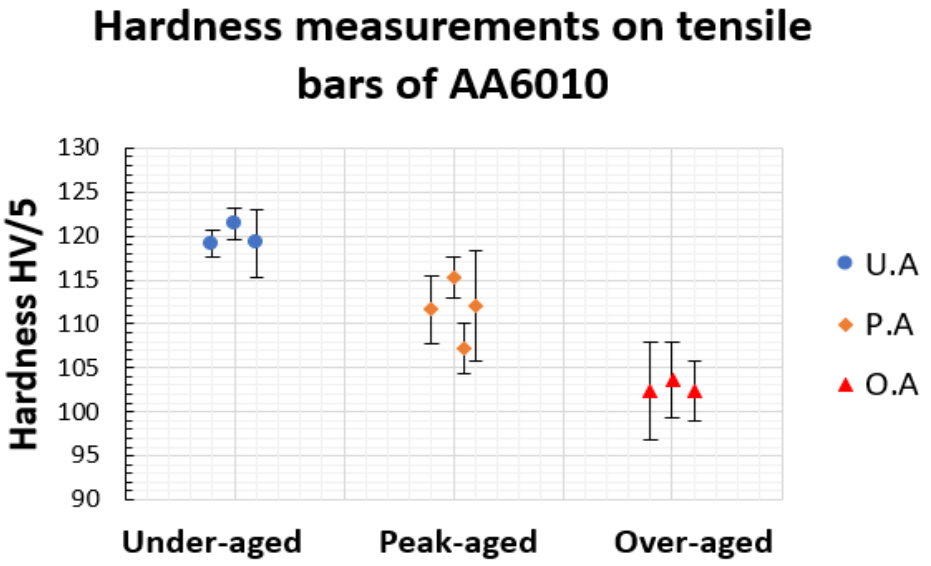


Figure 4.8: Hardness measurements on AA6010 tensile test bars that have been artificial aged to under-aged conditions (2 hours), peak-aged condition (5 hours), and over aged condition (20 hours).

Hardness measurements are proportional (match) with tensile tests measurements. Samples which have been aged to the under-aged points have higher hardness than samples which have been aged to the peak-hardness. Samples which have been aged to the over-aged point (40 minutes for AA6082 and 2 hours for AA6010) have lowest hardness and yield strength. From

the hardness measurements it appears that the samples that have the higher tensile strength have the higher hardness measurements.

## 4.4 Percentage reduction of area (Z) for tensile test bars

The images of the fracture of the tensile test bars were taken by the stereoscope.

Percentage reduction of area was calculated to compare between the percentage of reduction area and the yield strength values which have been obtained from the same tensile specimens. The reason of this comparison is that the results of tensile test at the under-aged condition do not match with the hardening curves. Because the average of the yield strength at the peak-aged state are lower than the average of the yield strength at the over-aged state.Figure 4.9 and figure 4.10 show the results of percentage of reduction area at the three different aging states for AA6082 and AA601, respectively.

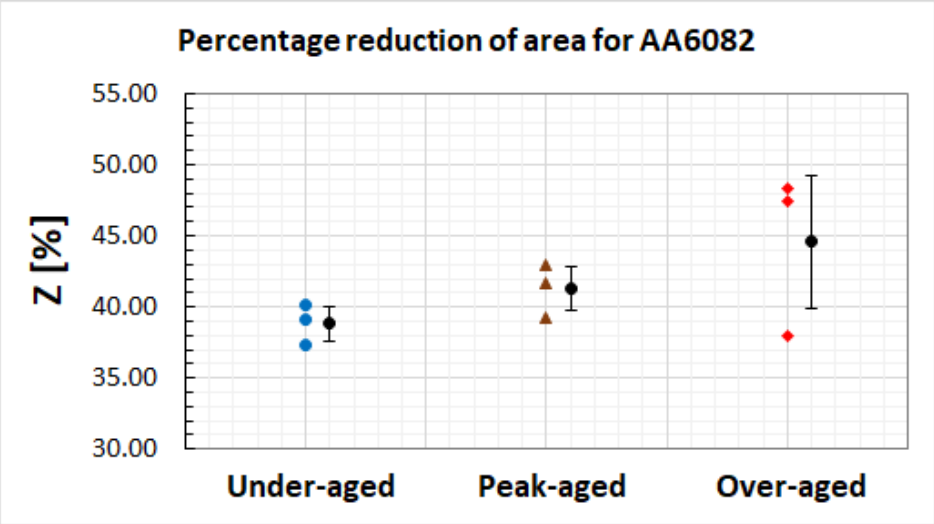


Figure 4.9: The percentage reduction of area Z [%] for the tensile test bars at the three aging states for AA6082. Together with the average and standard deviation.

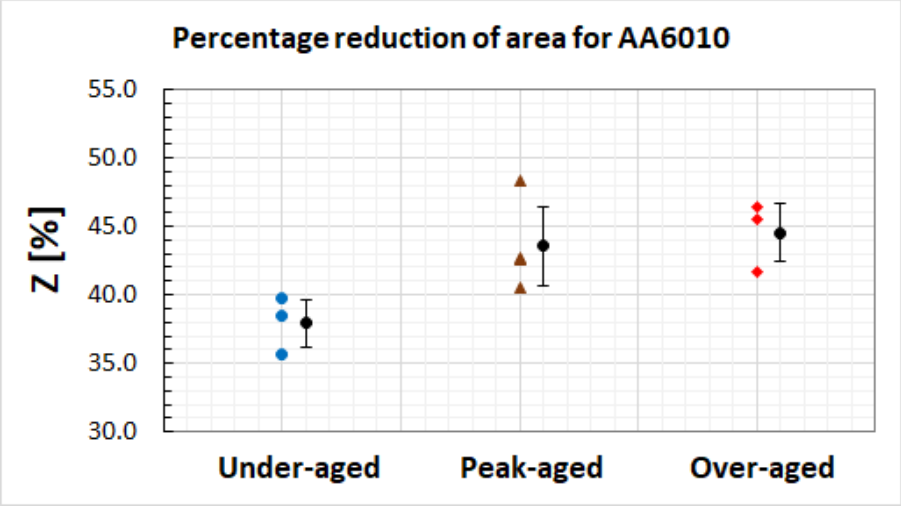


Figure 4.10: The percentage reduction of area Z [%] for the tensile test bars at the three aging states for AA6010. Together with the average and standard deviation.

Results show that at the Under-aged condition the percentage reduction of area is the lowest, and at the over-aged condition the percentage reduction of area is the highest. It means that specimens that have the higher yield strength have the lowest percentage reduction of area, which seems logical.

## 4.5 Low cycle fatigue behavior

Fatigue tests results are presented in S-N curves, the stress amplitude versus number of cycles to failure. Figure 4.11 shows the results of AA6082 samples for under-aged condition, peak-aged condition and over-aged conditions.

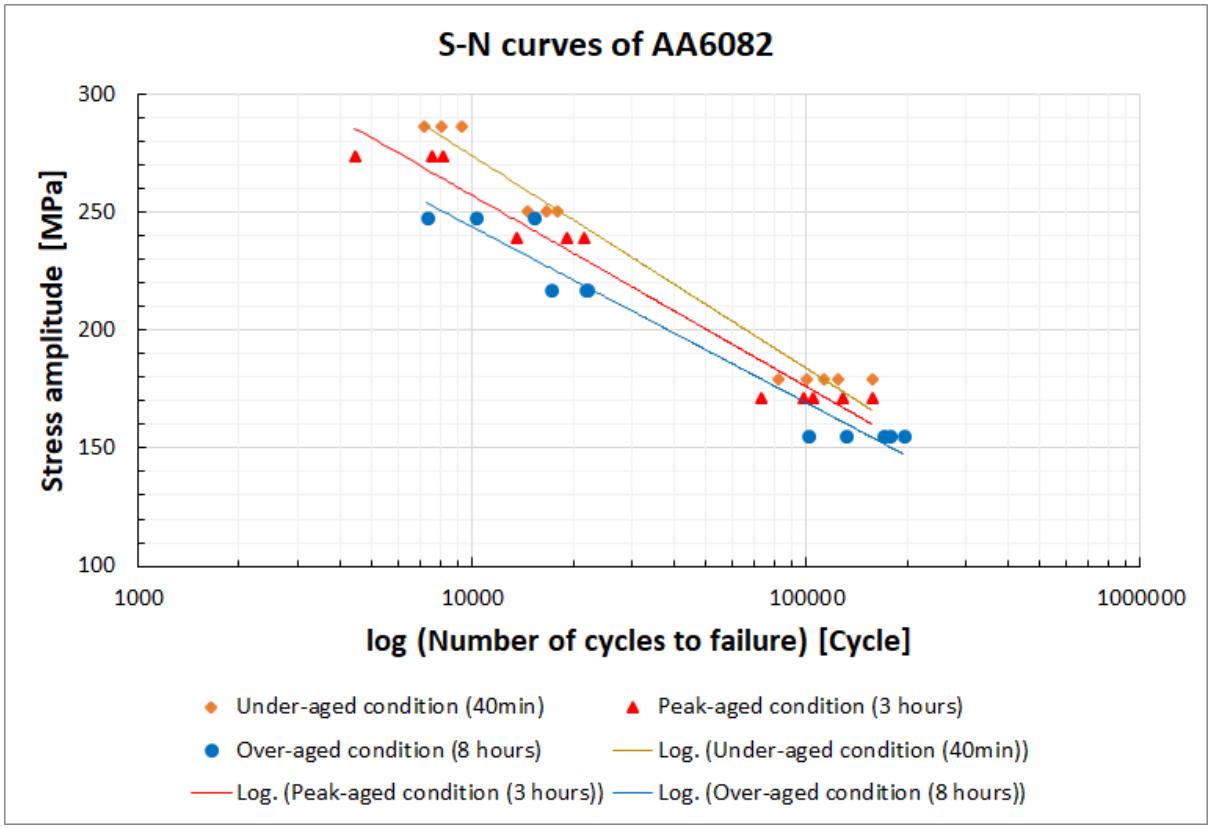


Figure 4.11: Stress amplitude versus number of cycles to failure for AA6082 samples at under-aged, peak-aged and over-aged conditions.

For AA6082, the longest fatigue life has been obtained for the specimens which have been conducted to the over-aged condition. This result was expected because AA6082 specimens at the over-aged condition had the lowest tensile strength compared to the other samples which have been aged to the under-aged and to the peak-aged conditions. Figure 4.12 shows the results of AA6010 samples for under-aged condition, peak-aged condition and over-aged condition, respectively.

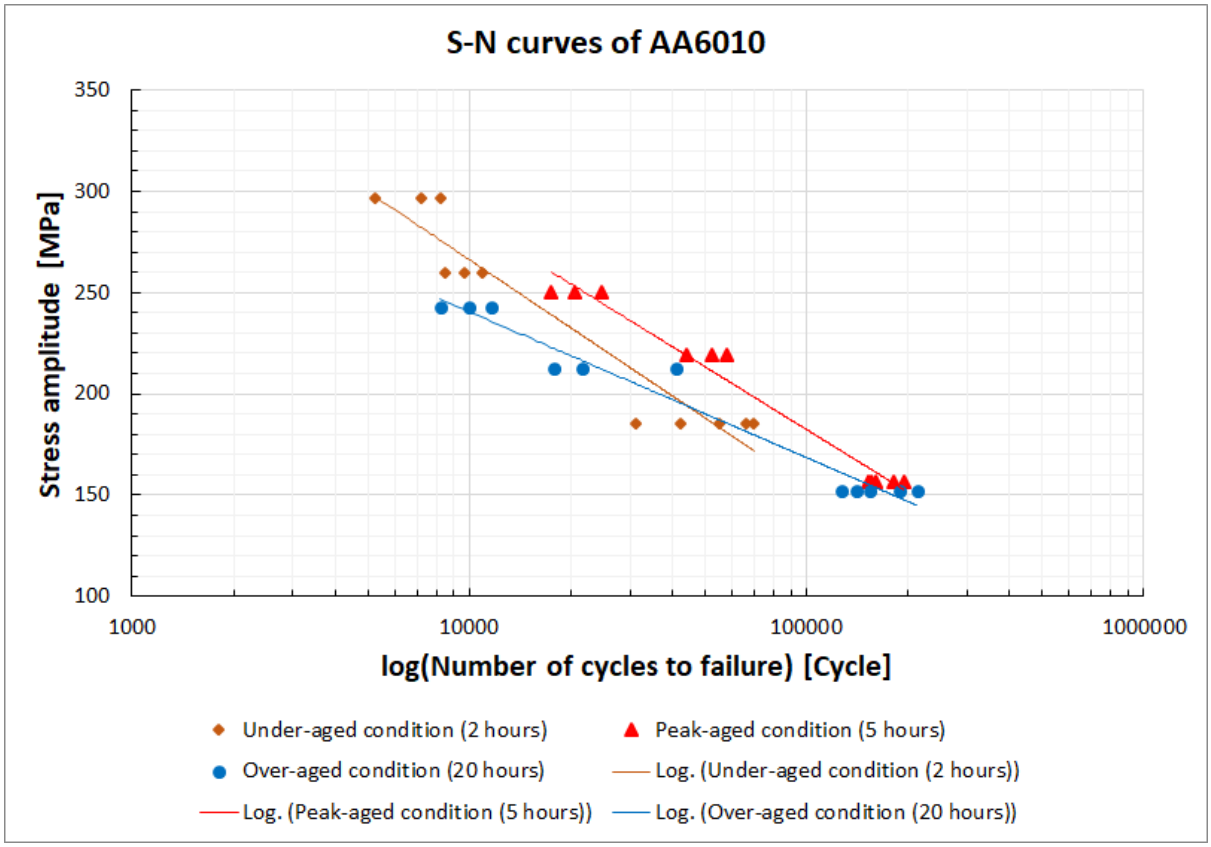


Figure 4.12: Stress amplitude versus number of cycles to failure for AA6010 samples at under-aged, peak-aged and over-aged conditions.

For AA6010, the longest fatigue life has been obtained for the specimens which been conducted to the over-aged condition. This result was expected because AA6010 specimens at the over-aged condition had the lowest tensile strength compared to the other samples which been aged to the under-aged and to the peak-aged conditions.

Both AA6082 and AA6010 specimens shows the highest fatigue life at the over-aged condition. However, the fatigue life for AA6010 at the over-aged condition is higher than the fatigue life for AA6082 at the over-aged condition.

## 4.6 Metallography

### 4.6.1 Grain structure

Grain structure was studied by the light microscope to examine the shape of the grain structure after the deformation and heat treatment. Figure 4.13 shows the grain structure in the longitudinal plane for AA6082.

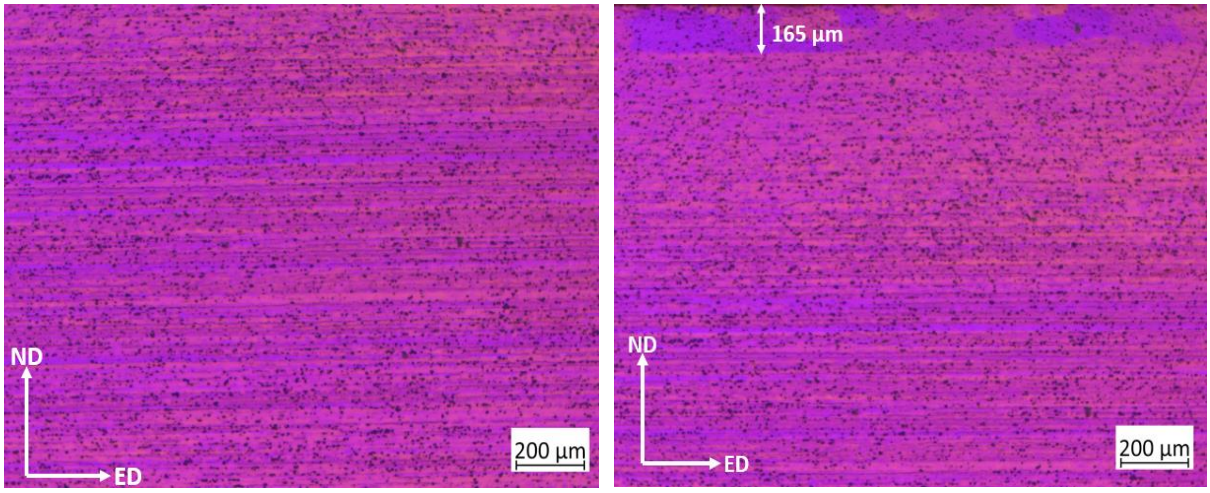


Figure 4.13: The grain structure in the longitudinal plane for AA6082 samples after the deformation and heat treatment at magnification 5x.

The images in figures 4.13 shows the elongated grains after solution heat treatment, deformation and quenching by the pressing tool, and artificial aging. All the grains have almost the same color because they have the same direction. Images show that the grains are elongated in the ED directions. Thin recrystallized layer (160 µm) appears in the image on the right side. It seems that the recrystallized layer has variation in the width along the longitudinal direction.

The images in figures 4.14 show the grains for AA6010 samples after solution heat treatment, deformation and quenching by the pressing tool, and artificial aging. The images exhibit the grain structure from the transverse plane. The black points are SiC particles obtained from the grinding by SiC papers.

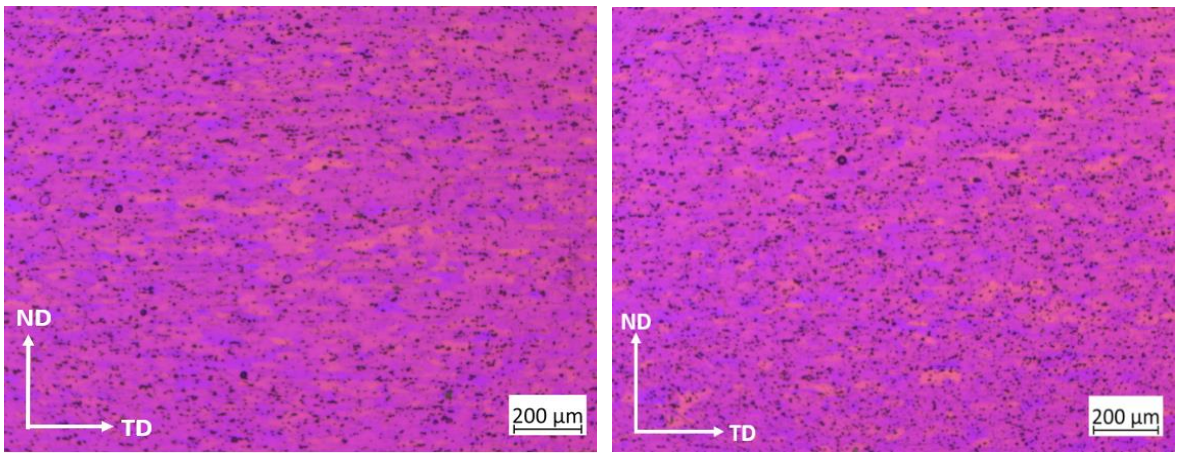


Figure 4.14: The grain structure in the transverse plane for AA6010 after the deformation and heat treatment at magnification 5X.

Figure 4.15 and figure 4.16 exhibit the shape and the direction of the grains by using the secondary electron microscopy and EBSD detector. Images were taken from the transverse and longitudinal planes for both AA6082 and AA6010. The EBSD patterns were obtained from the fibrous grain structure area in the longitudinal plane and in the transverse plane with a magnification of 200X, accelerating voltage of 20kV, aperture of 300 μm, high probe current and a tilt angle of 70°. Detection of secondary electrons (SE2) was used as imaging mode.

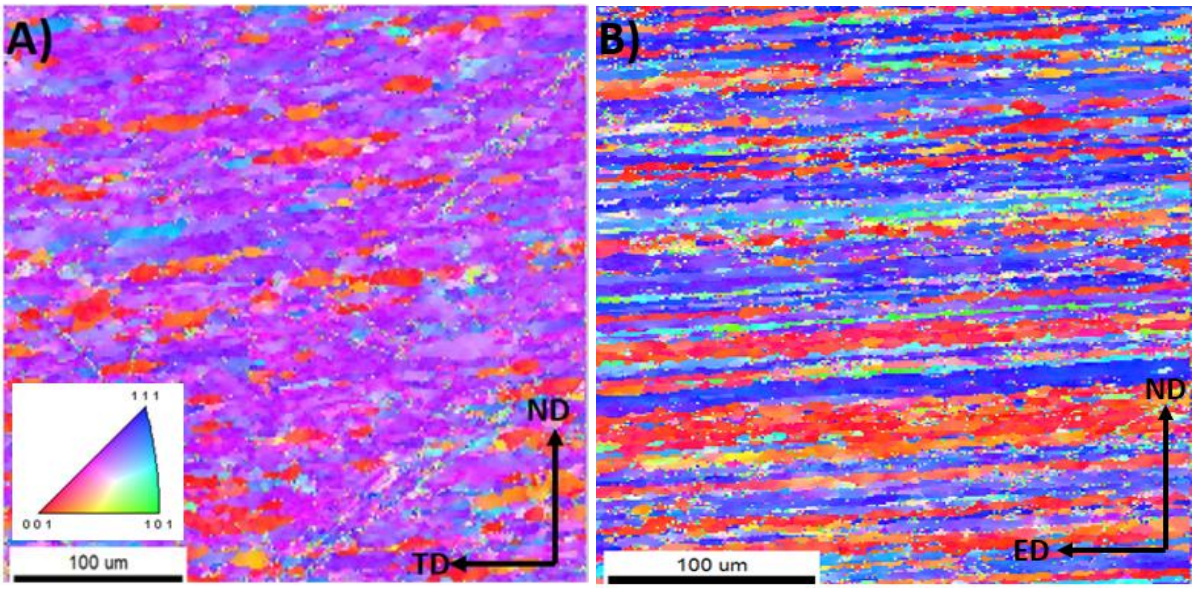


Figure 4.15: Scan area in EBSD of the deformed AA6082 specimens. The scan area in A) is obtained from the transverse plane, and the scan area in B) is obtained from the longitudinal plane.

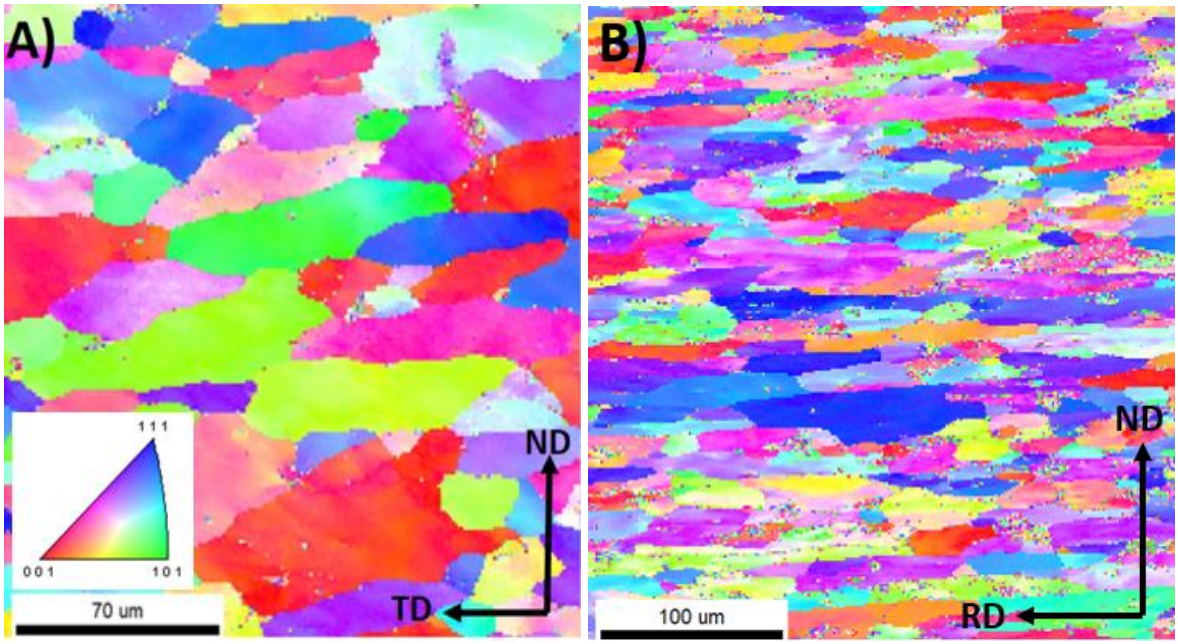


Figure 4.16: Scan area in EBSD of the deformed AA6010 specimens. The scan area in A) is obtained from the transverse plane, and the scan area in B) is obtained from the longitudinal plane.

Figures 4.15 and 4.16 show how the grains are elongated in the longitudinal plane due to the deformation process, and how the grains look different from the transverse plane. That exhibits how the samples are anisotropic.

### 4.6.2 Fractography

Fractographs were taken on selected specimens from both AA6082 and AA6010. The fractographs were taken to underline the fatigue properties, and not to establish the entire fracture surface of all specimens. Numbers 1, 2 and 3 represent the fracture initiation, fracture propagation and the final fracture, respectively. Figure 4.17 shows the fracture surface for an AA6082 specimen that had been over-aged and conducted to stress-controlled low cycle fatigue test with stress amplitude equals to 80% of the yield strength of this sample.

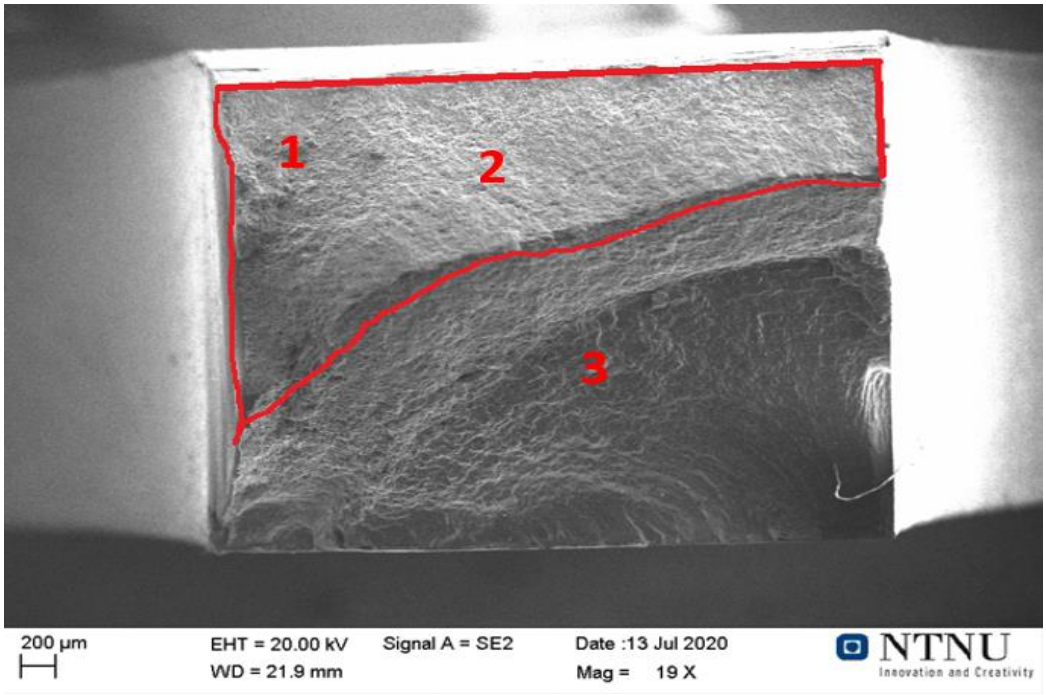


Figure 4.17: An overview of the fractured surface of an AA6082 specimen with short fatigue life.

Figure 4.18 shows the fractured surface for an AA6082 specimen that was over-aged and conducted to stress-controlled low cycle fatigue test with stress amplitude equals to 70% of the yield strength of this sample.

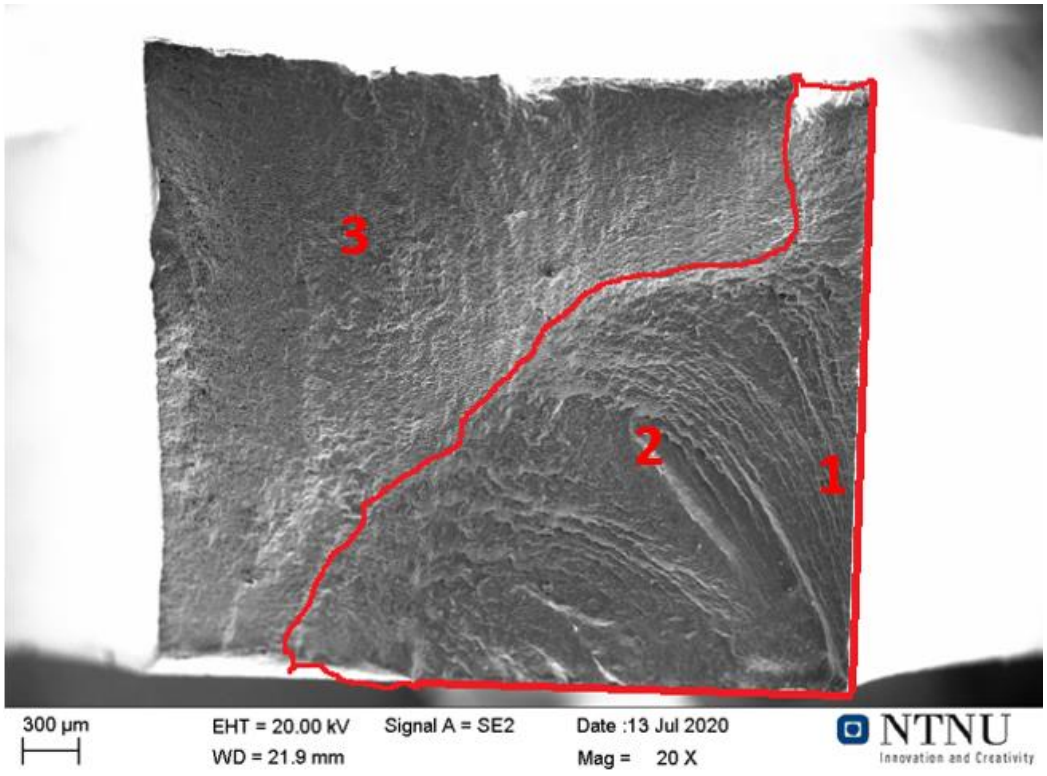


Figure 4.18: An overview of the fractured surface of an AA6082 specimen.

Figure 4.19 shows the fractured surface for an AA6010 specimens that been over-aged and conducted to stress-controlled low cycle fatigue test with stress amplitude equals to 50% of the yield strength of this sample.

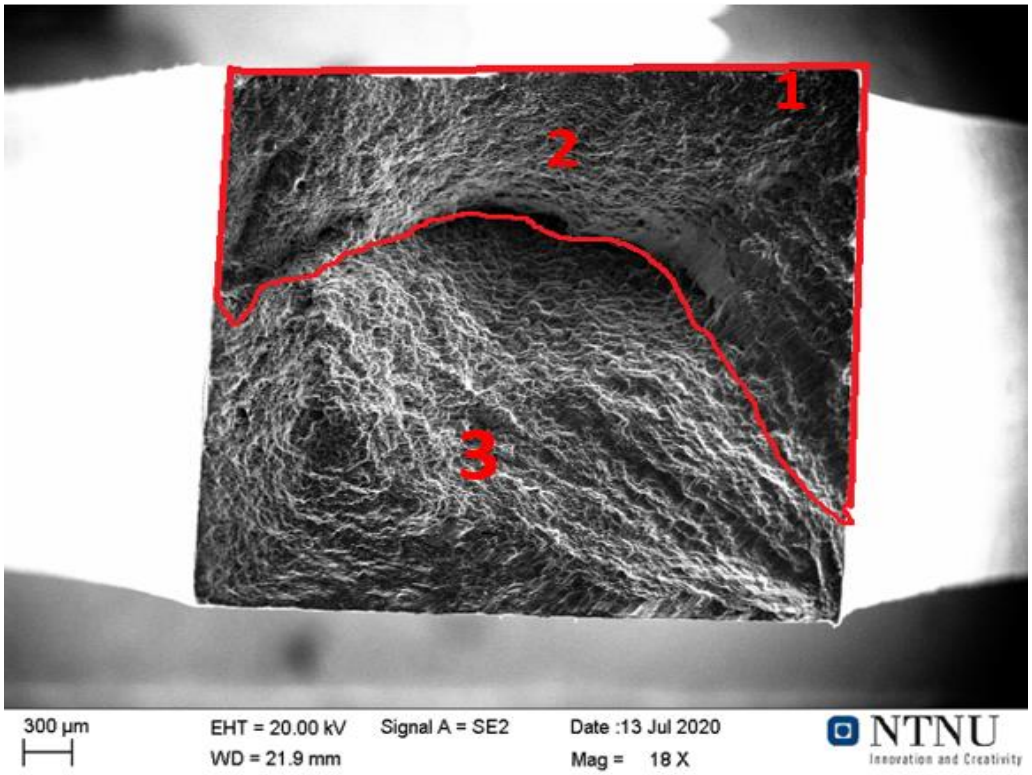


Figure 4.19: An overview of the fractured surface of an AA6010 specimen with long fatigue life.

Figure 4.20 show overview of the fractured surfaces of selected specimens from different viewing angles.

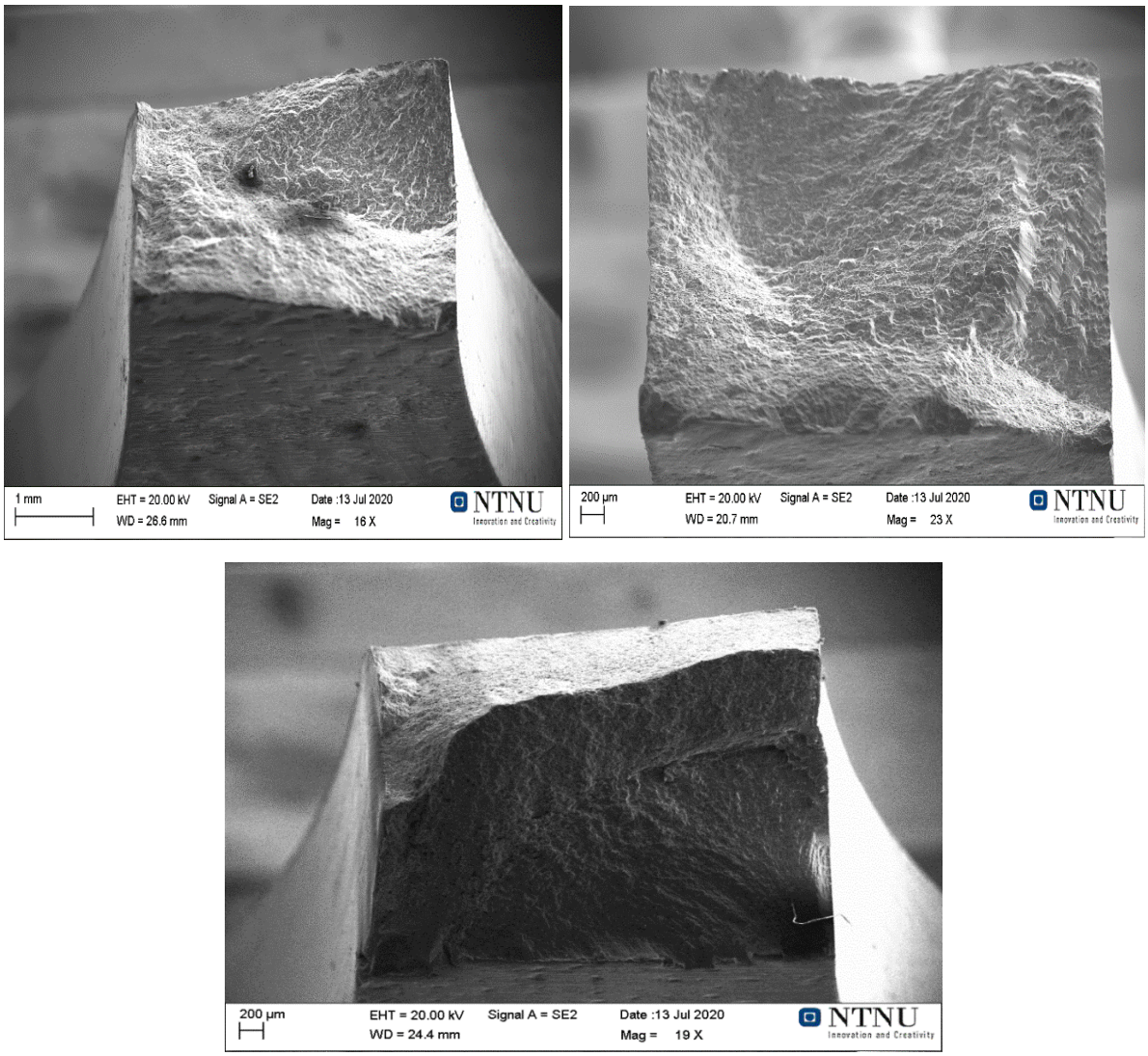


Figure 4.20: An overview of the fractured surfaces of three random selected specimens from different viewing angels.

Figures 4.18, 4.19 and 4.20 show that the areas of the initial fracture (number 1) and fracture propagation (number 2) are rough while the areas of the finial fracture (number 3) are smoother.

# 5. Discussion

## 5.1 Pressing tool effect on the hardening

Under-aged, peak-aged and, over-aged states were taken from the hardening curves performed for both AA6082 and AA6010. Results from tensile tests show that the yield strength at the under-aged condition are the highest and at the over-aged condition the lowest. Hardness measurements on the tensile test bars show that specimens that were aged to the under-aged condition have the highest hardness and specimens that were aged to the over-aged condition have the lowest hardness. However, percentage reduction of area has been calculated for all the specimens that conducted to the tensile tests. Percentage reduction of area for the specimens that were aged to the under-aged state is the lowest, while the highest percentage reduction of area was for the specimens that have been aged to the over-aged state. Percentage reduction of area and the hardness measurements on the tensile bars exhibit that tensile tests results are correct. Specimens that have the higher yield strength have the higher hardness and the lower percentage reduction of area. However, these tensile tests results do not fit with the hardening curves because samples that been aged to the peak-aged states should have the higher tensile strength. Hardening curves were done like all the classic hardening curves by quenching by water, while the quenching during the experimental work was done by integrated hot forming and in-die quenching. From the tensile tests results that have been given in figure 4.5 and figure 4.6, it's clear that the values that were used to age the samples to the under-aged states gave results as the peak-aged state due to the highest hardness and the highest tensile strength that been obtained at this state. Values that were obtained from the hardening curves for the peak-aged and the over-aged states are equivalent to the over-aged state for the samples that were quenched by the pressing tools. That means that the peak-aged and the over-aged states obtained during the experimental works are equivalent to the over-aged state (over-aged state (1) and over-aged state (2)), and the under-aged state are equivalent to the peak-aged state, and that is illustrated in figure 5.1 and figure 5.2.

However, hardness measurements at under-aged state, peak-aged state, and over-aged state for specimens that were conducted to solution heat treatment followed by integrated hot forming and in-die quenching are lower than hardness measurements for samples that were conducted to solution heat treatment followed by cooling by water. Figure 5.1 and figure 5.2 illustrate how the hardness differs between samples that were solution heat treated followed by cooling by water, then artificially aged, and the samples that were conducted to

solution heat treatment followed by integrated hot forming and quenching, then artificially aged.

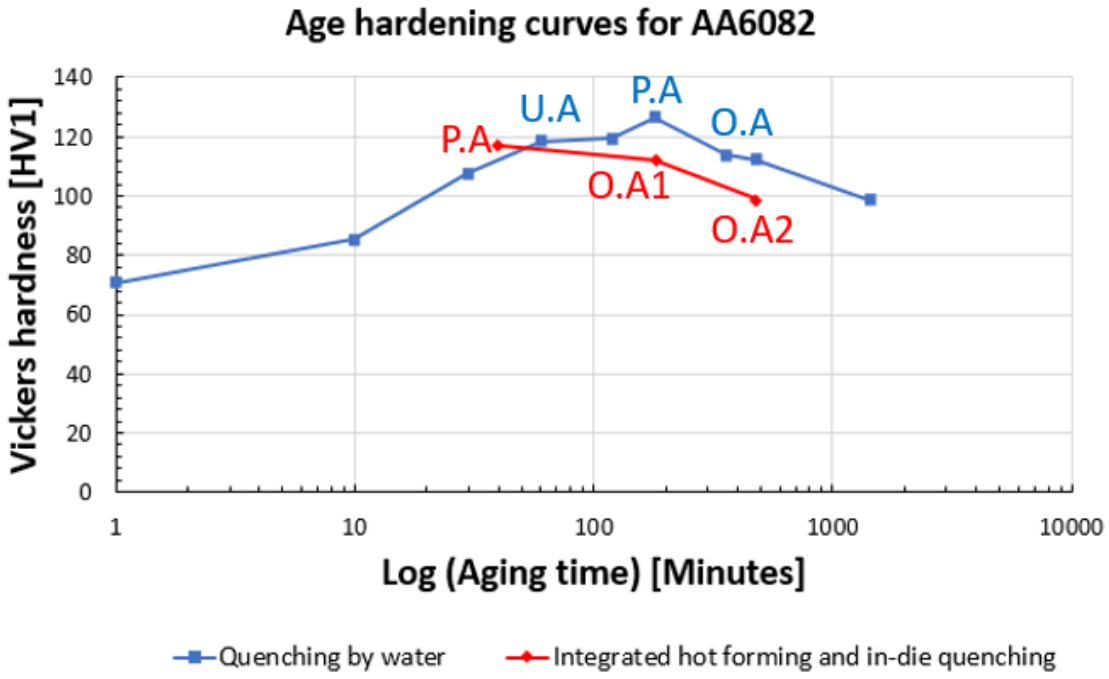


Figure 5.1: Comparison of the hardening curve obtained by quenching by water, and hardness measurements after integrated hot forming and in-die quenching for AA6082.

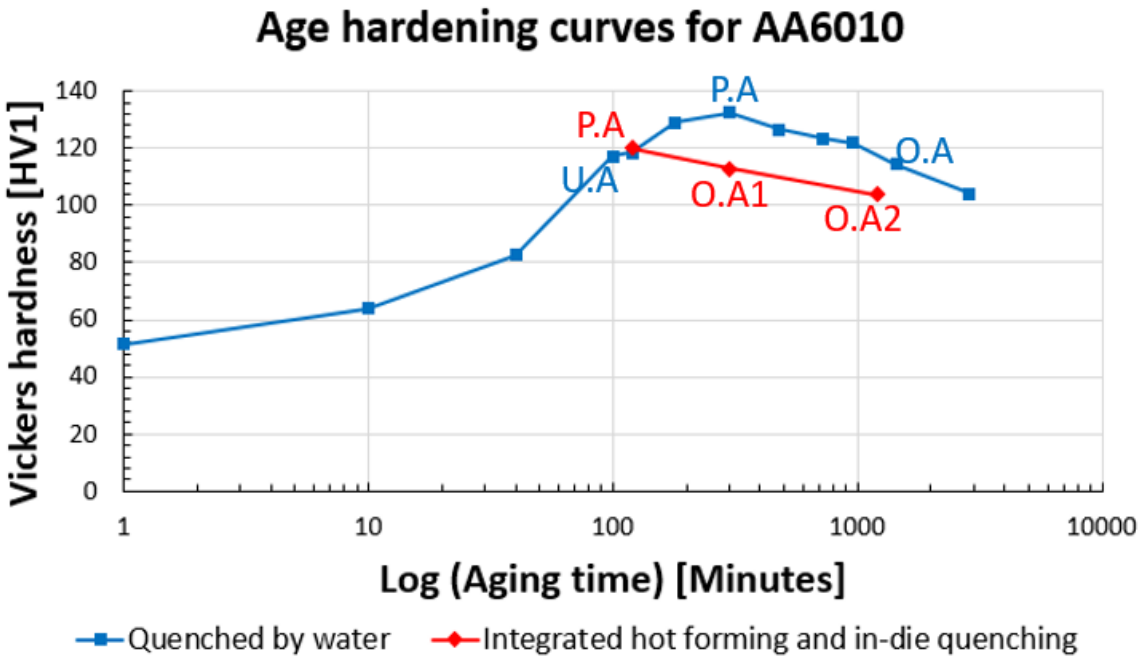


Figure 5.2: Comparison of the hardening curve obtained by quenching by water, and hardness measurements after integrated hot forming and in-die quenching for AA6010.

Figure 5.1 and figure 5.2 exhibit that specimens that were subjected to solution heat treatment, integrated hot forming and in die-quenching, and artificially aged at different periods have lower hardness in general and different peak-hardness compared to the hardening curves that were obtained by solution heat treatment followed by cooling by water, and artificial aging. However, artificial aging was done at 185 °C for both specimens that conducted to integrated hot forming and in-die quenching, and in the hardening curves.

## 5.2 Effect of aging on the low cycle fatigue

Low cycle fatigue tests have been done on the specimens that were aged at three different aging conditions, under-aged, peak-aged, and over aged conditions. Low cycle fatigue tests should be strain-controlled, but in this study low cycle fatigue tests were stress-controlled. The reasons were that the specimens were very small, and the gauge length was short, around 15 mm. The gauge length was 14 mm before the deformation but after the deformation the gauge length was nearly 15mm. Therefore, the extensometer couldn't fit this length of gauge length. Samples have this short length to fit the pressing tool that was built already to fit these parameters of samples. However, stress-controlled tests were beneficial to examine how the stress amplitude versus the fatigue life varies at the different artificial aging states. Results that have been presented in figure 4.11 and figure 4.12 exhibit that the specimens that have been aged to the over-aged state and have the lower yield strength, have the highest number cycle of failures, and that was expected already. Figure 5.3 for AA6082 and figure 5.4 for AA6010 exhibit how the number of cycles to failure became higher at the lower yield strength.

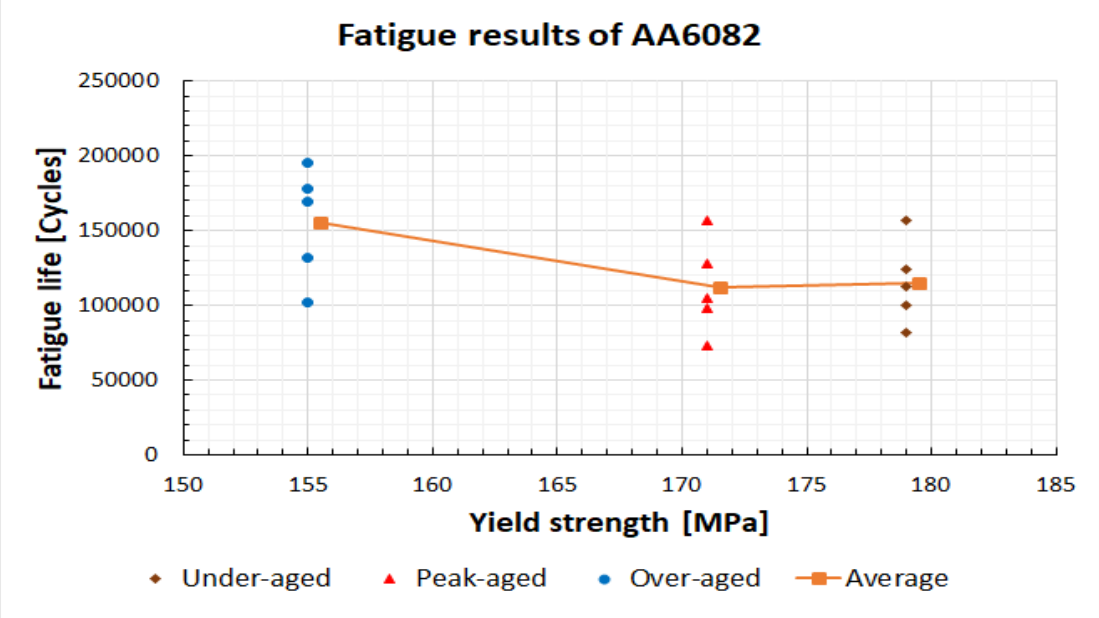


Figure 5.3: Yield strength versus number of cycles to failure at $10^5$ level for AA6082.

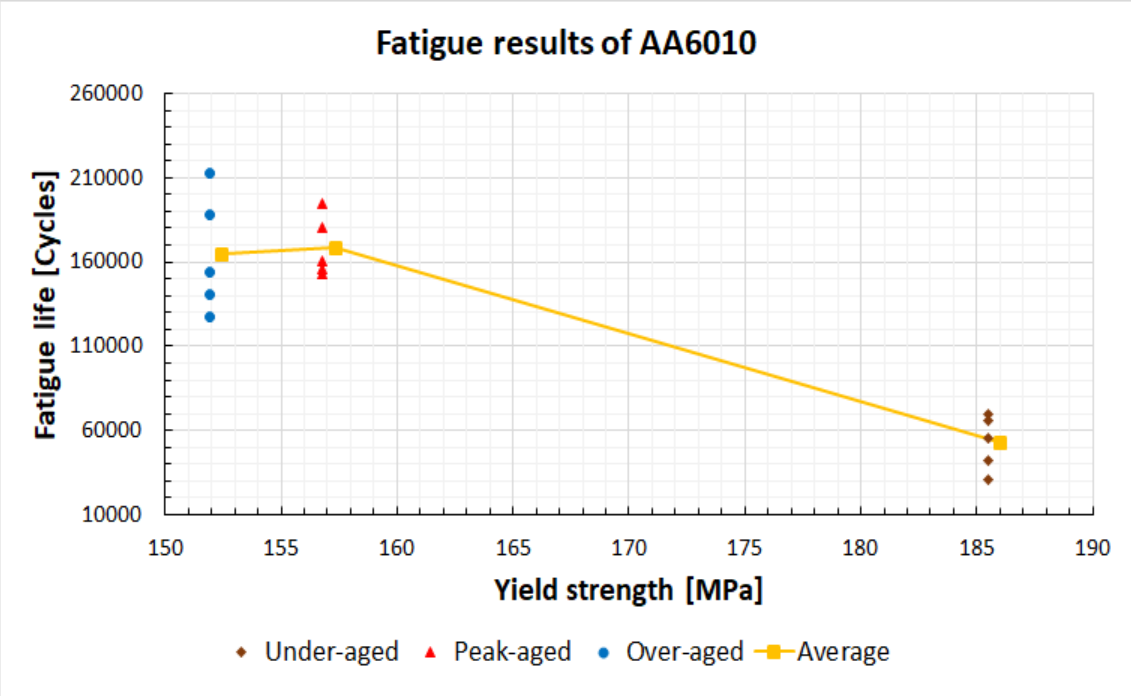


Figure 5.4: Yield strength versus number of cycles to failure at $10^5$ level for AA6010.

The results presented in figure 5.3 and 5.4 were expected already. Specimens that have the higher yield strength, have the higher number of cycles to failure because the ductility increases when the strength of a metal decreases. That means aging the AA6082 and AA6010 to the over-aged or to the under-aged conditions may give longer fatigue life.

# 6. conclusion

In this study, the effect of artificial aging on the low cycle fatigue of extruded AA6082 and rolled AA6010 have been investigated. Both alloys were tested at three different artificial aging states. Under-aged, peak-aged and over-aged states. The heat treatment sequence of the alloys involved: resolution heat treatment, integrated hot forming and in-die quenching, and artificial aging. The changes between hardening curves that have been done by solutions heat treatment followed by quenching by water, and the samples that have been conducted to solution heat treatment followed by integrated hot forming and in-die quenching have also been investigated.

Findings in this study:

- The setup of the pressing tool that was used to do the integrated hot forming and in-die quenching works well.
- Hardness of samples that were conducted to the integrated hot forming and in-die quenching by the pressing tool is lower than for specimens that were cooled by water.
- The peaks of hardness that have been obtained from the hardening curves made by solution heat treatment followed by quenching by water, and then artificial aging were changed during the experimental work du to quenching by the pressing tool instead of water.
- Under-aged, peak-aged, and over-aged conditions obtained from the hardening curves have been changed to the peak-aged, over-aged (1), and over-aged (2) conditions, respectively due to the pressing tool-effect.
- The fatigue properties are better for both alloys when the specimens are aged to the over-aged state.
- Specimens that have lower hardness, have the lower yield strength and the higher ductility.

# 7. Recommendation for further work

- An analysis of the fractured area at different artificial aging states.
- TEM images of the strengthening particles formed during the artificial aging to decide their shape, size and distribution.
- An analysis of the primary particles. These particles are likely to govern ductile dimple growth characteristics.

# 8. Reference


1. AZoM, W.b. *Aluminium / Aluminum 6010 Alloy (UNS A96010)*. 2013; Available from: https://www.azom.com/article.aspx?ArticleID=8612.
2. Branco, R., F. Berto, and A. Kotousov, *Special Issue on "Mechanical Behaviour of Aluminium Alloys".* Applied sciences, 2018. **8**(10): p. 1854.
3. Dieter, G.E., *Mechanical Metallurgy*. SI Metric Edition ed. 1989: McGraw-Hill Book Company.
4. Funatani, K., L. Xie, and G.E. Totten, *Handbook of metallurgical process design*. Materials engineering. Vol. 24. 2004, New York: Marcel Dekker.
5. Howard, R.D., *Aluminum heat treatment processes, applications and equipment.* Industrial Heating, 2007. **74**(2): p. 61-65.
6. Hu, P., et al., *Theories, Methods and Numerical Technology of Sheet Metal Cold and Hot Forming: Analysis, Simulation and Engineering Applications*. Analysis, Simulation and Engineering Applications. 2013, London: Springer London, London.
7. Humphreys, F.J. and M. Hatherly, *Recrystallization and Related Annealing Phenomena*. 2004, GB: Pergamon: GB.
8. Jensrud, O., *Forming technology of light alloys manufacturing of high performance products.* 2019.
9. Jensrud, O., *Personal communication*. 2020.
10. John, H., S.R. Gregory, and R. Anthony, *Chapter 13 - Hot Deformation and Dynamic Restoration*. 2017, Elsevier Ltd. p. 469-508.
11. Kammer, C., *Aluminium handbook: Vol. 1 : Fundamentals and materials*. Vol. Vol. 1. 1999, Düsseldorf: Aluminium-Verlag.
12. Lentz, M. *High strength 6xxx sheet alloys HA6070-D, HA6070S*. 2019.
13. materia, t. *Temper Designation System for Heat Treatable Aluminium Alloys*. 2001.
14. Miller, W.S., et al., *Recent development in aluminium alloys for the automotive industry*. Materials science & engineering. A, Structural materials : properties, microstructure and processing, 2000. **280**(1): p. 37-49.
15. Mughrabi, H. and H. Mughrabi, *Microstructural mechanisms of cyclic deformation, fatigue crack initiation and early crack growth.* Philosophical transactions. Series A, Mathematical, physical, and engineering sciences, 2015. **373**(2038).

16. Mukhopadhyay, P., *Alloy Designation, Processing, and Use of AA6XXX Series Aluminium Alloys.* ISRN metallurgy, 2012. **2012**: p. 1-15.
17. Nandy, S., et al., *Influence of ageing on the low cycle fatigue behaviour of an Al-Mg-Si alloy.* Philosophical Magazine, 2017. **97**(23): p. 1978-2003.
18. Noseda Grau, V., et al., *Solute clustering behavior between 293K and 373K in a 6082 Aluminum alloy.* Journal of Alloys and Compounds, 2016. **684**: p. 481-487.
19. Polmear, I.J., *Light Alloys: From Traditional Alloys to Nanocrystals*. 2006, GB: Butterworth Heinemann: GB.
20. Polmear, I.J., *Physical Metallurgy of Aluminium Alloys*. 2006, Elsevier. p. 1-4.
21. Polmear, I.J., *Wrought Aluminium Alloys*. 2006, Elsevier. p. 1-1.
22. Prasad, K., et al., *Influence of test temperature on cyclic deformation behavior of a near α titanium alloy.* Materials Science & Engineering A, 2016. **662**: p. 373-384.
23. Rösler, J., M. Bäker, and H. Harders, *Mechanical Behaviour of Engineering Materials: Metals, Ceramics, Polymers, and Composites*. 2007, Berlin, Heidelberg: Springer Berlin Heidelberg: Berlin, Heidelberg.
24. Phillips, A.L. and D.V. Volcox, *Aluminium and aluminium alloys*. [5th ed.]. ed. 1966, New York.
25. Srivatsan, T.S., M.A. Imam, and R. Srinivasan, *Fatigue of Materials III : Advances and Emergencies in Understanding*. 2016, Springer International Publishing : Imprint: Springer: Cham.
26. Suresh, S., *Cyclic deformation in polycrystalline ductile solids*. 1998. p. 86-131.
27. Xiong, J.J. and R.A. Shenoi, *Fatigue and Fracture Reliability Engineering*. 2011, Springer London: Imprint: Springer: London.
28. Ma, W.-y., et al., *Influence of process parameters on properties of AA6082 in hot forming process.* Transactions of Nonferrous Metals Society of China, 2017. **27**(11): p. 2454-2463.
29. Costa, J.D., et al., *Fatigue behaviour of AA6082 friction stir welds under variable loadings.* International Journal of Fatigue, 2012. **37**: p. 8-16.
30. Krupp, L.B., *Fatigue*. The Most common complaints series. 2003, Philadelphia: Butterworth-Heinemann.

# 9. Appendix

## Appendix A: Tensile test results for AA6082

| Condition of aging | Specimen | Area: Thickness*Width [$mm^2$] | Tensile strength [MPa] | Yield strength [MPa] | Modulus [GPa] |
|---|---|---|---|---|---|
| Under-aged condition | 1 | 3.31*3.97=13.4 | 368.7 | 348.5 | 71.144 |
| | 2 | 3.32*3.91=12.98 | 391.8 | 369.7 | 73.946 |
| | 3 | 3.29*3.90=12.83 | 379.3 | 356.7 | 80.291 |
| Peak-aged condition | 1 | 3.15*3.92=12.35 | 360.9 | 340.3 | 76.521 |
| | 2 | 3.25*3.92=12.74 | 370.9 | 352.5 | 75.955 |
| | 3 | 3.24*3.92=12.7 | 351.4 | 333.7 | 74.368 |
| Over-aged condition | 1 | 3.30*3.90=12.87 | 307.0 | 279.2 | 72.355 |
| | 2 | 3.39*3.90=13.22 | 346.4 | 322.9 | 75.983 |
| | 3 | 3.35*3.9=13.06 | 346.5 | 322.9 | 76.849 |
| | 4 | 3.35*3.91=13.10 | 339.9 | 315.7 | 77.050 |

Table 9.1: Tensile tests results of AA6082

## Appendix B: Tensile test results for AA6010

| Condition of aging | Specimen | Area: Thickness*Width [$mm^2$] | Tensile strength [MPa] | Yield strength [MPa] | Modulus [GPa] |
|---|---|---|---|---|---|
| Under-aged condition | 1 | 3.31*3.91=12.94 | 400.8 | 383.1 | 80.799 |
| | 2 | 3.40*3.90=13.26 | 372.1 | 350.9 | 75.549 |
| | 3 | 3.38*3.90=13.18 | 401.7 | 380.3 | 76.207 |
| Peak-aged condition | 1 | 3.35*3.92=13.13 | 350.1 | 329.1 | 73.615 |
| | 2 | 3.33*3.90=12.99 | 317.0 | 295.1 | 86.169 |
| | 3 | 3.32*3.91=12.98 | 316.5 | 295.2 | 73.676 |
| | 4 | 3.27*3.91=12.79 | 353.6 | 335.2 | 76.669 |
| Over-aged condition | 1 | 3.26*3.93=12.81 | 293.5 | 269.1 | 74.631 |
| | 2 | 3.38*3.90=13.18 | 350.8 | 329.5 | 79.965 |
| | 3 | 3.34*3.92=13.09 | 336.0 | 313.0 | 79.072 |

Table 9.2: Tensile tests results of AA6010

# Appendix C: Hardness measurements on the tensile test bars For AA6082

| Condition of aging | Specimen | Hardness measurements on the tensile test specimens HV/ 5 | | | | | Average |
|---|---|---|---|---|---|---|---|
| | | 1 | 2 | 3 | 4 | 5 | |
| Under-aged condition | 1 | 116.6 | 112.4 | 115.6 | 119 | 118.9 | 116.5 |
| | 2 | 120.3 | 118 | 121.4 | 112.2 | 116.7 | 117.72 |
| | 3 | 112 | 114.1 | 117 | 119.3 | 118.7 | 116.22 |
| Peak-aged condition | 1 | 113.5 | 110 | 117.5 | 116.9 | 112.5 | 114.08 |
| | 2 | 110 | 113.2 | 117.1 | 108.4 | 108 | 111.34 |
| | 3 | 113.1 | 113 | 111.1 | 108 | 110.2 | 111.08 |
| Over-aged condition | 1 | 96 | 94.8 | 95.8 | 96.7 | 94.2 | 95.5 |
| | 2 | 92.4 | 94 | 104 | 95.1 | 95.9 | 96.28 |
| | 3 | 105.2 | 101.6 | 99.9 | 102.9 | 103.1 | 102.54 |
| | 4 | 102 | 99.4 | 98.4 | 102 | 102.3 | 100.82 |

Table 9.3: Hardness measurements of AA6082

# Appendix D: Hardness measurements on the tensile test bars For AA6010

| Condition of aging | Specimen | Hardness measurements on the tensile test specimens HV/ 5 | | | | | Average |
|---|---|---|---|---|---|---|---|
| | | 1 | 2 | 3 | 4 | 5 | |
| Under-aged condition | 1 | 119.5 | 119 | 121 | 119.3 | 116.7 | 119.1 |
| | 2 | 116 | 119.9 | 115.1 | 120 | 124.9 | 119.18 |
| | 3 | 124 | 120.8 | 121.2 | 119 | 122 | 121.4 |
| Peak-aged condition | 1 | 106.7 | 110.1 | 116.9 | 113.7 | 110.8 | 111.64 |
| | 2 | 116.6 | 115.9 | 116.8 | 116.2 | 111.2 | 115.34 |
| | 3 | 115.9 | 105 | 105.6 | 116.8 | 117 | 112.06 |
| | 4 | 110.3 | 106.2 | 105.6 | 110 | 104 | 107.22 |
| Over-aged condition | 1 | 97.5 | 98.2 | 109 | 107.9 | 99.3 | 102.38 |
| | 2 | 98.1 | 107.3 | 105.7 | 100 | 107 | 103.62 |
| | 3 | 100.5 | 102 | 104.8 | 106.7 | 97.9 | 102.38 |

Table 9.4: Hardness measurements of AA6010.

# Appendix E: Images obtained from the stereoscope to calculate the percentage reduction of area for AA6082

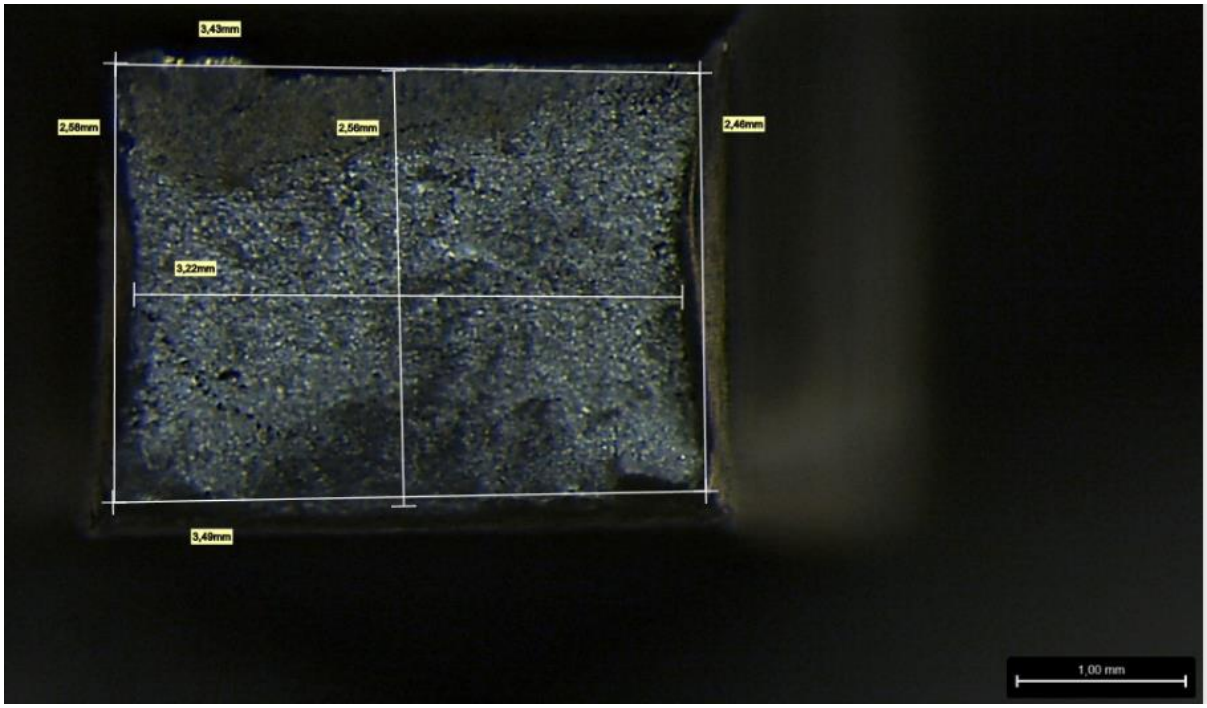


Figure 9.1: Specimen (1) that have been artificial aged to the under-aged state.

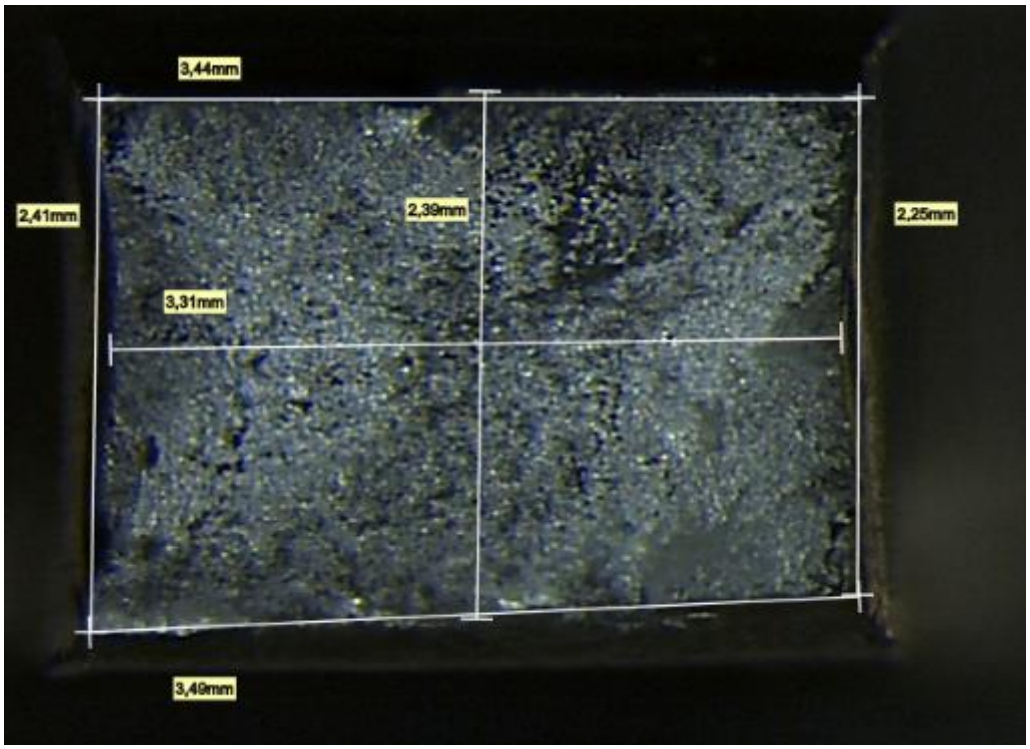


Figure 9.2: Specimen (2) that have been artificial aged to the under-aged state.

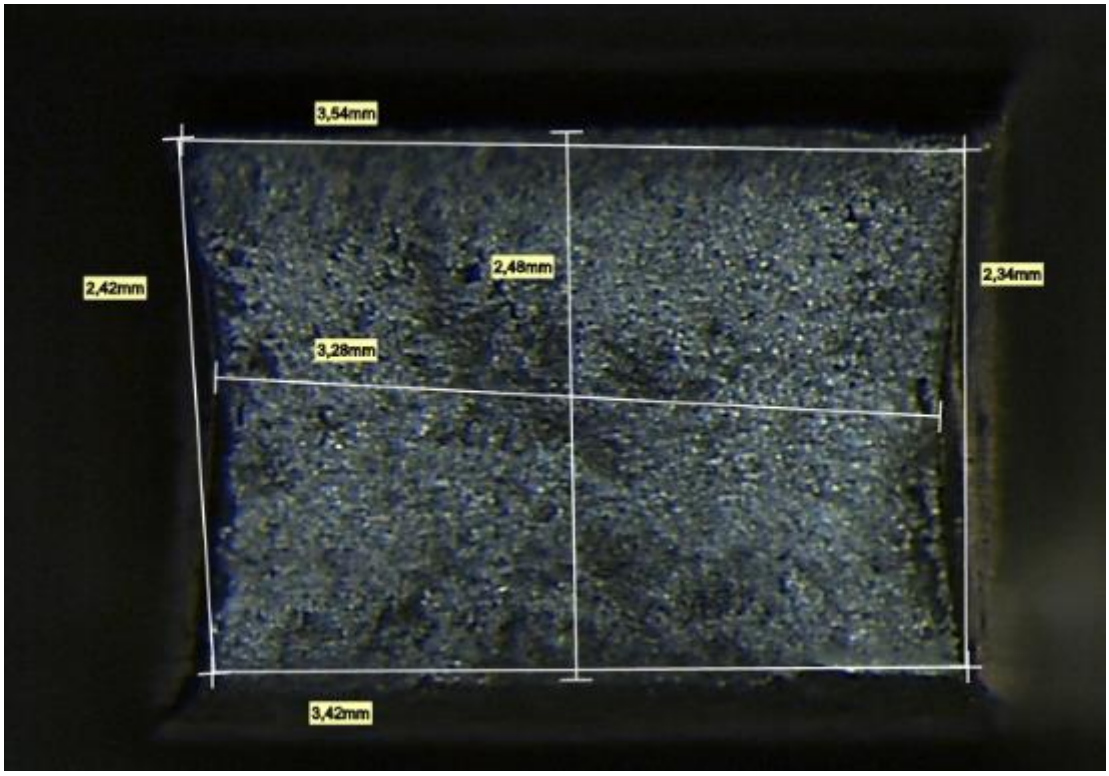


Figure 9.3: Specimen (3) that have been artificial aged to the under-aged state.

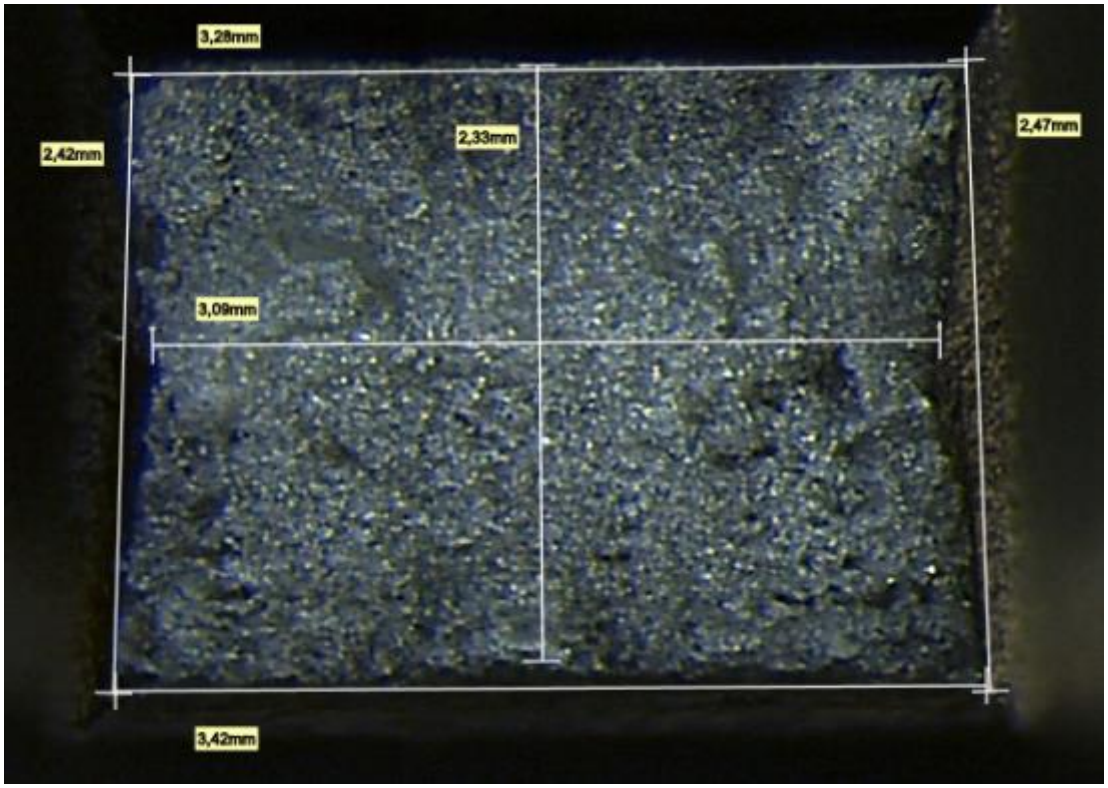


Figure 9.4: Specimen (1) that have been artificial aged to the peak-aged state.

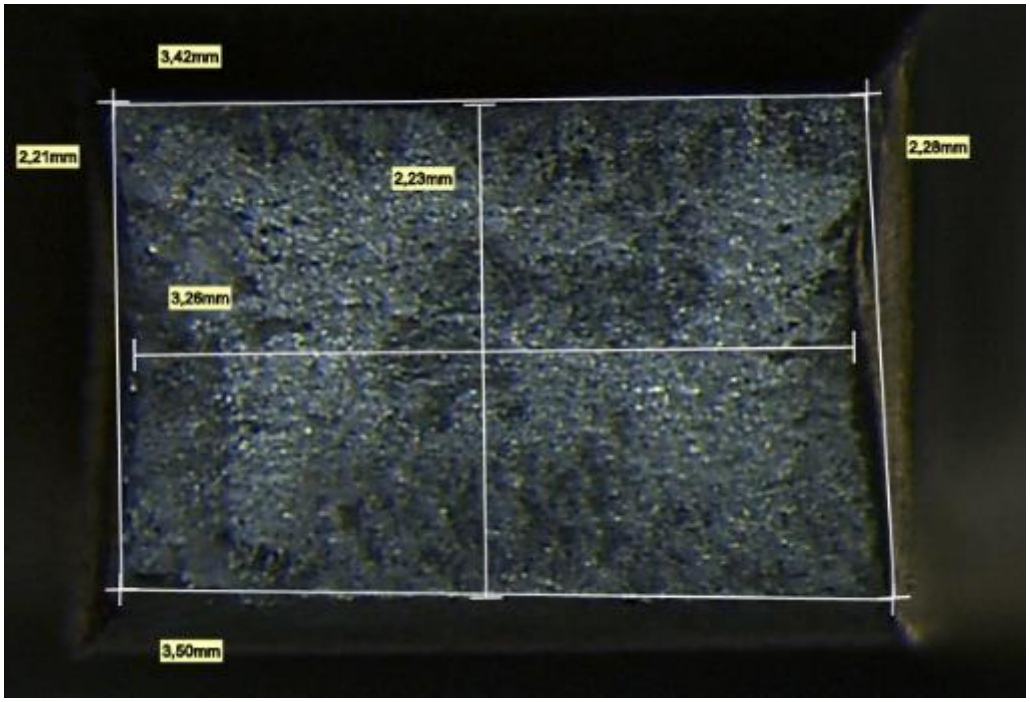


Figure 9.5: Specimen (2) that have been artificial aged to the peak-aged state.

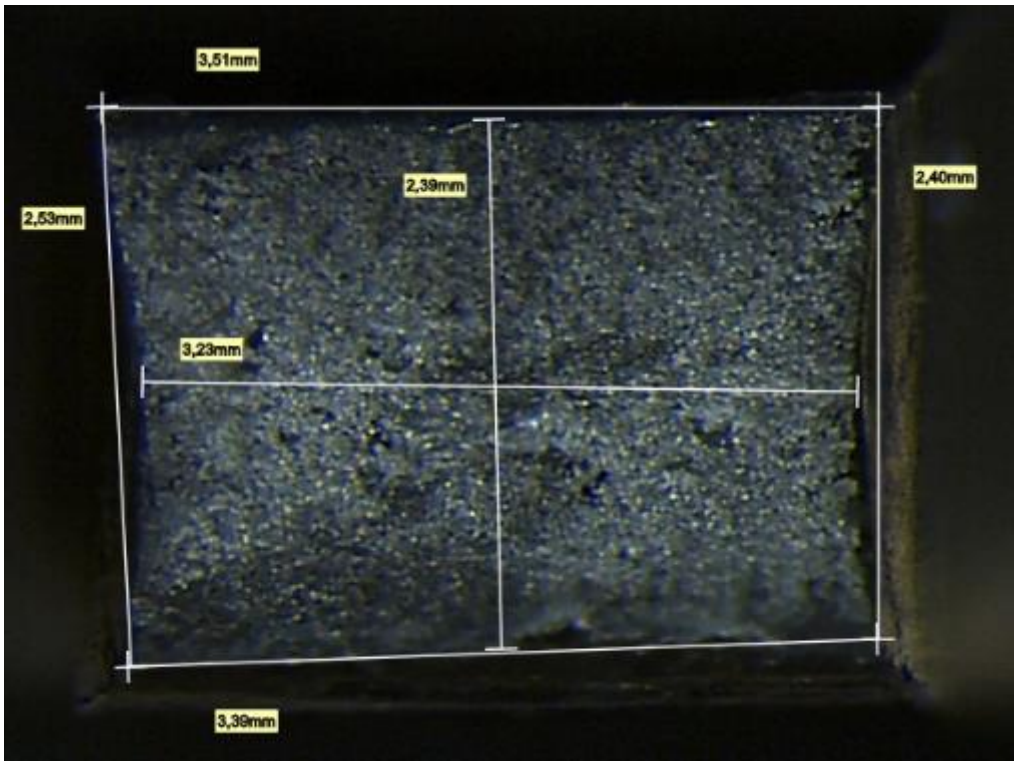


Figure 9.6: Specimen (3) that have been artificial aged to the peak-aged state.

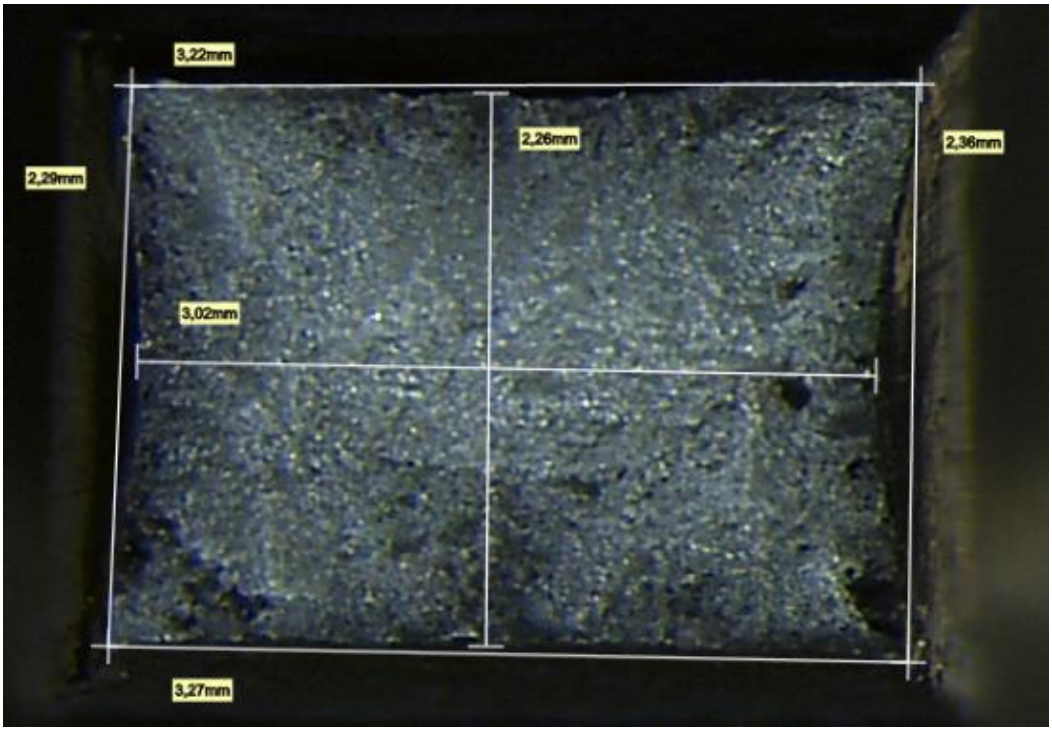


Figure 9.7: Specimen (1) that have been artificial aged to the over-aged state.

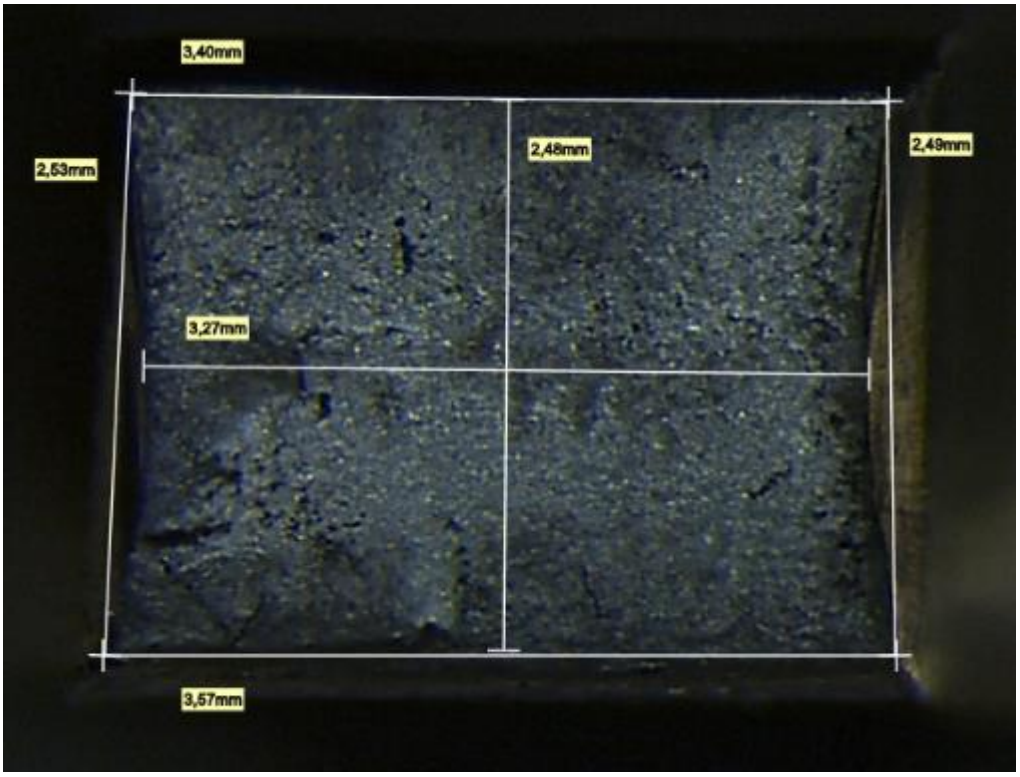


Figure 9.8: Specimen (2) that have been artificial aged to the over-aged state.

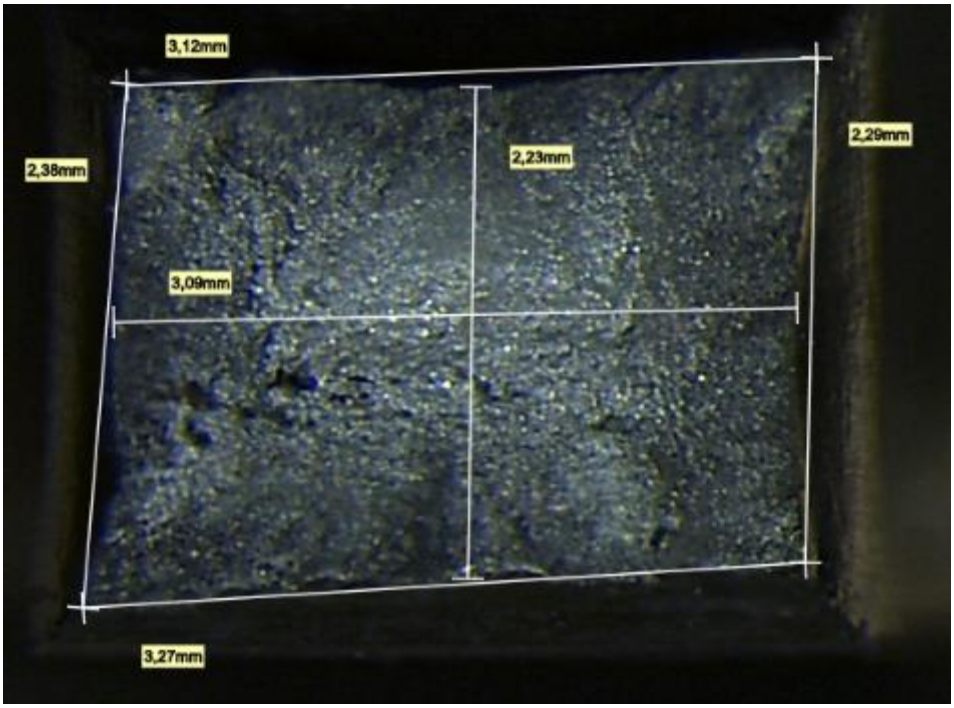


Figure 9.9: Specimen (3) that have been artificial aged to the over-aged state.

# Appendix F: Images obtained from the stereoscope to calculate the percentage reduction of area for AA6010

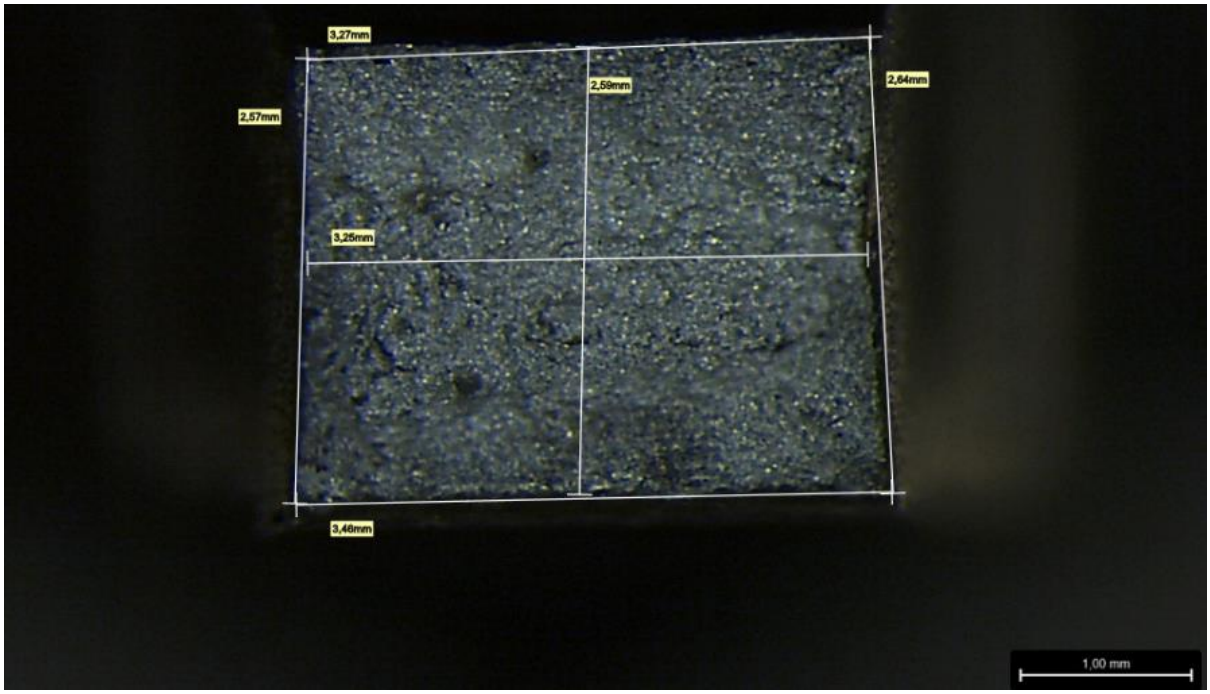


Figure 9.10: Specimen (1) that have been artificial aged to the under-aged state.

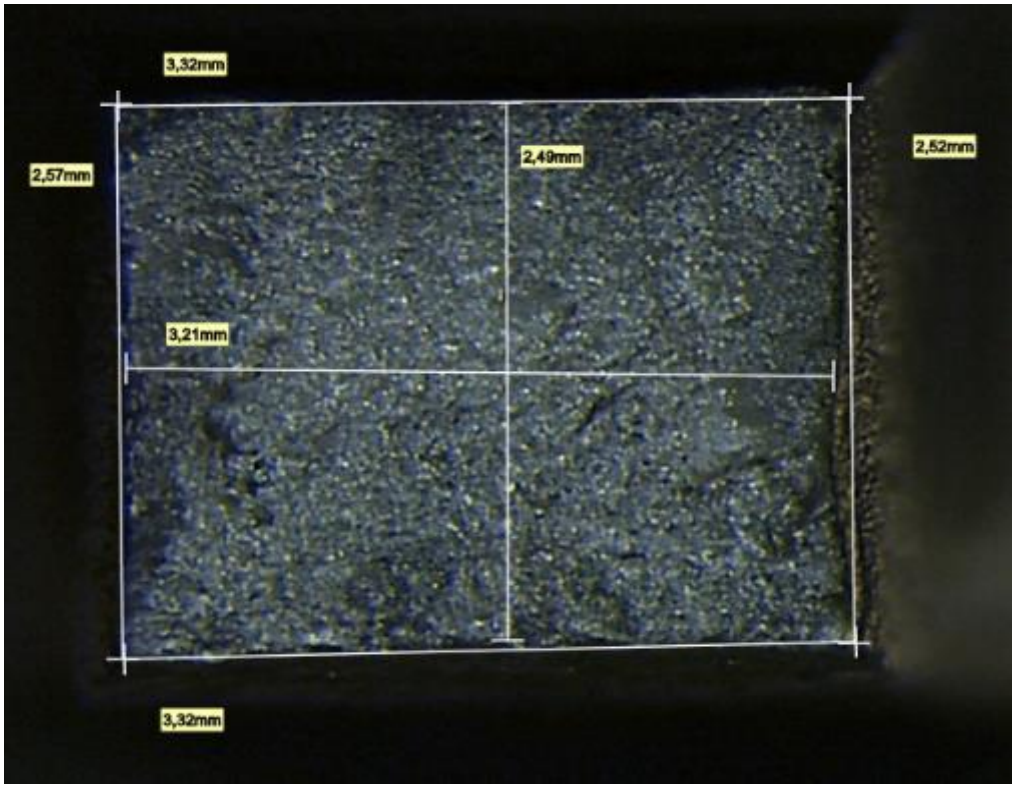


Figure 9.11: Specimen (2) that have been artificial aged to the under-aged state.

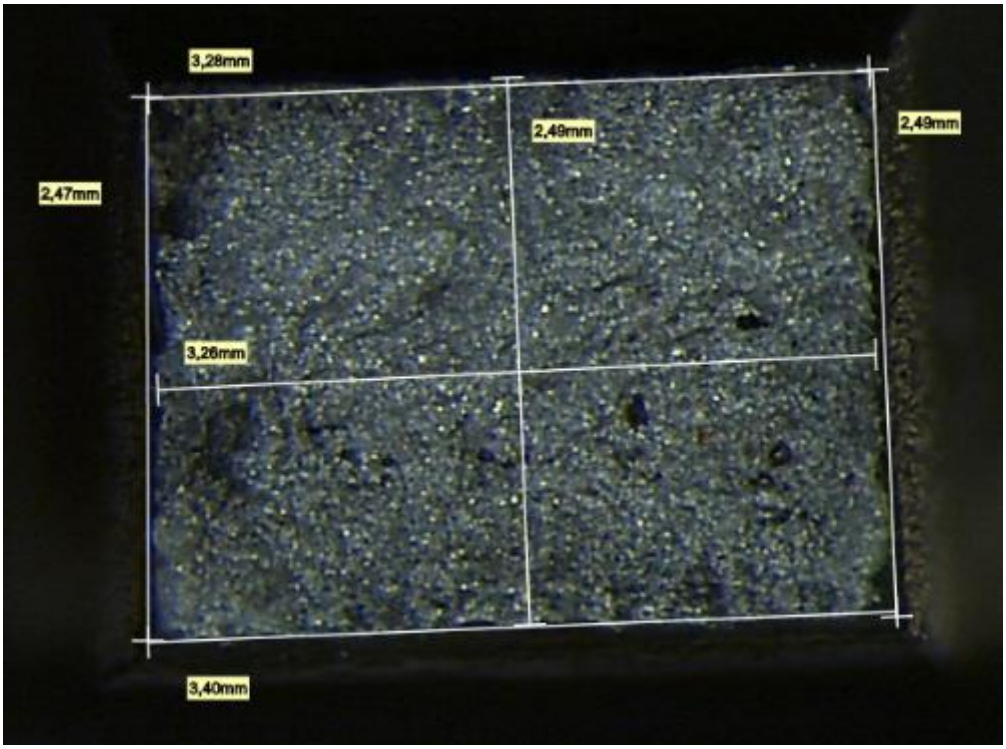


Figure 9.12: Specimen (3) that have been artificial aged to the under-aged state.

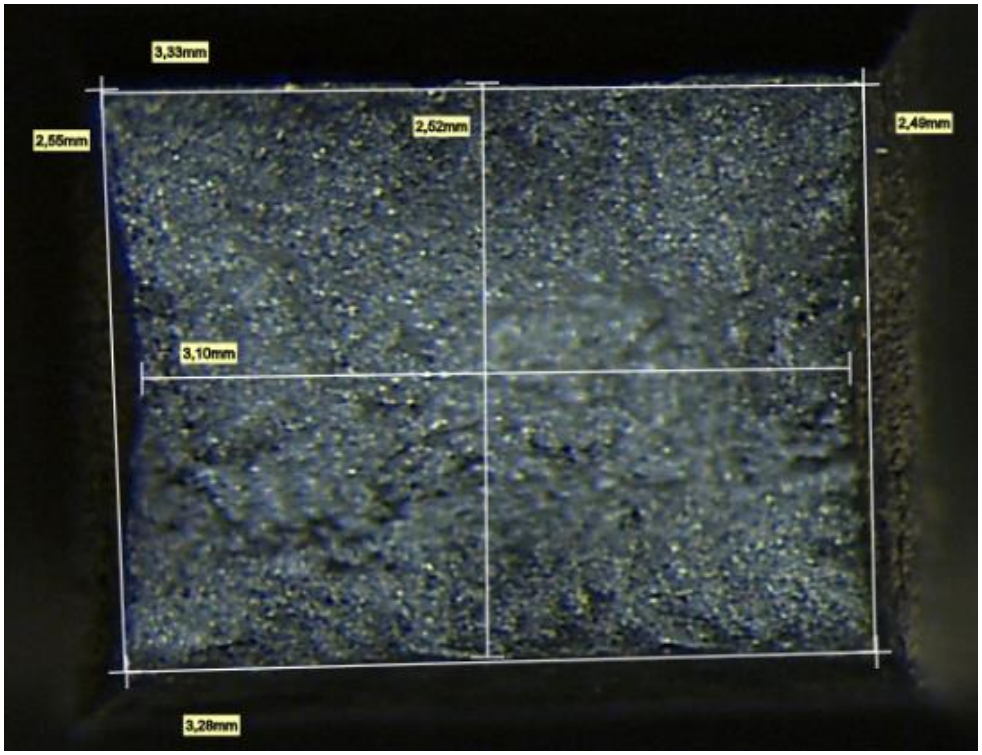


Figure 9.13: Specimen (1) that have been artificial aged to the peak-aged state.

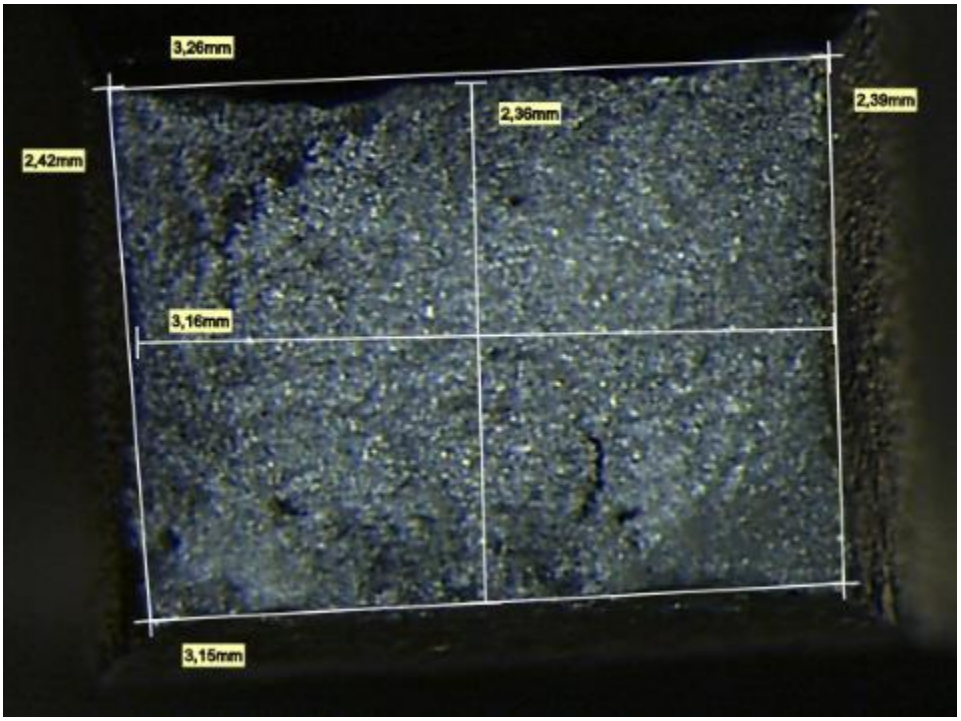


Figure 9.14: Specimen (2) that have been artificial aged to the peak-aged state.

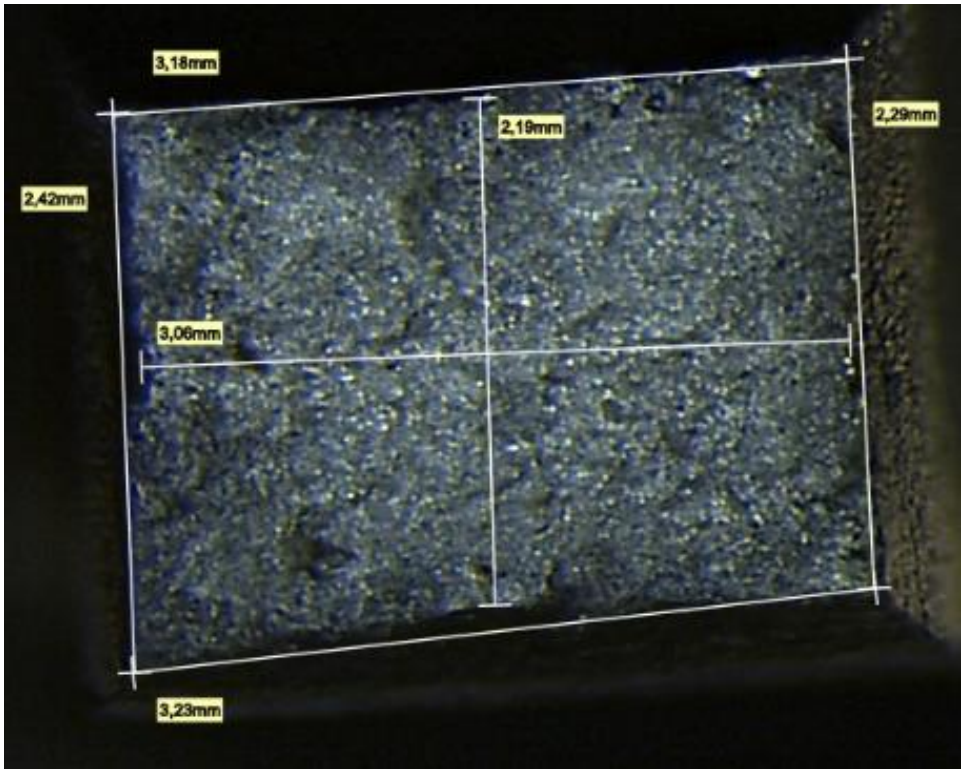


Figure 9.15: Specimen (3) that have been artificial aged to the peak-aged state.

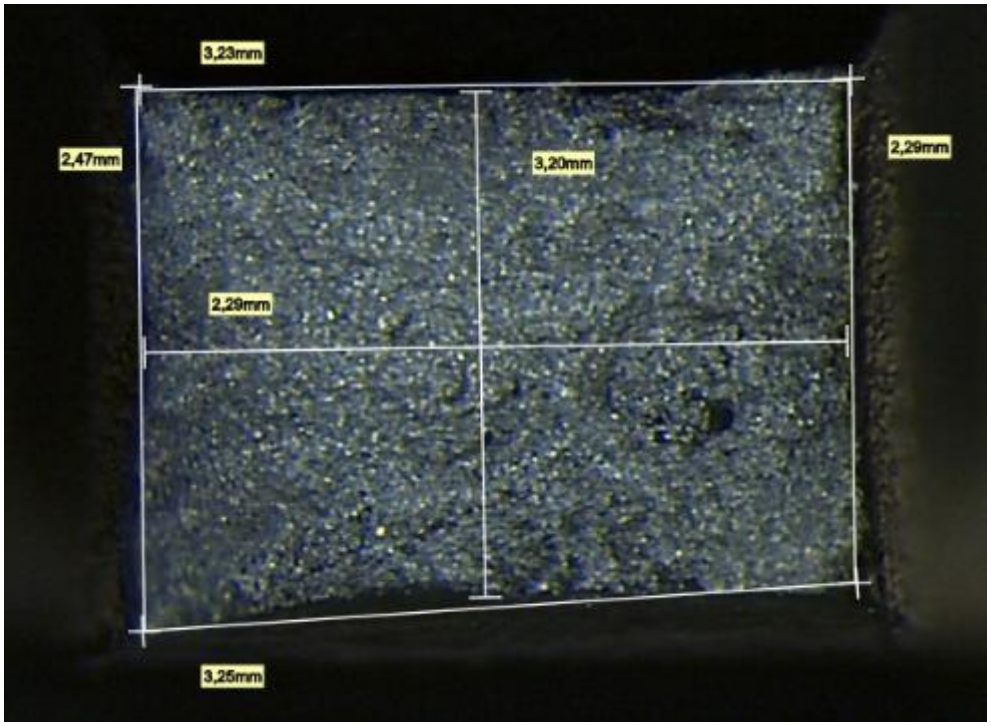


Figure 9.16: Specimen (4) that have been artificial aged to the peak-aged state.

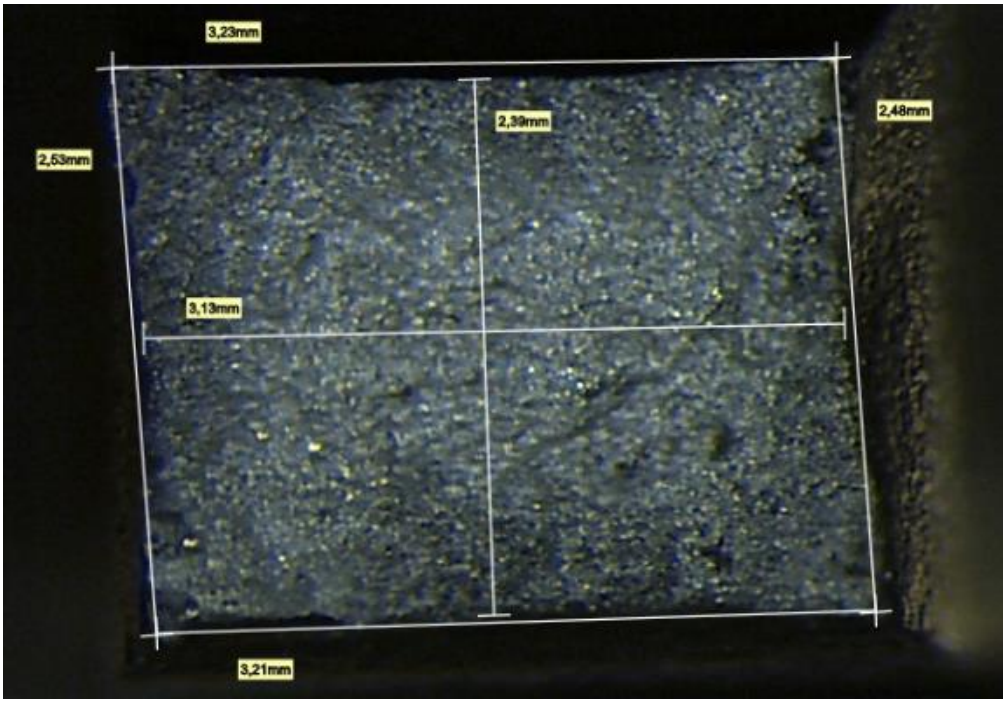


Figure 9.17: Specimen (1) that have been artificial aged to the over-aged state.

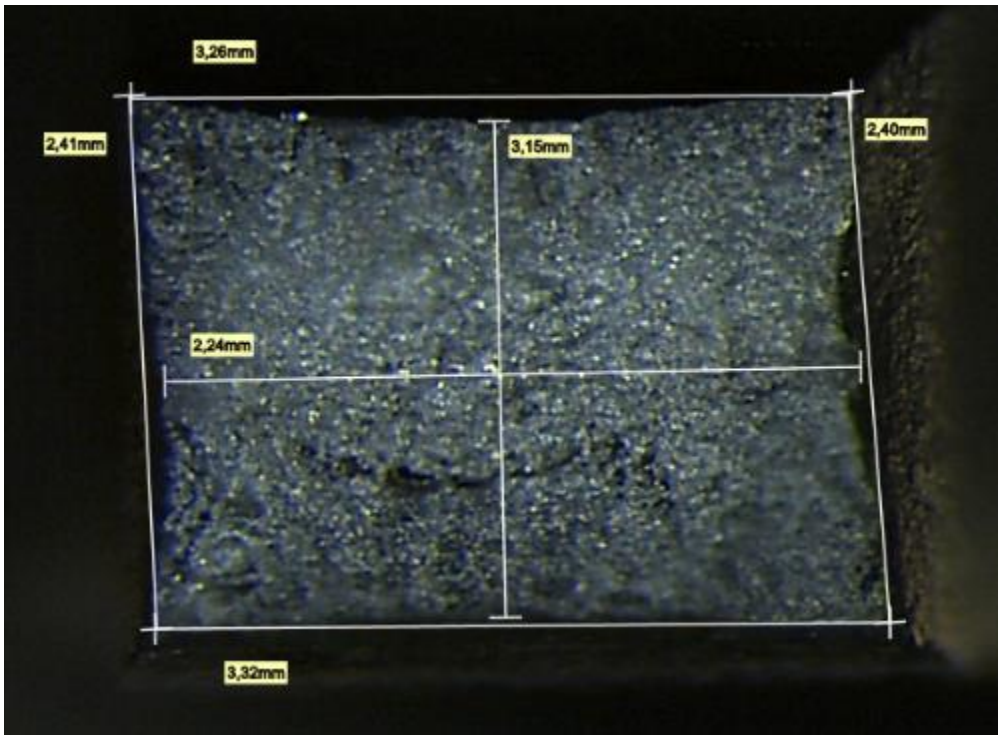


Figure 9.18: Specimen (2) that have been artificial aged to the over-aged state.

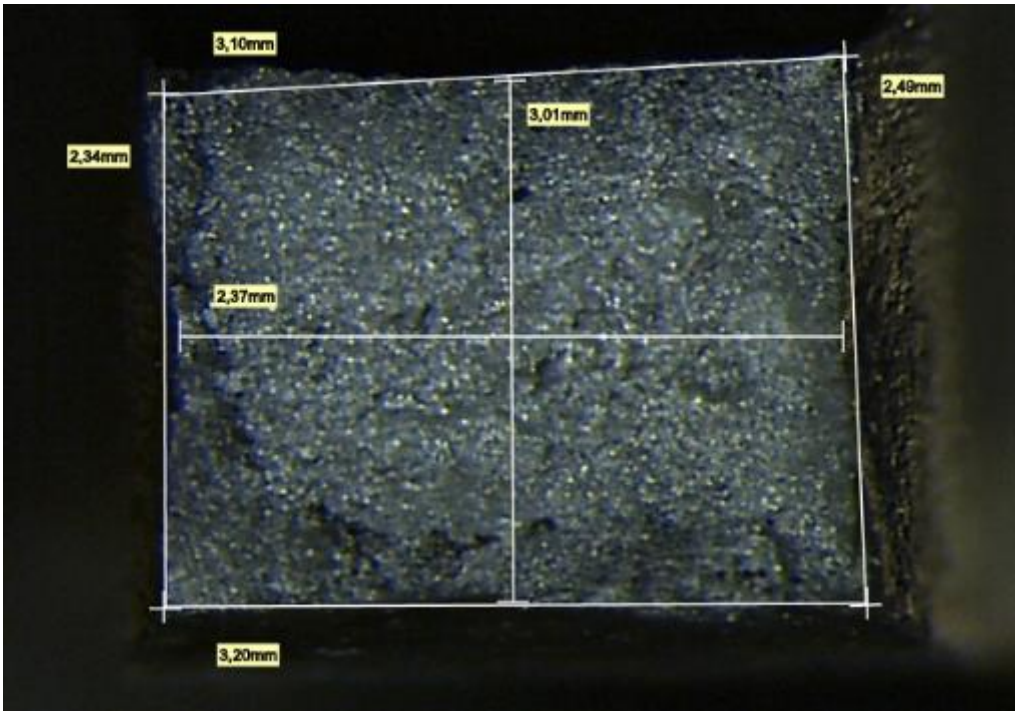


Figure 9.19: Specimen (3) that have been artificial aged to the over-aged state.

# Appendix G: Percentage reduction of area for AA6082

| AA 6082 | | Thickness after testing [mm] | Width after testing [mm] | Su [$mm^2$] | Thickness before testing [mm] | Width before testing [mm] | So [$mm^2$] | Z [%] |
|---|---|---|---|---|---|---|---|---|
| Under-aged state | 1 | 2.56 | 3.22 | 8.2432 | 3.31 | 3.97 | 13.1407 | 37.27 |
| | 2 | 2.39 | 3.31 | 7.9109 | 3.32 | 3.91 | 12.9812 | 39.06 |
| | 3 | 2.34 | 3.28 | 7.6752 | 3.29 | 3.9 | 12.831 | 40.18 |
| Peak-aged state | 1 | 2.33 | 3.09 | 7.1997 | 3.15 | 3.92 | 12.348 | 41.69 |
| | 2 | 2.23 | 3.26 | 7.2698 | 3.25 | 3.92 | 12.74 | 42.94 |
| | 3 | 2.39 | 3.23 | 7.7197 | 3.24 | 3.92 | 12.7008 | 39.22 |
| Over-aged state | 1 | 2.26 | 3.02 | 6.8252 | 3.39 | 3.9 | 13.221 | 48.38 |
| | 2 | 2.48 | 3.27 | 8.1096 | 3.35 | 3.9 | 13.065 | 37.93 |
| | 3 | 2.23 | 3.09 | 6.8907 | 3.35 | 3.91 | 13.0985 | 47.39 |

Table 9.5: Percentage reduction of area of AA6082

# Appendix H: Percentage reduction of area for AA6010

| AA 6010 | | Thickness after testing [mm] | Width after testing [mm] | Su [$mm^2$] | Thickness before testing [mm] | Width before testing [mm] | So [$mm^2$] | Z [%] |
|---|---|---|---|---|---|---|---|---|
| Under-aged state | 1 | 2.59 | 3.25 | 8.4175 | 3.31 | 3.95 | 13.0745 | 35.6 |
| | 2 | 2.49 | 3.21 | 7.9929 | 3.4 | 3.9 | 13.26 | 39.7 |
| | 3 | 2.49 | 3.26 | 8.1174 | 3.38 | 3.9 | 13.182 | 38.4 |
| Peak-aged state | 1 | 2.52 | 3.1 | 7.812 | 3.35 | 3.92 | 13.132 | 40.5 |
| | 2 | 2.36 | 3.16 | 7.4576 | 3.33 | 3.9 | 12.987 | 42.6 |
| | 3 | 2.19 | 3.06 | 6.7014 | 3.32 | 3.91 | 12.9812 | 48.4 |
| | 4 | 3.2 | 2.29 | 7.328 | 3.27 | 3.91 | 12.7857 | 42.7 |
| Over-aged state | 1 | 2.39 | 3.13 | 7.4807 | 3.26 | 3.93 | 12.8118 | 41.6 |
| | 2 | 3.15 | 2.24 | 7.056 | 3.38 | 3.9 | 13.182 | 46.5 |
| | 3 | 3.01 | 2.37 | 7.1337 | 3.34 | 3.92 | 13.0928 | 45.5 |

Table 9.6: Percentage reduction of area of AA6010

# Appendix I: Fatigue test results for AA6082 at under-aged condition

| Specimen | Thickness [mm] | Width [mm] | Area [$mm^2$] | Stress Amplitude [MPa] | Applied force [N] | Number of cycles to failure [cycle] |
|---|---|---|---|---|---|---|
| 1 (80% of Rp0.2) | 3.36 | 3.9 | 13.1 | 286.6 | 3755.6 | 7143 |
| 2(80% of Rp0.2) | 3.3 | 3.9 | 12.9 | 286.6 | 3688.5 | 8108 |
| 3(80% of Rp0.2) | 3.35 | 3.9 | 13.1 | 286.6 | 3744.4 | 9268 |
| 4(70% of Rp0.2) | 3.29 | 3.9 | 12.8 | 250.8 | 3218.0 | 14609 |
| 5(70% of Rp0.2) | 3.25 | 3.9 | 12.7 | 250.8 | 3178.9 | 16639 |
| 6(70% of Rp0.2) | 3.3 | 3.9 | 12.9 | 250.8 | 3227.8 | 17969 |
| 7(50% of Rp0.2) | 3.25 | 3.9 | 12.7 | 179 | 2268.8 | 82033 |
| 8(50% of Rp0.2) | 3.49 | 3.9 | 13.6 | 179 | 2436.4 | 99793 |
| 9(50% of Rp0.2) | 3.25 | 3.9 | 12.7 | 179 | 2268.8 | 112487 |
| 10(50% of Rp0.2) | 3.25 | 3.9 | 12.7 | 179 | 2268.8 | 123880 |
| 11(50% of Rp0.2) | 3.35 | 3.9 | 13.1 | 179 | 2338.6 | 157095 |

Table 9.7: Fatigue tests parameters of AA6082 at under-aged condition.

# Appendix J: Fatigue test results for AA6082 at peak-aged condition

| Specimen | Thickness [mm] | Width [mm] | Area [$mm^2$] | Stress Amplitude [MPa] | Applied force [N] | Number of cycles to failure [cycle] |
|---|---|---|---|---|---|---|
| 1 (80% of Rp0.2) | 3.23 | 3.9 | 12.6 | 273.6 | 3446.5 | 4445 |
| 2(80% of Rp0.2) | 3.25 | 3.9 | 12.7 | 273.6 | 3467.9 | 7579 |
| 3(80% of Rp0.2) | 3.23 | 3.9 | 12.6 | 273.6 | 3446.5 | 8193 |
| 4(70% of Rp0.2) | 3.2 | 3.92 | 12.5 | 239.4 | 3003.0 | 13563 |
| 5(70% of Rp02) | 3.29 | 3.93 | 12.9 | 239.4 | 3095.4 | 19154 |
| 6(70% of Rp0.2) | 3.22 | 3.92 | 12.6 | 239.4 | 3021.8 | 21510 |
| 7(50% of Rp0.2) | 3.22 | 3.96 | 12.8 | 171 | 2180.5 | 73396 |
| 8(50% of Rp0.2) | 3.22 | 3.95 | 12.7 | 171 | 2174.9 | 97918 |
| 9(50% of Rp0.2) | 3.23 | 3.95 | 12.8 | 171 | 2181.7 | 104647 |
| 10(50% of Rp0.2) | 3.28 | 3.93 | 12.9 | 171 | 2204.3 | 128154 |
| 11(50% of Rp0.2) | 3.29 | 3.96 | 13.0 | 171 | 2227.9 | 157071 |

Table 9.8: Fatigue tests parameters of AA6082 at peak-aged condition.

# Appendix K: Fatigue test results for AA6082 at over-aged condition

| Specimen | Thickness [mm] | Width [mm] | Area [$mm^2$] | Stress Amplitude [MPa] | Applied force [N] | Number of cycles to failure [cycle] |
|---|---|---|---|---|---|---|
| 1 (80% of Rp0.2) | 3.35 | 3.9 | 13.1 | 248 | 3240.1 | 7301 |
| 2(80% of Rp0.2) | 3.34 | 3.95 | 13.2 | 248 | 3271.9 | 10200 |
| 3(80% of Rp0.2) | 3.34 | 3.91 | 13.1 | 248 | 3238.7 | 15294 |
| 4(70% of Rp0.2) | 3.35 | 3.92 | 13.1 | 217 | 2849.6 | 17116 |
| 5(70% of Rp02) | 3.39 | 3.91 | 13.3 | 217 | 2876.3 | 21723 |
| 6(70% of Rp0.2) | 3.39 | 3.91 | 13.3 | 217 | 2876.3 | 22113 |
| 7(50% of Rp0.2) | 3.39 | 3.93 | 13.3 | 155 | 2065.0 | 101665 |
| 8(50% of Rp0.2) | 3.44 | 3.93 | 13.5 | 155 | 2095.5 | 131665 |
| 9(50% of Rp0.2) | 3.37 | 3.92 | 13.2 | 155 | 2047.6 | 169126 |
| 10(50% of Rp0.2) | 3.39 | 3.93 | 13.3 | 155 | 2065.0 | 177961 |
| 11(50% of Rp0.2) | 3.43 | 3.95 | 13.5 | 155 | 2100.0 | 195421 |

Table 9.9: Fatigue tests parameters of AA6082 at over-aged condition.

# Appendix L: Fatigue test results for AA6010 at under-aged condition

| Specimen | Thickness [mm] | Width [mm] | Area [$mm^2$] | Stress Amplitude [MPa] | Applied force [N] | Number of cycles to failure [cycle] |
|---|---|---|---|---|---|---|
| 1 (80% of Rp0.2) | 3.4 | 3.9 | 13.3 | 296.8 | 3935.6 | 5241 |
| 2(80% of Rp0.2) | 3.35 | 3.9 | 13.1 | 296.8 | 3877.7 | 7200 |
| 3(80% of Rp0.2) | 3.35 | 3.9 | 13.1 | 296.8 | 3877.7 | 8220 |
| 4(70% of Rp0.2) | 3.33 | 3.93 | 13.1 | 259.7 | 3398.7 | 8500 |
| 5(70% of Rp02) | 3.31 | 3.93 | 13.0 | 259.7 | 3378.3 | 9674 |
| 6(70% of Rp0.2) | 3.3 | 3.92 | 12.9 | 259.7 | 3359.5 | 10958 |
| 7(50% of Rp0.2) | 3.32 | 3.96 | 13.1 | 185.5 | 2438.8 | 31074 |
| 8(50% of Rp0.2) | 3.42 | 3.94 | 13.5 | 185.5 | 2499.6 | 42414 |
| 9(50% of Rp0.2) | 3.35 | 3.96 | 13.3 | 185.5 | 2460.8 | 55112 |
| 10(50% of Rp0.2) | 3.36 | 3.95 | 13.3 | 185.5 | 2462.0 | 65912 |
| 11(50% of Rp0.2) | 3.38 | 3.95 | 13.4 | 185.5 | 2476.6 | 69870 |

Table 9.10: Fatigue tests parameters of AA6010 at under-aged condition.

# Appendix M: Fatigue test results for AA6010 at peak-aged condition

| Specimen | Thickness [mm] | Width [mm] | Area [$mm^2$] | Stress Amplitude [MPa] | Applied force [N] | Number of cycles to failure [cycle] |
|---|---|---|---|---|---|---|
| 1 (80% of Rp0.2) | 3.41 | 3.93 | 13.4 | 250 | 3350.3 | 17536 |
| 2(80% of Rp0.2) | 3.4 | 3.95 | 13.4 | 250 | 3357.5 | 20552 |
| 3(80% of Rp0.2) | 3.4 | 3.9 | 13.3 | 250 | 3315.0 | 24674 |
| 4(70% of Rp0.2) | 3.37 | 3.95 | 13.3 | 219 | 2915.2 | 43930 |
| 5(70% of Rp02) | 3.32 | 3.93 | 13.0 | 219 | 2857.4 | 52567 |
| 6(70% of Rp0.2) | 3.32 | 3.93 | 13.0 | 219 | 2857.4 | 57981 |
| 7(50% of Rp0.2) | 3.31 | 3.96 | 13.1 | 156.8 | 2055.3 | 152929 |
| 8(50% of Rp0.2) | 3.32 | 3.96 | 13.1 | 156.8 | 2061.5 | 155720 |
| 9(50% of Rp0.2) | 3.39 | 3.96 | 13.4 | 156.8 | 2104.9 | 160973 |
| 10(50% of Rp0.2) | 3.4 | 3.95 | 13.4 | 156.8 | 2105.8 | 180600 |
| 11(50% of Rp0.2) | 3.35 | 3.96 | 13.3 | 156.8 | 2080.1 | 194613 |

Table 9.11: Fatigue tests parameters of AA6010 at peak-aged condition.

# Appendix N: Fatigue test results for AA6010 at over-aged condition

| Specimen | Thickness [mm] | Width [mm] | Area [$mm^2$] | Stress Amplitude [MPa] | Applied force [N] | Number of cycles to failure [cycle] |
|---|---|---|---|---|---|---|
| 1(80% of Rp0.2) | 3.3 | 3.9 | 12.9 | 243 | 3127.4 | 8210 |
| 2(80% of Rp0.2) | 3.31 | 3.9 | 12.9 | 243 | 3136.9 | 9927 |
| 3(80% of Rp0.2) | 3.3 | 3.9 | 12.9 | 243 | 3127.4 | 11610 |
| 4(70% of Rp0.2) | 3.23 | 3.9 | 12.6 | 212.6 | 2678.1 | 17779 |
| 5(70% of Rp0.2) | 3.36 | 3.91 | 13.1 | 212.6 | 2793.1 | 21528 |
| 6(70% of Rp0.2) | 3.35 | 3.95 | 13.2 | 212.6 | 2813.2 | 40960 |
| 7(50% of Rp0.2) | 3.31 | 3.95 | 13.1 | 151.9 | 1986.0 | 127341 |
| 8(50% of Rp0.2) | 3.32 | 3.94 | 13.1 | 151.9 | 1987.0 | 140399 |
| 9(50% of Rp0.2) | 3.41 | 3.95 | 13.5 | 151.9 | 2046.0 | 154318 |
| 10(50% of Rp0.2) | 3.47 | 3.93 | 13.6 | 151.9 | 2071.5 | 188313 |
| 11(50% of Rp0.2) | 3.26 | 3.95 | 12.9 | 151.9 | 1956.0 | 212970 |

Table 9.12: Fatigue tests parameters of AA6010 at over-aged condition.